

University of Windsor

Scholarship at UWindor

Electronic Theses and Dissertations

Theses, Dissertations, and Major Papers

8-29-2022

Overcurrent Protection Schemes for Inverter-Based Islanded Microgrids

Talal Sati

University of Windsor

Follow this and additional works at: <https://scholar.uwindsor.ca/etd>



Part of the [Electrical and Computer Engineering Commons](#)

Recommended Citation

Sati, Talal, "Overcurrent Protection Schemes for Inverter-Based Islanded Microgrids" (2022). *Electronic Theses and Dissertations*. 9124.

<https://scholar.uwindsor.ca/etd/9124>

This online database contains the full-text of PhD dissertations and Masters' theses of University of Windsor students from 1954 forward. These documents are made available for personal study and research purposes only, in accordance with the Canadian Copyright Act and the Creative Commons license—CC BY-NC-ND (Attribution, Non-Commercial, No Derivative Works). Under this license, works must always be attributed to the copyright holder (original author), cannot be used for any commercial purposes, and may not be altered. Any other use would require the permission of the copyright holder. Students may inquire about withdrawing their dissertation and/or thesis from this database. For additional inquiries, please contact the repository administrator via email (scholarship@uwindsor.ca) or by telephone at 519-253-3000ext. 3208.

Overcurrent Protection Schemes for Inverter-based Islanded Microgrids

By

Talal Sati

A Dissertation
Submitted to the Faculty of Graduate Studies
through the Department of Electrical and Computer Engineering
in Partial Fulfillment of the Requirements for
the Degree of Doctor of Philosophy
at the University of Windsor

Windsor, Ontario, Canada

2022

©2022 Talal Sati

Overcurrent Protection Schemes for Inverter-based Islanded Microgrids

by

Talal Sati

APPROVED BY:

H. Farag, External Examiner
York University

O. Jianu
Department of Mechanical, Automotive and Materials Engineering

N. Kar
Department of Electrical and Computer Engineering

E. Abdel-raheem
Department of Electrical and Computer Engineering

M. Azzouz, Advisor
Department of Electrical and Computer Engineering

August 17th, 2022

Declaration of Co-authorship/Previous Publication

I. Co-Authorship

I hereby declare that this thesis incorporates material that is result of joint research, as follows:

Chapters 3 and 4 of the thesis include the outcome of publications co-authored with Dr. Maher Azzouz, who provided supervision and guidance during the research, writing process, and manuscript editing.

Chapter 5 and 6 incorporates unpublished material co-authored with Dr. Maher Azzouz and Dr. Mostafa Shaaban. Dr. Azzouz provided guidance and feedback on refining ideas and editing the manuscript; Dr. Shaaban contributed feedback on improving ideas. The key ideas, primary contributions, data analysis, interpretation, and writing were performed by the author.

I am aware of the University of Windsor Senate Policy on Authorship, and I certify that I have properly acknowledged the contribution of other researchers to my thesis and have obtained written permission from each of the co-author(s) to include the above material(s) in my thesis.

I certify that, with the above qualification, this thesis, and the research to which it refers, is the product of my own work.

II. Previous Publication

This thesis includes three original papers that have been previously published/submitted to journals for publication, as follows:

Thesis Chapter	Publication title/full citation	Publication Status
Chapter 3	T. E. Sati and M. A. Azzouz, “An Adaptive Virtual Impedance Fault Current Limiter for Optimal Protection Coordination of Islanded Microgrids,” <i>IET Renew. Power Gener.</i> , vol. 16, iss. 8, pp. 1719–1732, Jun. 2022.	Published
	T. E. Sati, M. A. Azzouz, and Mostafa Shaaban, “Optimal Protection Coordination of Islanded Microgrids Utilizing an Adaptive Virtual Impedance Fault Current Limiter,” <i>in Proc. IEEE Texas Power and Energy Conference, (TPEC)</i> , pp. 1–6, Feb. 2022, invited to be submitted to <i>IEEE Trans. Ind. Appl.</i>	Published
Chapter 4	T. E. Sati and M. A. Azzouz, “Optimal Protection Coordination for Inverter Dominated Islanded Microgrids Considering N-1 Contingency,” <i>IEEE Trans. Power Deliv.</i> , vol. 37, no. 3, pp. 2256–2267, Jun. 2022.	Published
Chapter 5	T. E. Sati, M. A. Azzouz, and Mostafa Shaaban, “Adaptive Harmonic-based Dual-setting Directional Overcurrent Protection for Islanded Microgrids,” <i>IEEE Trans. Smart Grid.</i>	Requested revisions
Chapter 6	T. E. Sati, M. A. Azzouz, and Mostafa Shaaban, “Adaptive Harmonic-based Optimal Protection Coordination for Inverter-dominated Islanded Microgrids Considering N-1 Contingency,” <i>IEEE Trans. Power Deliv.</i>	To be submitted

I certify that I have obtained a written permission from the copyright owner(s) to include the above published material(s) in my thesis. I certify that the above material describes work completed during my registration as a graduate student at the University of Windsor

III. General

I declare that, to the best of my knowledge, my thesis does not infringe upon anyone's copyright nor violate any proprietary rights and that any ideas, techniques, quotations, or any other material from the work of other people included in my thesis, published or otherwise, are fully acknowledged in accordance with the standard referencing practices. Furthermore, to the extent that I have included copyrighted material that surpasses the bounds of fair dealing within the meaning of the Canada Copyright Act, I certify that I have obtained a written permission from the copyright owner(s) to include such material(s) in my thesis.

I declare that this is a true copy of my thesis, including any final revisions, as approved by my thesis committee and the Graduate Studies office, and that this thesis has not been submitted for a higher degree to any other University or Institution.

Abstract

Integration of distributed generators (DGs) into distribution networks results in active distribution networks (ADNs) characterized by bidirectional power flow and can evolve into microgrids. Microgrids could host synchronous-based DGs (SBDGs) or inverter-interfaced DGs (IIDGs). These networks have many advantages, including power loss reduction, deferring network upgrades, and backup for the main grid. Despite these advantages, IIDGs have limited fault current contributions, adversely impacting the protection coordination.

This dissertation investigates the overcurrent protection challenges faced by inverter-based islanded microgrids (IBIM). The aim is to devise reliable overcurrent protection schemes for IBIM in the fundamental and harmonic domains taking advantage of the flexibility of the IIDG controllers. Optimal protection coordination (OPC) is achieved by developing a new short-circuit current calculation (SCC) algorithm for IIDGs in the fundamental domain and using a harmonic short-circuit current calculation (HSCC) algorithm.

An effective method is proposed by modifying the IIDG controller to include a virtual impedance-fault current limiter (VI-FCL) in the positive-sequence frame. The new SCC algorithm incorporates VI-FCLs to enable modeling droop-based IIDGs as a voltage source behind an impedance and protect inverter switches from overcurrent. The VI-FCL is implemented as an additional control loop in the inverter control scheme to limit IIDG fault currents and achieve OPC. Further, the VI-FCL is adaptively adjusted to enhance overcurrent protection sensitivity. A two-stage OPC algorithm for directional overcurrent relays (DOCRs) is developed. An optimal value for the adaptive VI-FCLs and relay currents is calculated in Stage I. Stage II aims at obtaining optimal DOCRs settings by solving the OPC problem as a constrained nonlinear programming problem. Time-domain simulations are used to demonstrate the effectiveness of the proposed adaptive VI-FCL and the accuracy of the proposed SCC algorithm.

OPC is usually solved for the original network topology with all lines, loads, and generation intact. However, power grids may experience contingencies due to transient events, e.g., generation or line outages. Low fault currents of IIDGs necessitate a sensitive and reliable protection scheme. The protection scheme utilizes adaptive VI-FCLs to limit IIDGs fault currents and achieve protection coordination. The two-stage OPC algorithm is modified to include the islanded topology and each possible topology following an N-1 contingency.

Limited fault currents in IBIM impose immense challenges on conventional overcurrent protection schemes. Therefore, a sensitive and selective protection scheme is proposed for islanded microgrids using a third harmonic voltage generated by IIDGs. The generated harmonic voltage results in a harmonic layer formed during short-circuit faults and is decoupled from the fundamental fault current, i.e., limited by IIDGs. Further, the generated harmonic voltage is adaptively adjusted based on fault severity. The proposed protection scheme utilizes harmonic directional overcurrent relays (HDOCRs) equipped with a dual time-current-voltage setting that senses the generated harmonic voltages and currents at the relay location to ensure an OPC of islanded microgrids. The OPC with the proposed dual setting is formulated as a constrained nonlinear program to determine the optimal forward and reverse relays' settings. The results ensure the ability of the proposed scheme to protect islanded microgrids without communication and its capability to reduce relays' operation times.

Lastly, the adaptive harmonic generation is utilized to develop a new harmonic-based overcurrent protection scheme for IBIM considering N-1 contingency. The proposed scheme employs HDOCRs with only forward trip characteristics. The OPC problem is formulated as a constrained nonlinear program to obtain the HDOCRs' setting. A two-stage OPC algorithm is developed to include the main topology and each possible single IIDG and line outage. The results confirm that a single set of relay settings can achieve OPC up to the maximum resistive fault on the main network topology while satisfying the N-1 criterion.

Dedication

*To my mother and father souls',
beloved wife, dear kids.*

Acknowledgments

“My success can only come from Allah; in him I trust, and unto him, I look.”

I owe my deepest gratitude to my advisor Dr. Maher Azzouz, who guided me through my five years of Ph.D. studies. His valuable advice and continual encouragement has always motivated me. With his valuable input, I was able to look at my research from a different perspective. My appreciation is extended to my committee members for their time and beneficial insights. Thanks extend to my external examiner Dr. H. Farag.

My most profound appreciation to my wife, Rida, to whom I owe gratitude for the endless support and patience during the five years of my Ph.D. studies, and to my siblings for their continuous prayers and support.

Table of Contents

Declaration of Co-authorship/Previous Publication	iii
Abstract	vi
Dedication	viii
Acknowledgments	ix
List of Figures	xiii
List of Tables	xv
List of Abbreviations	xvii
1 Introduction	1
1.1 Preface	1
1.2 Research Motivation	2
1.3 Research Objectives	4
1.4 Dissertation Outline	4
2 Background and Literature Review	6
2.1 Islanded Microgrid Operation	6
2.2 Droop Control Implementation	8
2.3 Steady State Analysis of Islanded Microgrids	13
2.4 Literature Review	13
2.4.1 Fundamental Domain Protection	15
2.4.2 Harmonic Domain Protection	17
2.5 Discussion	19
3 Adaptive VI-FCL for Protection Coordination of IBIM	20
3.1 Proposed SCC Considering VI-FCLs	20
3.1.1 Modified IIDG Control	20
3.1.2 VI-FCL Design	21
3.1.3 Current Control	26
3.1.4 System Modeling	28
3.1.5 Levenberg-Marquardt Algorithm	30
3.2 Proposed Optimal Protection Coordination	31
3.2.1 OPC Problem Formulation	31
3.2.2 SCC Algorithm for IIDGs	33

3.2.3	Solving Method	35
3.3	Performance Evaluation	36
3.3.1	Test Microgrid	36
3.3.2	SCC Algorithm Validation and Results	37
3.3.3	Unbalanced faults	44
3.4	Enhanced Adaptive VI-FCL Design	47
3.4.1	Proposed adaptive VI-FCL Characteristics Results	49
3.5	Conclusion	52
4	Protection Coordination of IBIM Considering N-1 Contingency	54
4.1	Adaptive Piecewise VI-FCL Design	54
4.2	Proposed Optimal Protection Coordination	56
4.2.1	OPC Problem Formulation	56
4.2.2	OPC Program for IIDGs with VI-FCLs	58
4.3	Microgrid Adequacy and Models Under Contingencies	61
4.3.1	Microgrid Adequacy	61
4.3.2	Models Considering Contingencies	62
4.4	Results and Analysis	64
4.5	Conclusion	74
5	Harmonic-based Dual-setting Protection for IBIM	75
5.1	Proposed Harmonic-based Protection	75
5.1.1	IIDG controller and harmonic generation characteristic	75
5.1.2	Trip characteristics of HDOCRs	81
5.1.3	The harmonic directional element	82
5.2	Harmonic Short Circuit Calculations	83
5.3	Proposed Protection Coordination	85
5.3.1	OPC problem formulation	85
5.3.2	OPC program	87
5.4	Performance Evaluation	89
5.4.1	Test system	89
5.4.2	The harmonic layer measurements	89
5.4.3	OPC using constant and adaptive harmonic voltage generation	93
5.5	Conclusion	98
6	Harmonic-based Protection of IBIM Considering N-1 Contingency	100
6.1	Proposed Harmonic-based Protection	100
6.1.1	OPC problem formulation	100
6.1.2	OPC program	102
6.2	Performance Evaluation	104
6.3	Conclusion	111

7	Conclusions	112
7.1	Summary	112
7.2	Contributions	113
7.3	Future Work	115
	Bibliography	116
	Appendix A	127
	Vita Auctoris	128

List of Figures

2.1	IIDG droop characteristics.	9
2.2	Generic control of droop-based IIDG operating in an islanded microgrid.	10
2.3	Droop-based IIDG: (a) Droop control. (b) Outer loops for voltage control. (c) Inner loops for current control.	12
3.1	Droop-controlled IIDG with VI-FCL: (a) The IIDG control scheme with VI-FCL. (b) IIDG circuit model with VI-FCL.	21
3.2	Adaptive VI-FCL.	23
3.3	Simple test microgrid.	24
3.4	Responses during F_1 and after restoration: (a) Fault current of IIDG1. (b) The simple test microgrid frequency.	26
3.5	Fault currents measured by relay R1: (a) Hard limiter. (b) VI-FCL.	27
3.6	PV source V-I characteristic.	28
3.7	Flow chart of the proposed OPC program.	35
3.8	Single line diagram of the test microgrid.	37
3.9	Comparison of relays' currents during F_{15}	40
3.10	Comparison of total relays' operation times for the test microgrid (Case study I) N, M, and F are the near-end, midline, and far-end faults, respectively.	44
3.11	Modified sequence networks for SLG faults.	45
3.12	Impedance characteristics of the adaptive VI-FCL.	48
4.1	Impedance characteristic of the adaptive VI-FCL.	55
4.2	A 4-bus microgrid with two IIDGs and one SBDG.	59
4.3	Flow chart of the proposed OPC program.	60
4.4	Network topologies of a sample microgrid: (a) Islanded topology. (b) IIDG2 outage topology. (c) Line 4-5 outage topology.	62

5.1	The IIDG control block diagram with the proposed adaptive harmonic generation.	76
5.2	A sample microgrid.	78
5.3	Microgrid equivalent model in the harmonic layer.	78
5.4	Proposed adaptive harmonic voltage characteristics.	79
5.5	Flow chart of the proposed OPC program.	88
5.6	Single line diagram of the test microgrid.	90
5.7	IIDG1 currents during F_{10} : (a) output current. (b) harmonic current.	90
5.8	The harmonic current measured by R_4 during F_{10}	91
5.9	The harmonic current measured by R_1 during F_1	91
5.10	The harmonic torque angles measured by R_2 and R_3 during F_1	92
5.11	The magnitude of the harmonic currents measured by relay R_1 due to (a) SLG (b) LL (c) DLG during F_1	92
6.1	Flow chart of the proposed OPC program.	103

List of Tables

3.1	Validation Results with the Constant VI-FCLs	38
3.2	Validation Results with the Adaptive VI-FCLs	39
3.3	VI-FCLs Magnitudes in Per Unit (Case I)	40
3.4	Relays Optimal Settings for the Test Microgrid (Case I)	41
3.5	Operation Times in Seconds for Bolted Faults (Case I)	42
3.6	Relays Optimal Settings for the Test Microgrid (Case II)	43
3.7	Operation Times in Seconds for Selected Bolted Faults (Case II)	43
3.8	Operation Times for Selected Far-end Faults in Seconds	46
3.9	Relays Optimal Settings Considering SLG Faults	47
3.10	Relays Optimal Settings with Different VI-FCL Characteristics	50
3.11	Relays Total Operation Times at Different Fault Resistances with Different VI-FCL Characteristics	51
3.12	Operation Times in Seconds for Near-end and Far-end Bolted Faults	51
3.13	Operation Times in Seconds for Near-end and Far-end Faults Consid- ering 5 Ω Fault Resistance	52
4.1	OPC Models Description	63
4.2	Relays Optimal Settings for the Test Microgrid (Case I)	65
4.3	Sum of Operation Times for Bolted Faults in the Test Microgrid (Case I)	65
4.4	Coordination Violations for Bolted Faults in the Test Microgrid (Case I)	67
4.5	Operation Times for Selected Near-end and Far-end Bolted Faults in the Test Microgrid (Case I)	68
4.6	Operation Times for a Three-phase Fault at F ₄ with Selected Fault Resistances (Case I)	69
4.7	ITC vs TCV characteristic (Case I)	70
4.8	Relays Optimal Settings for the Test Microgrid (Case I)	70

4.9	Operation Times for Selected Near-end and Far-end Bolted Faults in the Test Microgrid (Case I)	71
4.10	Relays Optimal Settings for the Test Microgrid (Case II)	72
4.11	Operation Times for Selected Near-end Bolted Faults for the Test Microgrid (Case II)	73
5.1	Relays Total Operation Times in Seconds for Near-end Faults Considering Forward Characteristic	94
5.2	Relays Optimal Settings Considering Forward Characteristic	94
5.3	Relays Total Operation Times in Seconds for Near-end Faults with TCV Dual Setting and Various Characteristic	95
5.4	Relays Optimal Dual Setting with Piecewise Characteristic	95
5.5	Operation Times in Seconds for Bolted Faults Utilizing the Proposed Scheme with TCV Dual Setting	97
5.6	Operation Times in Seconds for 15 Ω Resistance Faults Utilizing the Proposed Scheme with TCV Dual Setting	98
6.1	Relays Optimal Settings for the Test Microgrid (Case I)	104
6.2	Coordination Violations for Considered Fault Resistances in the Test Microgrid	105
6.3	Operation Times for Selected Near-end and Far-end Bolted Faults with Fixed I_p (Case I)	106
6.4	Relays Optimal Settings for the Test Microgrid (Case II)	107
6.5	Operation Times for Selected Near-end and Far-end Bolted Faults with Variable I_p (Case II)	108
6.6	Reduction in Individual Relays' Operation Times for Selected Near-end Bolted Faults (Case II)	109
6.7	Operation Times for Selected Near-end and Far-end 15 Ω resistance Faults with Variable I_p (Case II)	110
6.8	Relays Total Operation Times Considering Near-end Faults	110
6.9	Protection Schemes Sensitivity	111

List of Abbreviations

ADN	Active Distribution Network
CT	Current Transformer
CTI	Coordination Time Interval
CTR	Current Transformer Ratio
DG	Distributed Generator
DLG	Double Line to Ground
DOA	Domain of Attraction
DOCR	Directional Overcurrent Relay
DVR	Dynamic Voltage Restorer
FCL	Fault Current Limiter
FFT	Fast Fourier Transform
FRT	Fault Ride Through
GA	Genetic Algorithm
HDOCR	Harmonic Directional Overcurrent Relay
HSCC	Harmonic Short-circuit Current Calculation
HTCV	Harmonic Time Current Voltage
IBIM	Inverter-Based Islanded Microgrids
IBFS	Improved Backword-Forward Sweep
IIDG	Inverter-Interfaced Distributed Generator
IMFO	Improved Moth-Flame Optimization

ITC	Inverse Time Current
LL	Line to Line
LP	Linear Programming
LPF	Low Pass Filter
MINLP	Mixed Integer Non Linear Programming
MNM	Modified Nodal Method
NERC	North-American Electric Reliability Corporation
NLP	Non Linear Programming
OPC	Optimal Protection Coordination
PCC	Point of Common Coupling
PLL	Phase Locked Loop
PV	Photovoltaic
SBDG	Synchronous-Based Distributed Generator
SCC	Short-circuit Current Calculation
SG	Synchronous Generator
SLG	Single Line to Ground
TCV	Time Current Voltage
TDS	Time Dial Setting
VI-FCL	Virtual Impedance-Fault Current Limiter

Chapter 1

Introduction

1.1 Preface

The continuous advancements in renewable energy technologies, rapid advances in power electronics, and incentives put forward by governments pave the way to rethink distribution systems by integrating small-scale distributed generators (DGs). This integration results in active distribution networks (ADNs) characterized by bidirectional power flow and could be self-sustained by forming microgrids [1]. Microgrids have two modes of operation, namely, grid-connected and islanded modes. In grid-connected mode, the DG operates in current control, supplying the grid with active and reactive powers, where the main grid regulates the system voltage and frequency. In islanded mode, the network is powered by a cluster of DGs that share system loading and maintain the voltage and frequency of the microgrid within their allowable limits. The Droop-based control represents a feasible method to control and operate an islanded microgrid, which does not rely on communication links [2].

Microgrids could host synchronous-based DGs (SBDGs) or inverter-interfaced DGs (IIDGs). Inverters facilitate the integration of renewable energy sources to microgrids. IIDGs have limited fault current contributions, which may adversely impact the protection coordination or render the coordination of protective devices infeasible [1]. Despite the low fault current contributions of IIDGs, relying on hard limiters may result in reference current saturation from the IIDG controller perspective. Consequently, outer control loops may suffer from poor dynamic performance [3]. Further, the IIDG model may switch between a constant current source and a droop-based voltage source, complicating the short-circuit current calculation (SCC).

Islanded microgrids could be at risk if not adequately protected against short-circuit faults. The unavailability of an off-the-shelf protective relay to suit microgrid

protection leaves us with the existing protective relays, e.g., directional overcurrent relays (DOCRs), distance relays, and differential relays, as potential candidates. Distance and differential relays are uneconomical options for microgrids. DOCRs represent simple and economical relays for overcurrent protection of grids with bidirectional fault currents, such as ADNs and microgrids [4]–[6]. The DOCRs need to be time coordinated to isolate faults reliably and ensure minimum load interruption.

1.2 Research Motivation

The limited fault currents of the IIDGs have a negative impact on conventional overcurrent protection schemes, which depend on fault current magnitude. Several studies have presented solutions to the limited IIDGs fault currents [7], [8]. Nevertheless, the offered solutions require communication infrastructure that may not be available in distribution systems.

The protection challenges of inverter-dominated islanded microgrids include:

- Conventional distribution systems have unidirectional power flow from the substation to loads. Therefore, their overcurrent protection employs only overcurrent relays. In contrast, ADNs have bidirectional power flow due to the presence of DGs within the distribution network. During short-circuits, the bidirectional fault currents necessitate the use of DOCRs.
- IIDGs typically use droop characteristics to share loads in islanded microgrids. The IIDGs can be operated as a droop-controlled voltage source. However, built-in current hard limiters may suffer from reference current saturation due to high short-circuit faults. As a result, the IIDG model may switch between a voltage source and a current source complicating the SCC and deteriorating microgrid transient stability during short-circuit faults. A virtual impedance-fault current limiter (VI-FCL) is employed to limit the inverter’s fault current and avoid the reference current saturation, which enhances microgrid transient stability [3]. Further, the VI-FCL keeps the voltage source model intact, which

reduces the complexity of SCC. The VI-FCL is adaptively adjusted and included in the formulation of a new SCC algorithm.

- Power systems experience network topology changes due to transient contingencies such as generation or line outages. For instance, an IIDG being out of service results in lower short-circuit current levels in the microgrid. On the other hand, the microgrid topology splits into two separate sub-microgrids with the removal of a line. As a result, lower short-circuit current levels exist in the sub-microgrids. Ignoring contingencies resulting from IIDGs and line outages leads to protection coordination violations. Therefore, an optimal protection coordination (OPC) formulation is proposed in which a model simultaneously considers all topologies resulting from all single IIDG and line outages as well as the main topology. The OPC problem is solved considering N-1 contingency, including a single line and an IIDG outage during the islanding mode. Including contingencies guarantees the proper operation of the assigned primary and backup DOCRs under planned or transient outages. Therefore, a single set of relays' settings is obtained utilizing a comprehensive model, which works for all possible topologies.
- In the fundamental domain, relays pickup currents must be selected to have a safe margin of 25%–50% above the rated load current of the protected element. This constraint ensures that DOCRs only trip when a fault occurs. Fulfilling this condition, relay pickup current may be set at close and tight margins to the fault currents. As a consequence, relays have high operation times. In contrast, employing a harmonic-based generation system that is independent of load currents implemented within the IIDG controller results in higher multiples of pickup current and hence lower relay operation time.

1.3 Research Objectives

The main goal of this research was to devise protection schemes that overcome the limited IIDG fault currents hindrance. The aim is to obtain an OPC while protecting inverter switches from overcurrent.

The following objectives have driven this dissertation:

- Development of control algorithms for inverters to enable the reliable operation of the inverter-dominated islanded microgrids.
- Development of overcurrent protection scheme based on fundamental layer measurements.
- Development of overcurrent protection scheme based on harmonic layer measurements.
- Development of reliable overcurrent protection schemes that consider N-1 contingencies.

1.4 Dissertation Outline

This dissertation is divided into two main parts: chapters 3 and 4 focus on fundamental current-based overcurrent protection schemes for islanded microgrids. Chapters 5 and 6 concentrate on harmonic-based overcurrent protection schemes for islanded microgrids.

The remainder of this dissertation is organized as follows:

Chapter 2 provides a background and literature survey relevant to SCC and control algorithms of ADNs.

Chapter 3 presents the newly developed SCC algorithm for IIDGs, which serves as a tool to calculate short-circuit currents measured by protective relays to achieve OPC.

Chapter 4 introduces power system contingencies and the N-1 criteria. All possible single IIDG and single line outages are considered in solving the OPC problem

to obtain a universal set of relays' settings.

Chapter 5 investigates the use of harmonic voltage generation utilizing the IIDG controller. The independence of fault and load currents results in a sensitive harmonic-based dual-setting overcurrent protection scheme. The OPC solution results in a single relays' settings that maintain protection coordination up to the maximum resistive faults.

Chapter 6 proposes a harmonic-based overcurrent protection scheme employing harmonic voltage generation considering N-1 contingency. The proposed scheme can preserve protection coordination under different contingencies using a universal set of relays' settings.

Chapter 7 concludes the dissertation, highlights its contributions, and suggests topics for future work.

Chapter 2

Background and Literature Review

2.1 Islanded Microgrid Operation

In the grid-connected mode of operation, IIDGs supply a pre-specified amount of active and reactive powers to fulfill system requirements (e.g., exporting power to the main grid). The discrepancy between the active and reactive power generated by the IIDGs and the microgrid total demand is either supplied or absorbed by the main grid. Consequently, the IIDGs can be controlled as PQ or PV buses [9]. In this operation mode, the IIDGs voltage reference is often taken from the grid voltage sensed by a phase-locked-loop (PLL); an inner current control loop ensures the IIDG act as a current source. In contrast, in the islanded mode of operation, the IIDG units within the microgrid cannot be controlled as PV or PQ buses due to:

- (i) Operating the generation units in a conventional power system as a PV or a PQ bus relies on a slack bus capable of stabilizing and maintaining the system frequency at a constant value by supplying the difference between the load and the pre-scheduled generation. Nevertheless, in islanded microgrids, no IIDG unit can act as a slack bus since all IIDGs are relatively small and have comparable ratings.
- (ii) IIDGs do not have a reference signal to control their generation, requiring a separate control measure to control the islanded microgrid voltage and frequency. Connecting the IIDGs without such a control measure, depending only on the control of the IIDGs' output voltage to pre-defined values, result in large circulating currents flow between these IIDGs due to system components' tolerances [10].
- (iii) In conventional grids with IIDGs operating as PV or PQ, the slack bus com-

pensates for any increase in the system loading until the settings of the PV or PQ buses are increased by the dispatch center. Therefore, in the absence of the slack bus in the islanded mode, the total power generated by the IIDGs must match the total islanded microgrid demand.

Most IIDGs are coupled with a passive output filter [11], [12]. Different techniques have been proposed in the literature to accommodate IIDGs with the previously mentioned challenges and or requirements. These techniques are broadly categorized into two approaches centralized and decentralized control approaches.

The centralized control approach depends on a central controller that controls the operation of all IIDGs in the islanded microgrid. This approach enfoldes two main control strategies: single master operation and multi-master operation. In single master operation mode, one master IIDG serves as a slack bus (voltage reference). At the same time, the other enslaved IIDGs operate in active/reactive power dispatch mode by regulating their output current. Several IIDGs are set as masters in multi-master operation mode to regulate the microgrid voltage and frequency. The slave IIDGs operate in PQ control mode [13]. In this case, the PQ control is implemented by measuring the load powers and sending them to the supervisory control level, which calculates and sends the reference PQ to each IIDG. The IIDG built-in current controller regulates the measured output current to track the reference current [12], [14]. Given its single point of failure, the centralized control lacks the required operation redundancy and depends on communication which adds extra cost and decreases reliability.

The decentralized control approach is widely accepted in the industry and literature to overcome the drawbacks of centralized control [15], [16]. This approach depends on the local controllers of the IIDGs and uses the system frequency as means of communication between these controllers. Further, the approach utilizes the droop control strategy to mimic the behavior of conventional synchronous generators (SGs). In droop control, the IIDG's local controller emulates the characteristics of an SG by decreasing proportional amounts of the output active and reactive powers from the system frequency and IIDG's output voltage magnitude, respectively (i.e., imple-

menting specific droop characteristics). Hence, it guarantees that the IIDGs in the islanded microgrid always stabilize at the required load sharing.

2.2 Droop Control Implementation

In decentralized (interactive) islanded microgrid operation, the DGs mimic the behavior of SGs by implementing droop characteristics [16]. Figure 2.1 displays the static droop characteristics implemented by the IIDG controller to emulate SG characteristics. Assuming an inductive impedance between the grid and the point of common coupling (PCC), the power exchange between an IIDG and the grid is given by

$$P_G = \frac{V_o V_{grd}}{X_{eq}} \sin(\delta) \quad (2.1)$$

$$Q_G = \frac{V_o V_{grd} \cos(\delta) - V_{grd}^2}{X_{eq}} \quad (2.2)$$

where X_{eq} is the network equivalent reactance, and δ is the phase angle between the DG output voltage V_o and the grid voltage V_{grd} . The above equations reveal that the generated active power, P_G , relies on δ , and the generated reactive power, Q_G , depends on the magnitude of the output voltage V_o . The instantaneous active power, p , and the instantaneous reactive power, q , in the synchronous d - q frame are given by

$$p = \frac{3}{2}(V_{od}I_{od} + V_{oq}I_{oq}) \quad (2.3)$$

$$q = \frac{3}{2}(V_{oq}I_{od} - V_{od}I_{oq}) \quad (2.4)$$

Then, the average powers P_G and Q_G can be calculated by filtering the instantaneous powers using a low-pass filter (LPF) having a cut-off frequency, ω_c , to enhance power quality injection:

$$P_G = \frac{\omega_c}{s + \omega_c} p \quad (2.5)$$

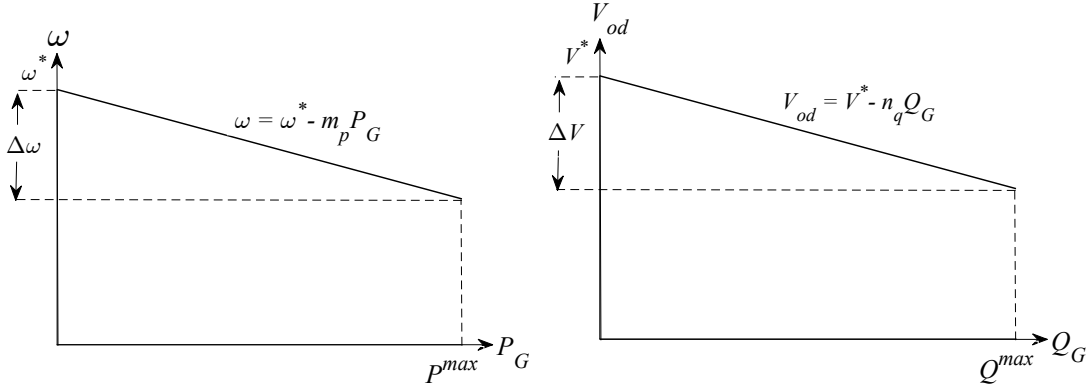


Figure 2.1: IIDG droop characteristics.

$$Q_G = \frac{\omega_c}{s + \omega_c} q \quad (2.6)$$

The droop characteristics determine the reference voltage and frequency of the outer control loops:

$$\omega = \omega^* - m_p P_G \quad (2.7)$$

$$V_{od}^{ref} = V^* - n_q Q_G \quad (2.8)$$

where V_{od}^{ref} and ω are the magnitudes of the d -axis reference voltage from the power controller and DG frequency, respectively, V^* and ω^* are the magnitudes of the reactive power droop control voltage at no load and nominal system frequency, respectively, m_p and n_q are the frequency and voltage droop coefficients, respectively. For low voltage microgrids that typically have a high R/X ratio, the droop characteristics exchange their role and are given by [17]

$$\omega = \omega^* + m_p Q_G \quad (2.9)$$

$$V_{od}^{ref} = V^* - n_q P_G \quad (2.10)$$

m_p and n_q are calculated based on the allowable frequency and voltage regulation

$$m_p = \frac{\omega^{max} - \omega^{min}}{P_{max}} \quad (2.11)$$

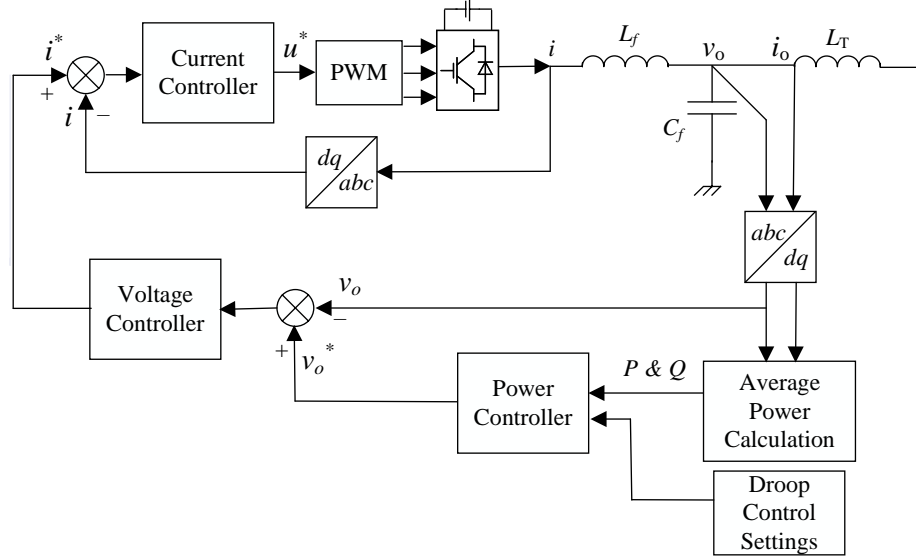


Figure 2.2: Generic control of droop-based IIDG operating in an islanded microgrid.

$$n_q = \frac{|V_{od}|^{max} - |V_{od}|^{min}}{Q^{max}} \quad (2.12)$$

where ω^{min} and ω^{max} are the minimum and maximum permissible frequencies, respectively. $|V_{od}|^{min}$ and $|V_{od}|^{max}$ are the minimum and maximum allowable voltage magnitudes, respectively. P^{max} and Q^{max} are the maximum active and reactive power of the DG, respectively. As noted by (2.10), the output voltage is aligned with the d -axis; in other words, $V_{oq}^{ref} = 0$, so as V_{od} has full controllability of the reactive power Q_G .

The control strategy of the IIDGs typically includes two cascaded loops; outer and inner. The internal loop is a current control loop that regulates the DG's inverter current. The outer control loop can have different control objectives depending on the microgrid mode of operation, i.e., grid-connected or islanded. Figure 2.2 illustrates the block diagram of the power circuit and the control circuit of a droop-based IIDG operating in islanded mode [12], [16]. The power circuit comprises the LC filter to remove the switching harmonics and the interfacing inverter. The controller has a cascaded structure with an outermost power-sharing control loop that achieves the required power-sharing by generating the reference magnitude and frequency of the

output voltage across the LC filter following the droop characteristics given by (2.7) and (2.8). The innermost control loop is a current controller, which provides control over the filter inductor current by generating the inverter reference voltage u^* , i.e., gating signals. The middle loop is the voltage controller that regulates the voltage across the filter capacitor by generating a reference signal for the current controller.

An IIDG inverter's model in the d - q reference frame represents the dynamics of the interfacing filter, which is given by

$$L_f \frac{dI_d}{dt} = -R_f I_d + V_d - V_{od} + \omega L_f I_q \quad (2.13)$$

$$L_f \frac{dI_q}{dt} = -R_f I_q + V_q - V_{oq} - \omega L_f I_d \quad (2.14)$$

$$C_f \frac{dV_{od}}{dt} = I_d - I_{od} + \omega C_f V_{oq} \quad (2.15)$$

$$C_f \frac{dV_{oq}}{dt} = I_q - I_{oq} - \omega C_f V_{od} \quad (2.16)$$

where R_f , L_f , and C_f are the IIDG interfacing filter resistance, inductance, and capacitance, respectively, and ω is the microgrid frequency. V_{dq} and V_{odq} pertain to the d - q components of the inverter terminal voltage and the IIDG voltage at the PCC, respectively. I_{dq} and I_{odq} denote the d - q components of the inverter output current and the IIDG current at the PCC, respectively. New terms are defined to provide a decoupled control for V_{od} and V_{oq} :

$$I'_d = I_d - I_{od} + \omega C_f V_{oq} \quad (2.17)$$

$$I'_q = I_q - I_{oq} - \omega C_f V_{od} \quad (2.18)$$

Substituting (2.17) and (2.18) in (2.15) and (2.16) respectively yields

$$C_f \frac{dV_{od}}{dt} = I'_d \quad (2.19)$$

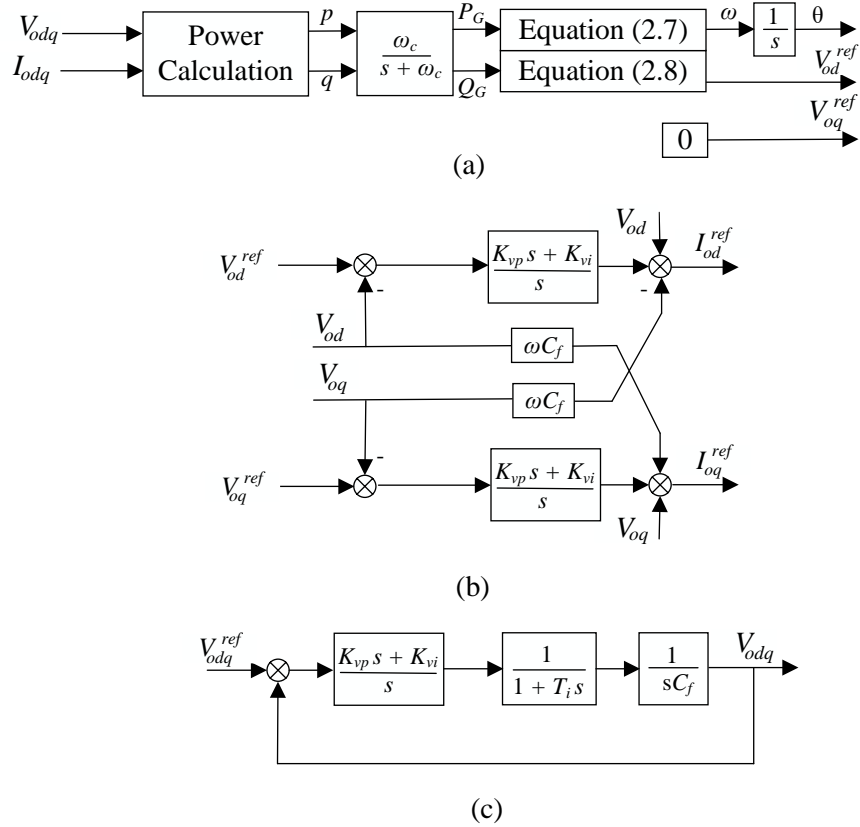


Figure 2.3: Droop-based IIDG: (a) Droop control. (b) Outer loops for voltage control. (c) Inner loops for current control.

$$C_f \frac{dV_{oq}}{dt} = I'_q \quad (2.20)$$

Equations (2.19) and (2.20) represent a decoupled model for V_o . Figure 2.3(a) shows the utilization of droop characteristics to generate the reference voltage and frequency, which dynamically controls the angle. Figure 2.3(b) shows the voltage controller outer loops. Figure 2.3(c) displays the current and voltage controllers ignoring the decoupling terms. The voltage control loop must be designed to be three to five times slower than the inner current loop to maintain the stability and reference current tracking [18]. On the other hand, the inner current controller is typically designed to have a time constant, T_i , in the range of 3–5 ms [19].

2.3 Steady State Analysis of Islanded Microgrids

The successful implementation of the microgrid concept requires the conduction of planning and operational studies by power distribution utilities. These studies include but are not limited to:

1. Planning studies.
2. Contingency analysis.
3. Optimal allocation of DG units.
4. Restoration and reconfiguration.
5. Protection coordination studies.

2.4 Literature Review

The majority of the OPC studies which consider islanded microgrids use time-domain simulation software (SIMULINK or PSCAD/EMTP) to obtain steady-state values for the short-circuit currents measured by the protective relays [20], [21]. The simulation software solves the differential equations set describing the system response at every sampling instant. Therefore, employing this method to solve for the system's steady-state values is time-consuming, computationally expensive, and limited to relatively small test systems. In contrast, an SCC algorithm only solves the nonlinear algebraic equations at the steady-state operating point. Hence, using an SCC algorithm for the islanded microgrid is computationally much less expensive than time-domain simulations, which solve a larger number of differential equations at different points of time until it reaches the steady-state.

Islanded microgrids could be at risk if not adequately protected against short-circuit faults. The typical line protection scheme design involves assigning a primary protective relay backed up by another protective relay for each microgrid line. Protection coordination involves the procedure carried out to determine the operation

sequence of primary and backup relay sets for each fault location to isolate faults reliably.

In the event of a fault, DGs contribute differently to microgrid fault currents depending on the DG type, which can be SBDG or IIDG. IIDGs in islanded microgrids adopting droop characteristics can be operated as a droop-controlled voltage source. The SBDGs have a more profound effect on fault current, unlike IIDGs, which have a limited short-circuit capacity. An SCC method should be first performed to coordinate DOCRs. Conventional fault analysis methods used with SBDGs are inadequate to analyze microgrids with IIDGs because they do not consider inverter controllers. This requires a model to capture the IIDG behavior during faults and be used in fault analysis to obtain short-circuit currents seen by DOCRs [22], [23].

In [22], the authors utilize an SCC method for IIDGs based on the superposition theorem and an improved backward-forward sweep (IBFS) procedure. [24] proposes an iterative SCC method, where the fault current of a photovoltaic (PV) source is updated based on its terminal voltage. In [25], an SCC algorithm is developed for IIDGs that utilize sparsity methods. The authors of [26] develop an SCC algorithm for droop-based IIDGs. However, the algorithm does not consider current reference saturation.

In [27], an analytical fault analysis model is developed for grid-connected IIDGs, implementing a decoupled sequence control. The model is used to investigate the characteristics of the IIDG fault currents. The study in [28] proposes an analytical model to reflect the transient behavior of IIDG fault currents, considering the IIDG controller saturation. The PCC voltage is utilized to define a domain of attraction (DOA) that precisely estimates the PI controller's working status. [29] models grid-connected IIDGs as voltage-controlled current sources and considers fault ride-through (FRT). The model switches from a voltage-controlled current source to a voltage-controlled voltage source for limited modulation signals.

This dissertation focuses on inverter-based islanded microgrid (IBIM) protection, which is challenging due to the low fault current levels. On the other hand, the protection of grid-connected microgrids is not challenging and is well covered in the

literature.

2.4.1 Fundamental Domain Protection

The built-in current controller limits the IIDG fault currents to 150% of its rated current [30]. Although the IIDGs have limited contribution to fault currents, built-in current hard limiters may suffer from reference current saturation. The hard limiter is a saturation block that limits the IIDG output current following a grid disturbance. It limits the IIDG's fault current to a maximum value by controlling the reference values of the IIDG active and reactive current components in the d - q reference frame. As a result, the IIDG fault current may saturate at its threshold irrespective of the fault location. As mentioned in the preface, the IIDG model may switch between a droop-based voltage source and a constant current source. This behavior causes instability in the outer control loops [31].

Physical fault current limiters (FCLs) are used to limit fault currents [4], [32]; nevertheless, they have drawbacks, including high cost, bulkiness, and periodic maintenance. An alternative and feasible solution to limit the IIDG fault currents is using VI-FCLs. Controlling the IIDG as a voltage source behind a virtual impedance during faults protects the inverter switches from overcurrent or thermal damage and ensures the stable and reliable operation of islanded microgrids. In addition, VI-FCLs are not costly, allow IIDGs to remain connected during faults, and improve transient stability [33].

In [34], a modification in the IIDG secondary control is proposed to act as an intrinsic FCL. An adaptive protection scheme proposed in [35] utilizes a central controller to identify an optimal setting for DOCRs. A dynamic VI-FCL is presented in [36] to limit downstream fault currents and protect a dynamic voltage restorer (DVR). A virtual impedance is used to limit the inverter current when operating in parallel with SGs in islanded microgrids [31]. [37] introduces a review of control schemes based on virtual impedance for the current source and voltage source converters. VI-FCLs are integrated into the IIDG model to limit IIDG fault currents, protect inverter switches, and ensure islanded microgrids' reliable and stable opera-

tion [38]. However, OPC is not considered in the presence of IIDGs with VI-FCLs. Thus, a new SCC algorithm is required for islanded microgrids powered by IIDGs with VI-FCLs in order to solve the OPC problem.

The OPC problem is tackled using different optimization algorithms. The OPC problem is formulated as a linear programming (LP) problem and is solved using the simplex method [39]. In [40], an improved Moth-flame optimization (IMFO) algorithm is utilized to solve the DOCR coordination problem. Alternatively, in [41], a mixed-integer non-LP (MINLP) formulation is proposed, and the problem is solved by a fuzzy-based genetic algorithm (GA). The authors of [32], [42] consider GA and hybrid GA, respectively, to solve the protection coordination problem as a nonlinear programming (NLP) problem. A new objective function is defined to minimize the operation time of primary, backup DOCRs, and the coordination time; the problem is solved using GA [43].

The authors of [4], [32] explored the use of physical FCLs in series with the ADN to restore protection coordination considering grid-connected and islanded modes of operation. The study in [5] used dual-setting DOCRs capable of operating in forward and backward directions using a low bandwidth communication link. The proposed scheme is used to preserve protection coordination. Despite the low bandwidth used, the communication channel comes with extra cost. The study in [44] employs a hybrid symbiotic organism search algorithm to solve the OPC as an NLP problem. [45] solves the protection coordination problem, considering line outages. However, all of the studies [4], [5], [32], [44] and [45] considered only SBDGs.

Power systems experience network topology changes due to transient contingencies such as generation or line outages. These outages may result from fault isolation, conducting routine maintenance, and network reconfiguration. The North-American Electric Reliability Corporation (NERC) develops and enforces standards throughout North America to ensure power system reliability. Outages of any line (excluding radial lines) or a generator is considered an N-1 contingency, according to the NERC reliability standards [46]. Contingency analysis is a cornerstone in power system planning, which includes protection coordination [6]. Finding one set of relay settings that

accommodates all possible N-1 contingencies is crucial for the reliability of protection schemes.

In [47], the k-means clustering technique is used to design an adaptive protection scheme where the available set groups of overcurrent relays are matched to the possible resulting network topologies. The author of [48] introduces an online adaptive protection scheme that accommodates a power distribution network with different operating conditions. The OPC problem is solved, considering all possible single-line contingencies for a distribution system where an interval LP is implemented [49]. The study in [50] assessed only DG outages when solving the protection coordination problem. The differential evolution meta-heuristic algorithm is used as a solver. [51], [52] consider all network topologies resulting from the line, substation, and DG outage contingencies. The studies use particle swarm and hybrid GA-LP optimization techniques for protection coordination, respectively. However, all of the studies [49]–[52] consider SBDGs, not IIDGs.

2.4.2 Harmonic Domain Protection

Numerous non-communication methods are proposed to tackle inverter-interfaced islanded microgrid protection challenges. Faults in islanded microgrids are detected by monitoring the inverter’s current transient response [53]. In [54], faults are detected and classified based on a data-mining decision tree created using wavelet transform and the extracted features from sequence and phase currents. [55] proposes a digital protection scheme that detects faults based on the extracted and analyzed information of the current components in the d - q reference frame, using a wavelet transform. However, the proposed methods do not consider relay coordination and lack selectivity [53]–[55]. The study in [56] utilizes negative-sequence components to achieve protection coordination based on a definite-time grading method to protect islanded microgrids. Nonetheless, unbalanced loading conditions may challenge the negative-sequence-based protection schemes. An overcurrent protection scheme equipped with dual setting time-current-voltage DOCRs for distribution systems powered by DGs is suggested [57]. Despite the scheme’s capability to handle reverse DG fault cur-

rents, it considers only SBDGs. The authors of [58] propose to increase the IIDGs fault currents by integrating supercapacitors to obtain a single set of relays' settings for grid-connected and islanded modes. However, supercapacitors introduce an extra cost. VI-FCLs are employed in the IIDG control scheme to protect inverter switches from overcurrent and achieve protection coordination [3]. An overcurrent protection scheme for microgrids is proposed in [59], utilizing a non-standard trip characteristic.

Communication-assisted protection schemes have also been proposed to address microgrid protection challenges [60], [61]. In [60], a protection scheme based on mathematical morphology is proposed in which faults are detected utilizing current traveling waves. The traveling-wave-based protection schemes are immune against fault current levels but require high-frequency instrument transformers. An adaptive DOCR is proposed in [61], utilizing the superimposed positive and negative-sequence components. However, the relay's pickup current has to be accurately set to avoid nuisance tripping. Differential-based protection schemes are also suggested using the difference in negative-sequence impedance angle [62], power flow [63], relays' output binary state [64], and measured impedance [65]. The methods in [62]–[65] require communication infrastructure that is often unavailable in microgrids, comes with an extra cost, and may suffer from latency.

The flexibility of the IIDG controllers makes them a venue for recent research to fulfill different protection objectives [66]–[68]. These studies employ the IIDG controller to inject harmonics to assist in islanded microgrids protection. In [66], the IIDG controller injects a fifth-harmonic used for fault detection. A droop impedance is used to limit the fundamental fault current to enable coordination of upstream and downstream relays in an islanded microgrid. However, existing commercial relays may indicate incorrect fault directions [1], [69]. Moreover, [66] does not consider bidirectional fault currents.

The study in [67] proposes a protection scheme for islanded microgrids that utilize harmonic-DOCRs (HDOCRs). The IIDG control scheme is modified to include a function that makes the IIDG injects an n^{th} order harmonic current synthesized by the respective HDOCRs. The HDOCRs measure the injected harmonic currents at

different locations, which are employed to attain protection coordination. However, some backup relays have high operation times with moderate resistance faults. In [68] and following fault inception, the IIDG controller generates a constant third harmonic voltage, resulting in harmonic fault currents. The OPC of the developed HDOCRs is attained based on the locally measured harmonic voltages and currents. However, the constant harmonic voltage generation may result in fault currents being less than relays' pickup current. Furthermore, using a single relay trip characteristic for forward and reverse fault directions may lead to higher relays' operation times.

2.5 Discussion

The literature review presented in this chapter reveals that research has been conducted on IBIM overcurrent protection. However, the literature falls short in addressing several key challenges. First, no SCC algorithm has been developed for IBIM utilizing the fundamental current. Second, ignoring contingencies when solving the OPC impacts the protection scheme's reliability. Third, most methods that obtained relatively low speed for primary protection used communication, which may suffer from latency, data packet loss and add an extra cost to distribution utilities. Further, the methods proposed for OPC of IBIM employing harmonic injection or generation are not sensitive to high resistive faults. Sensitive protection schemes are crucial for the reliable and successful operation of IBIM.

Chapter 3

Adaptive VI-FCL for Protection Coordination of IBIM

Fault currents of IIDGs depend on inverter controllers. Thus, IIDGs fault currents are different than those of SBDGs, both from the magnitude and waveshape perspectives. Although the IIDGs have limited contribution to fault currents, built-in current hard limiters may suffer from reference current saturation. As a result, the droop-based IIDG fault current may saturate at its threshold, and the IIDG model may switch between a droop-based voltage source and a constant current source. This behavior complicates the SCC and causes instability in the outer control loops [31].

This chapter proposes a new SCC algorithm that incorporates VI-FCLs to enable modeling droop-based IIDGs as a voltage source behind an impedance. The VI-FCL is implemented as an additional control loop in the inverter control scheme to limit IIDG fault currents and achieve OPC.

3.1 Proposed SCC Considering VI-FCLs

This section first presents the modified IIDG control structure, followed by the VI-FCL design, an explanation of the current control concept, and system modeling for the proposed SCC algorithm.

3.1.1 Modified IIDG Control

The generic control block diagram for a droop-based IIDG with a VI-FCL is shown in Figure 3.1(a), where a cascaded structure has an innermost current control loop that provides control over its output current i_o . The outer control loop is a power control loop that achieves power-sharing by generating a voltage reference from the power

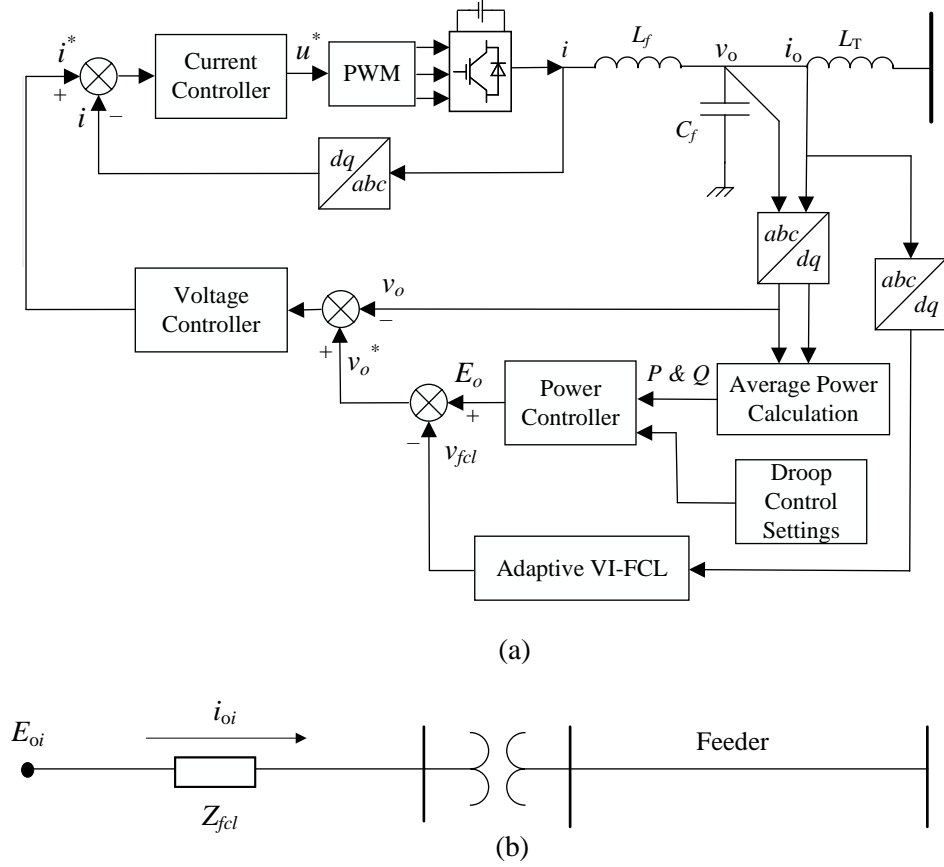


Figure 3.1: Droop-controlled IIDG with VI-FCL: (a) The IIDG control scheme with VI-FCL. (b) IIDG circuit model with VI-FCL.

controller, E_o , that is subtracted from the voltage drop across a VI-FCL, v_{fcl} , to provide voltage reference, v_o^* , for the output voltage v_o . A voltage controller regulates the voltage across the filter capacitor by generating a reference signal for a current controller. The innermost loop is the current controller, which controls the filter inductor current by generating the inverter reference voltage u^* , i.e., gating signals.

3.1.2 VI-FCL Design

Following fault inception, the inverter's output currents may saturate when using hard limiters in the current control loops of IIDGs. Thus, the IIDG model may switch between a constant current source and a droop-based voltage source, which complicates the SCC. The VI-FCLs make IIDGs modeled as a voltage source behind

an impedance similar to SGs. Hence, it maintains the voltage source model of IIDGs intact during faults. Therefore, a control method was devised to implement a VI-FCL as an additional control loop in the inverter control scheme to protect the IIDG switches against overcurrent and reduce the complexity of SCC.

The VI-FCL is implemented in the IIDG control circuit and only activated during faults to act as a high impedance. The VI-FCL can be viewed as a transient impedance that is engaged only during faults. It is added virtually by subtracting the voltage drop across the VI-FCL from the internal inverter voltage, E_{og} . The IIDG equivalent circuit after implementing the VI-FCL is shown in Figure 3.1(b). From which one can deduce

$$v_{o_k}^* = E_{o_k} - i_o Z_{fcl_k} \quad (3.1)$$

where k is the IIDG index. $v_{o_k}^*$ is the voltage reference for v_{o_k} , E_{o_k} , and i_{o_k} are the internal inverter voltage and IIDG output current, respectively, and Z_{fcl_k} includes the filter inductor impedance Z_{f_k} and VI-FCL impedance. The value of Z_{fcl} is determined by limiting the IIDG maximum fault current to 1.5 per unit (pu) for a bolted fault at the IIDG terminals, i.e., $v_{o_k} = 0$. Thus, $|Z_{fcl_k}|$ can be approximated by

$$|Z_{fcl_k}| = \frac{E_{o_k}}{I_{DG}^{max}} \quad (3.2)$$

where I_{DG}^{max} is the maximum IIDG current. The magnitude of Z_{fcl_k} in (3.2) is calculated for the worst-case scenario; hence any other IIDG fault currents can be limited using the same constant value. v_{o_k} drops under fault conditions; once a voltage sag below 0.9 is detected in v_{o_k} ; the VI-FCL is activated.

The constant VI-FCL limits the IIDG fault current irrespective of fault harshness, narrowing the range of fault scenarios considered for protection coordination. In contrast, using an adaptive VI-FCL provides a more gradual fault current profile, accommodating a broader range of fault resistances.

It is worth mentioning that the proposed adaptive VI-FCLs offer the following advantages:

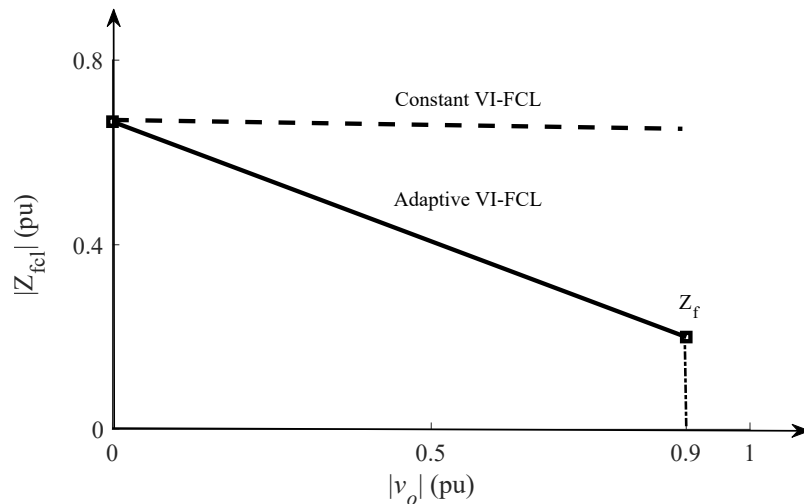


Figure 3.2: Adaptive VI-FCL.

- (i) Hard limiters may result in reference current saturation during faults. Consequently, outer control loops may suffer from a poor dynamic response [3]. On the contrary, VI-FCLs prevent current saturation and contribute to microgrid transient stability, as reported in [33].
- (ii) Unlike constant VI-FCLs—which are typically proposed by other researchers to fulfill different objectives other than OPC—the proposed adaptive VI-FCL allows appreciable fault current levels based on fault severity, thus, enhancing the protection sensitivity.
- (iii) IIDGs with VI-FCLs mimic the behavior of SGs. The farther the fault location from the IIDG, the lower the fault current. That behavior enhances the protection coordination selectivity.

The proposed adaptive VI-FCL is designed following the characteristic in Figure 3.2, which represents a linear droop. Using Figure 3.2, $|Z_{fcl_k}|$ can be written as a function of the FCL resistance and the network X/R ratio

$$\underbrace{|R_{fcl_k}| \sqrt{1 + a^2}}_{|Z_{fcl_k}|} = m|v_{o_k}| + b \quad (3.3)$$

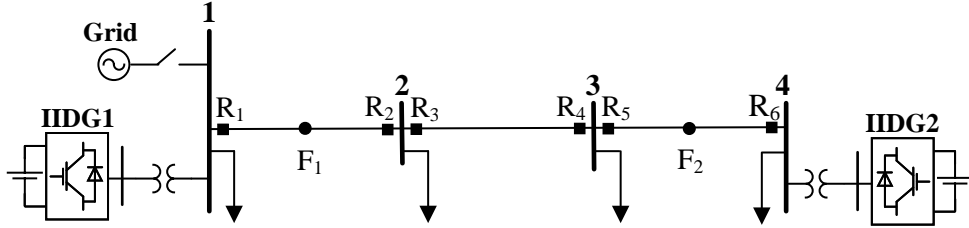


Figure 3.3: Simple test microgrid.

where a denotes the network X/R ratio. $|Z_{f_{cl_k}}|$ is expressed using the network X/R ratio to enable the correct operation of protective functions, such as phase selection and directional elements [70]. The impedance droop characteristic in (3.3) simulates an adaptive VI-FCL that senses the measured IIDG output voltage, v_o , during a fault and outputs a virtual impedance value depending on the fault severity. The constants m and b denote the parameters of the droop characteristic in Figure 3.2. The slope m is calculated using the two endpoints in Figure 3.2, assuming v_o dips to 0.9 pu at fault inception for the highest resistive fault while the constant b is equal to the impedance magnitude in (3.2).

The built-in hard current limiter in the primary IIDG controller typically limits fault currents to 150% of the IIDG rated current [30]. In the event of low resistive faults, the IIDG reference current may saturate, i.e., switch to a constant current source, which may result in instability of outer control loops [31]. On the other hand, engagement of VI-FCLs mitigates current saturation and enhances the microgrid transient stability [33]

To assess the performance of the proposed VI-FCL control scheme, the 4-bus microgrid depicted in Figure 3.3 is simulated by PSCAD/EMTDC. The microgrid is powered by two droop-based IIDGs rated at 2 MVA each and connected to buses 1 and 4 through a 2.5-MVA, 480/12.47 kV, dYg transformers with $Z_t = 0.0012 + j0.05$ pu. Lines 1-2, 3-4 are 1 km in length, and line 2-3 is 2 km. The line impedance $Z = 0.1529 + j0.1406$ Ω /km. The microgrid has 6 DOCRs (R_1 - R_6) installed for overcurrent protection. The rated loads consume 0.75 MVA at 0.9 power factor. A bolted fault F_1 is applied at $t = 1$ s and lasts for 1 s. Figure 3.4(a) shows a

comparison of IIDG1's fault currents with the hard limiter and the proposed VI-FCL control scheme for F_1 . The VI-FCL limits the IIDG fault current to a value below the saturation level and above the relay pick-up current, while the current is saturated with the hard limiter. Figure 3.4(b) compares the system frequency during and after the fault clearance. Without the VI-FCL, the system frequency during restoration drops beyond the lower permissible frequency bound (i.e., 59.3 Hz) and experiences more significant oscillations. When engaging the VI-FCL, the frequency remains within the acceptable limits (59.3–60.5 Hz), and oscillations are attenuated, which illustrates the VI-FCL benefit to the microgrid transient stability. This result also confines with [38].

Bolted faults at mid of the lines, i.e., denoted by F_1 and F_2 , are considered one at a time at $t = 1$ s to demonstrate the effectiveness of the proposed VI-FCL in maintaining the IIDG fault currents. Figure 3.5 displays the currents measured by R_1 during faults F_1 and F_2 with the hard limiter and the VI-FCL, respectively. The currents measured by R_1 have the same magnitude for two different fault locations due to the IIDGs fault currents saturation, as noted in Figure 3.5(a). This behavior, i.e., switching of the IIDG model from voltage mode to current mode, complicates the SCC. On the other hand, the fault currents measured by R_1 , utilizing VI-FCL, are limited below the threshold and sustained during faults. As shown in Figure 3.5(b), the nearer the fault to the IIDG terminals, the higher the fault current, enhancing the protection scheme selectivity. It is worth mentioning that transient current could exceed I_{DG}^{max} immediately after fault inception. Such a response is noted for hard limiters and VI-FCLs, as illustrated in Figure 3.5, because the current limitation is fully enforced when the proposed control scheme reaches a steady state. Therefore, two current limits exist, the steady-state current limit ($I_{DG}^{max} = 1.5$ pu) and a maximum current limit (I_{limit}), which accommodates transient currents. Inverters could contribute transient currents in the range 2.0–3.0 pu immediately after fault inception [30].

The proposed algorithm is developed for islanded microgrids where the grid has no contributions to the fault current. Therefore, only IIDGs can control the current flow in the microgrid during faults. The VI-FCLs limit the fault currents of the IIDGs

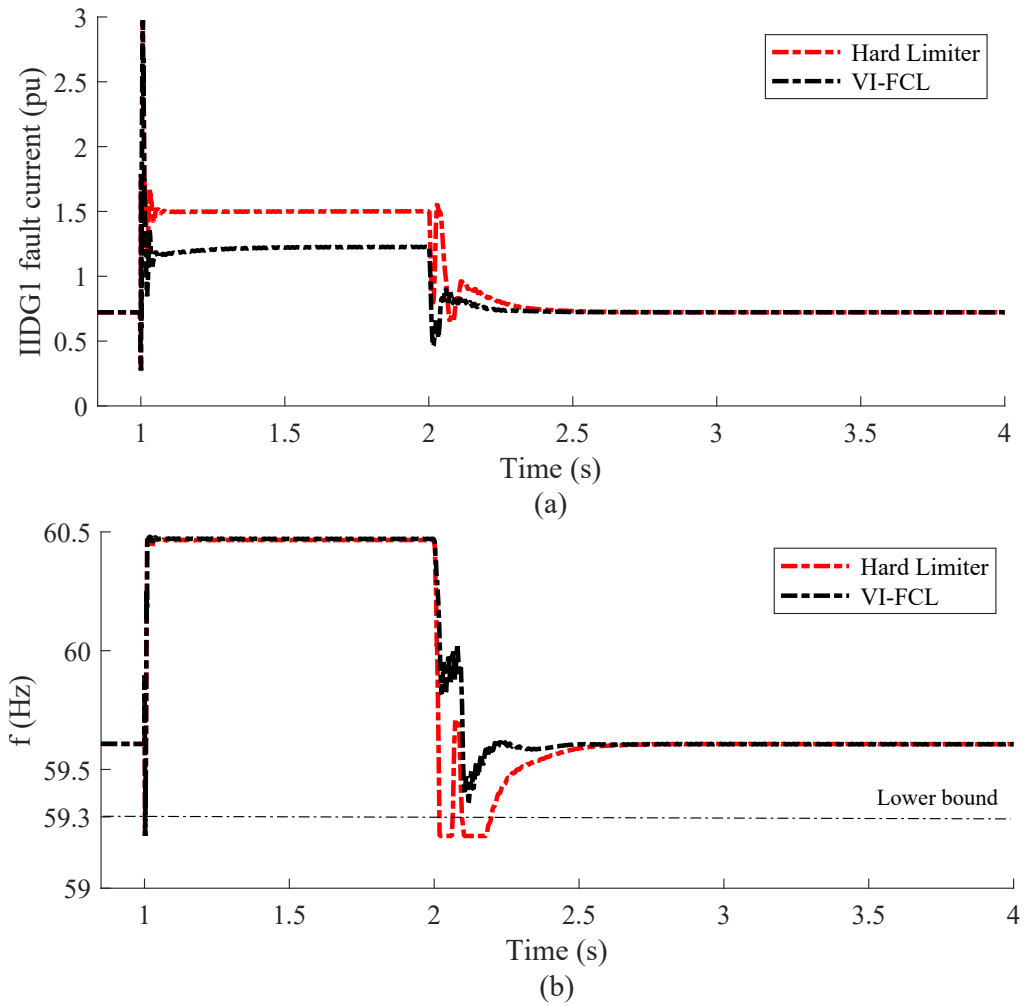


Figure 3.4: Responses during F_1 and after restoration: (a) Fault current of IIDG1. (b) The simple test microgrid frequency.

and protect the inverter's electronic switches from overcurrent.

3.1.3 Current Control

The power controller of a current-controlled IIDG estimates the reference currents to track the reference active and reactive powers. The magnitude of the current source depends on source reference power and terminal voltage. Current-controlled inverters adopt control algorithms to track the maximum power during normal operation.

During faults, the inverter continues to operate in a constant power mode for

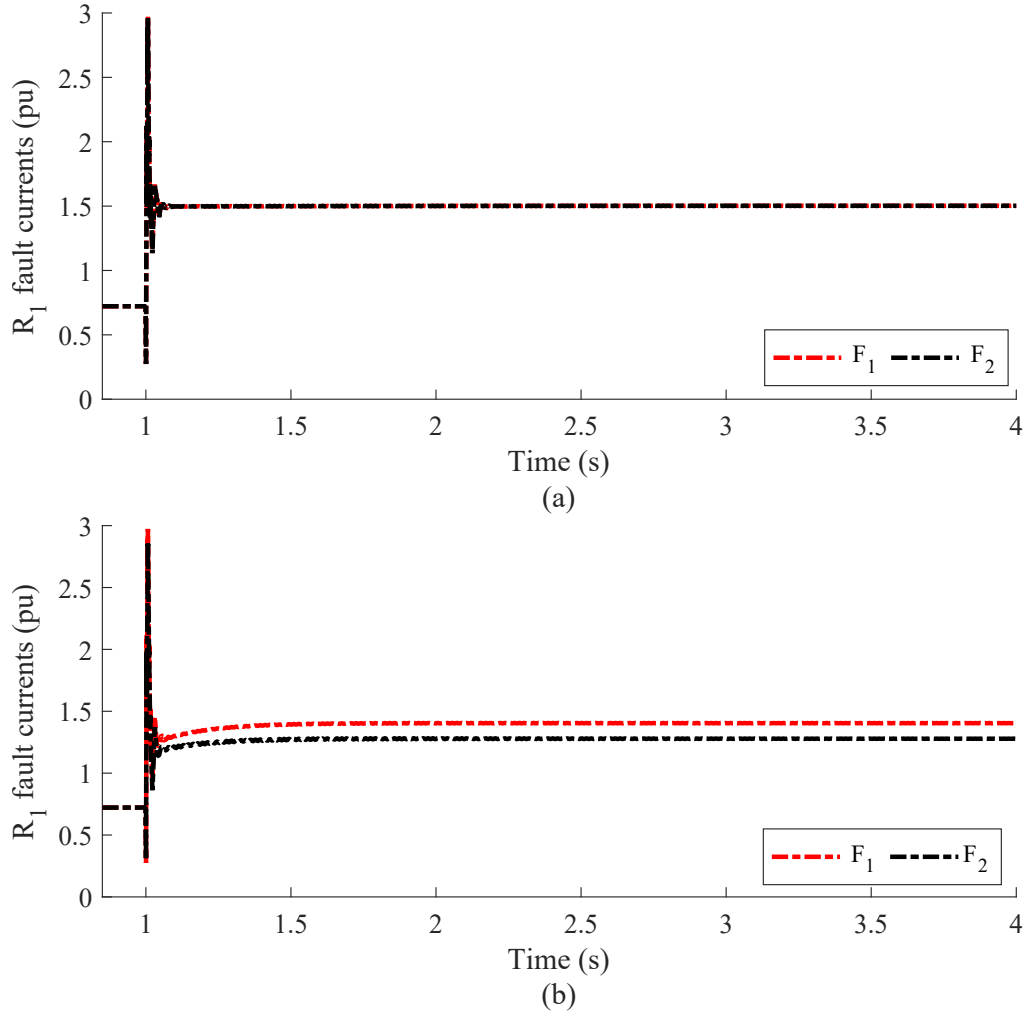


Figure 3.5: Fault currents measured by relay R1: (a) Hard limiter. (b) VI-FCL.

terminal voltages equal to or above $1/I_{DG}^{max}$. In contrast, for terminal voltages below $1/I_{DG}^{max}$, the current is limited to 1.5 pu, and the inverter operates in the constant current mode. The V-I characteristic of a PV source is displayed in Figure 3.6 and is interpreted by

$$I_{PV} = \begin{cases} I^{max}, & |V_{PV}| \leq P/I^{max} \\ P/|V_{PV}|, & P/I^{max} \leq |V_{PV}| < V_{nom} \end{cases} \quad (3.4)$$

where P , I^{max} , and V_{nom} are the PV source power, maximum current, and nominal voltage, respectively.

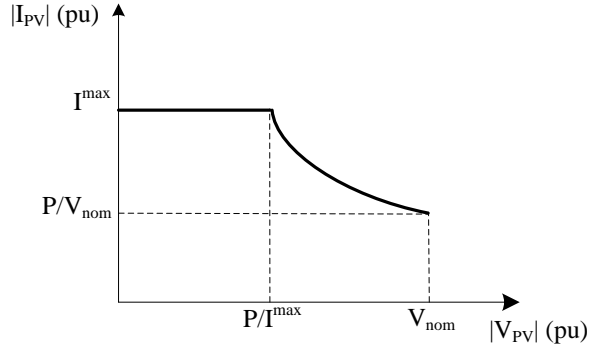


Figure 3.6: PV source V-I characteristic.

3.1.4 System Modeling

Loads can be modeled to reflect the variations in their consumed active and reactive powers P_{Li} and Q_{Li} at bus i due to changes in the microgrid voltage, i.e.,

$$P_{Li} = P_{oi}|V_i|^\alpha \quad (3.5)$$

$$Q_{Li} = Q_{oi}|V_i|^\beta \quad (3.6)$$

where P_{oi} and Q_{oi} are the nominal active and reactive powers, respectively, α and β are the active power and reactive power exponents. The constant impedance model for loads is adopted in this dissertation, where the active and reactive power exponents are equal to two. Injected active and reactive powers P_i and Q_i at bus i are given by

$$P_i = \sum_{j=1}^N |V_i||V_j||Y_{ij}(\omega)|\cos(\delta_i - \delta_j - \gamma_{ij}) \quad (3.7)$$

$$Q_i = \sum_{j=1}^N |V_i||V_j||Y_{ij}(\omega)|\sin(\delta_i - \delta_j - \gamma_{ij}) \quad (3.8)$$

where $|Y_{ij}(\omega)|$ and θ_{ij} are the magnitude and angle of line ij admittance, respectively. $|V_i|$ and δ_i denote the voltage magnitude and angle at bus i , respectively. Similarly, $|V_j|$ and δ_j pertain to bus j voltage magnitude and angle, respectively.

Two types of buses exist in an islanded microgrid: a droop bus and a PQ bus. Each PQ bus i , has two mismatch equations:

$$P_{G_i,sch} = P_{L_i}(|V_i|) - P_i(\omega, |V_i|, |V_j|, \delta_i, \delta_j) \quad (3.9)$$

$$Q_{G_i,sch} = Q_{L_i}(|V_i|) - Q_i(\omega, |V_i|, |V_j|, \delta_i, \delta_j) \quad (3.10)$$

where $P_{G_i,sch}$ and $Q_{G_i,sch}$ are the scheduled active and reactive power generation, respectively. P_{L_i} and Q_{L_i} are the load active and reactive powers, respectively. P_i and Q_i are the injected active and reactive powers to bus i , respectively. The unknown variables for PQ buses are

$$x_{PQ} = [x_{PQ,1} \ x_{PQ,2} \ \dots \ x_{PQ,i} \ \dots \ x_{PQ,n_{PQ}}]^T \quad (3.11)$$

where

$$x_{PQ,i} = [|V_i| \ \delta_i]^T \quad (3.12)$$

and n_{PQ} is the total number of PQ buses.

Each droop bus i has two power mismatch equations:

$$P_{G_i} = P_{L_i}(|V_i|) - P_i(\omega, |V_i|, |V_j|, \delta_i, \delta_j) \quad (3.13)$$

$$Q_{G_i} = Q_{L_i}(|V_i|) - Q_i(\omega, |V_i|, |V_j|, \delta_i, \delta_j) \quad (3.14)$$

Since the VI-FCL is adopted, v_o accurately tracks its reference v_o^* at the fault instant. Based on that and recalling (2.7) and (2.8) and substituting E_o for V_{od}^{ref} ,

$$P_{G_i} = \frac{1}{m_{p_i}}(\omega^* - \omega) \quad (3.15)$$

$$Q_{G_i} = \frac{1}{n_{q_i}}(V^* - |E_{o_i}|) \quad (3.16)$$

The voltage equation in (3.1) can be decomposed into its real and imaginary components and rewritten as

$$|E_{o_i}| \cos \delta_i - v_{oD_i} - i_{oD_i} R_{fcl_i} + i_{oQ_i} X_{fcl_i} = 0 \quad (3.17)$$

$$|E_{o_i}| \sin \delta_i - v_{oQ_i} - i_{oQ_i} R_{fcl_i} - i_{oD_i} X_{fcl_i} = 0 \quad (3.18)$$

where v_{oD_i} and v_{oQ_i} are direct and quadrature components of v_{oi} , respectively, R_{fcl_i} and X_{fcl_i} are the resistance and reactance of Z_{fcl_i} , respectively.

Each droop bus i is modeled for SCC by (3.13)–(3.18) in addition to (3.3). The unknown variables for the droop buses are

$$x_{drp} = [x_{drp,1} \ x_{drp,2} \ \dots \ x_{drp,i} \ \dots \ x_{drp,n_{drp}}]^T \quad (3.19)$$

where

$$x_{drp_i} = [|V_i| \ \delta_i \ i_{oD_i} \ i_{oQ_i} \ P_{G_i} \ Q_{G_i}]^T \quad (3.20)$$

and n_{drp} is the total number of droop buses. The total unknown variables X and the number of mismatch equations n in an islanded microgrid are given by

$$X = [\omega \ x_{pq} \ x_{drp}]^T \quad (3.21)$$

$$n = 2 \times n_{pq} + 6 \times n_{drp} \quad (3.22)$$

Phase relays subjected to balanced and unbalanced faults are considered in this study for phase fault protection. The fault is modeled by adding the fault resistance as an additional branch at the fault location. Then, a set of the nonlinear equations (3.9), (3.10), and (3.13)–(3.18) along with (3.3) of the VI-FCL are solved simultaneously as a minimization problem using the Levenberg-Marquardt algorithm (briefly described in Subsection 3.1.5). The solution provides the voltages at each bus during the fault; and hence, the lines' fault currents are calculated.

3.1.5 Levenberg-Marquardt Algorithm

The Levenberg-Marquardt algorithm is one of the powerful tools for solving nonlinear equations [71]. The set of nonlinear equations that models the various components in islanded microgrids is formulated as a minimization problem

$$\text{minimize } F_i(X) = f_i(X) - C_i = 0 \quad (3.23)$$

where $F_i(X)$ ($i = 1, 2, \dots, n$) is the system of nonlinear equations describing the islanded microgrid, i.e., (3.9), (3.10), (3.13)—(3.18), and (3.3), $f_i(X)$ and C_i are the variable dependent and constant terms, respectively, and n is the number of unknowns.

The unknowns are assigned an initial guess solution vector X_0 . The algorithm adopts a search direction, which is a solution of the linear set of equations, i.e.,

$$\left(J(x^k)^T J(x^k) + \mu^k I \right) d^k = -J(x^k)^T F(x^k) \quad (3.24)$$

where d^k is the step solution vector, μ^k is a scalar that controls d^k magnitude and direction, and $J(x^k)$ is an n -by- n Jacobian:

$$J(x^k) = \begin{bmatrix} \nabla F_1(x^k)^T \\ \nabla F_2(x^k)^T \\ \vdots \\ \nabla F_n(x^k)^T \end{bmatrix} \quad (3.25)$$

The solution vector x^k represents the unknown variables of X in the islanded microgrid. The algorithm toggles the update of the variable between the gradient descent update and the Gauss-Newton update. Small μ^k values result in a Gauss-Newton update and large values of μ^k result in a gradient descent update.

3.2 Proposed Optimal Protection Coordination

3.2.1 OPC Problem Formulation

The typical formulation of the protection coordination problem is developed as an optimization program to minimize the relays' total operation time while maintaining

coordination between primary and backup relay sets. Hence, the objective function is defined as the sum of all relays operation times, T , i.e.,

$$\min T = \sum_{r=1}^R \sum_{l=1}^L (t_{rl}^p + \sum_{b=1}^{BK} t_{rl}^{b_k}) \quad (3.26)$$

where l is the fault location identifier with total locations L , r is the relay identifier with R as the total number of relays. Each fault location is identified as a near-end, midline, and far-end fault. This identifier allows for covering the entire feeder length to ensure that the proposed algorithm can operate at all possible fault locations. The subscript p refers to a primary relay and b_k refers to a backup relay k , with BK denoting the total number of backup relays for each primary relay. t_{rl}^p is the operation time of relay r as a primary relay for fault location l , and $t_{rl}^{b_k}$ is the operation time of the backup relay b_k of relay r for fault location l .

The operation time of a DOCR is inversely proportional to the short-circuit current passing through it. The inverse-time-current (ITC) relay characteristic based on IEC 60255-151 standard characteristic is adopted [72]. The operation time is given by

$$t_{rl} = TDS_r \frac{A}{\left(\frac{I_{sc_{rl}}}{I_{pr}}\right)^B - 1} \quad (3.27)$$

where TDS_r is the time dial setting, K_r is a constant parameter, $I_{sc_{rl}}$ is the short-circuit current measured by relay r due to a fault at location l , I_{pr} is relay r pick-up current. The constants A and B are determined according to the DOCR characteristic employed. Assuming a standard inverse-time characteristic, the constants A and B are 0.14 and 0.02, respectively. The time-current-voltage (TCV) relay characteristic is proposed in [73] mainly for distribution systems. Due to its benefits, such as gaining the highest possible reduction in relay's operation time, it is utilized in the following case studies for islanded microgrids. That characteristic is based on the IEC 60255-151 standard characteristic, where the operation time of relay r is given by

$$t_{rl} = e^{(V_{rl}^f - 1)K_r} TDS_r \frac{A}{\left(\frac{I_{scrl}}{I_{pr}}\right)^B - 1} \quad (3.28)$$

where V_{rl}^f is the phase voltage magnitude measured at relay r due to a fault at location l .

The coordination time is the minimum time between a primary relay's operation and its backup that must be preserved. This time is known in the literature as the coordination time interval (CTI). The CTI is set at 0.2 s to comply with IEEE Standard 242-2001 [74], and thus, the following constraint is defined

$$t_{rl}^{bk} - t_{rl}^p \geq CTI \quad \forall r, [l, k] \quad (3.29)$$

Pick-up currents are selected to have fixed values with a significant margin of 30% above the respective protected line's rated load current. This condition ensures that DOCRs trip only when a fault occurs. Further, TDS and K can have continuous values. Therefore, the constraints on TDS , K , and minimum relay operation time are given by

$$K_{min} \leq K_r \leq K_{max} \quad \forall r \quad (3.30)$$

$$TDS_{min} \leq TDS_r \leq TDS_{max} \quad \forall r \quad (3.31)$$

$$t_{rl}^p, t_{rl}^{bk} \geq t_{min} \quad \forall r \quad (3.32)$$

where TDS_{min} and TDS_{max} are the lower and upper bounds of TDS_r , respectively, which are set at 0.01 and 1.0. K_{min} and K_{max} denote the lower and upper bounds of K_r , respectively, with values of 0 and 4.0 [68]. t_{min} is the minimum relay operation time, and t_{min} is set to 20 ms [75].

3.2.2 SCC Algorithm for IIDGs

In this study, the droop-based IIDG is modeled as a voltage source behind an impedance, owing to the integration of the proposed VI-FCL. This impedance comprises the filter inductor impedance and virtual impedance. The current-controlled IIDG is modeled

as a current source that updates its fault current based on the terminal voltage, as indicated by (3.4). The mismatch equations for load, current-controlled IIDGs (interpreted as a negative load with powers equal to the pre-fault settings), and droop buses are formulated, including the fault location as a virtual load bus. The adaptive VI-FCL in (3.3) ensures limiting the IIDG output current to a value less than the threshold (1.5 pu). The algorithm starts with building the system bus admittance matrix Y_{bus} . Then, a modified version of Y_{bus} , i.e., Y_{bus}^f , is generated to include the virtual fault bus, which is represented by the last row and column of Y_{bus}^f . Y_{bus}^f is a function of the fault location in each line. Thus, it is formulated for each fault scenario in the test microgrid. Three-phase faults are simulated at virtual buses, representing near-end, midline, and far-end locations. The algorithm involves a two-stage optimization, as displayed in Figure 3.7. In Stage I, the power mismatch equations are solved, including the VI-FCLs, to obtain bus voltages during short-circuit faults. The first stage is solved using MATLAB's Levenberg-Marquardt algorithm.

The algorithm restarts for each fault location, near, mid, and far, involving several fault resistances in one iteration for each fault location. A solution vector with all bus voltages for different fault locations is obtained for fault resistances simultaneously, i.e., $V_{ilR_{flt}}$, where i , l , and R_{flt} are subscripts indicating the bus number, fault location, and fault resistance, respectively. The solution vector also includes the frequency and IIDGs fault currents. Then, the short-circuit current seen by each relay is calculated using the obtained bus voltages during a fault. The relays' short-circuit currents are then mapped to their respective primary and backup relays.

Stage II determines the optimal values of the tuning variables TDS and K to achieve OPC. Due to the nonlinearity and intractability of the OPC problem, a meta-heuristic optimization method is employed. GA is an evolutionary optimization algorithm that outperforms other meta-heuristic techniques in terms of execution time and solution accuracy [76]. Thus, GA is selected to solve the OPC problem as suggested in [32]. The nonlinear constraints formulated using voltages and currents are obtained in Stage I, considering several values of R_{flt} in the range 0.1—10 Ω and solved simultaneously using the GA.

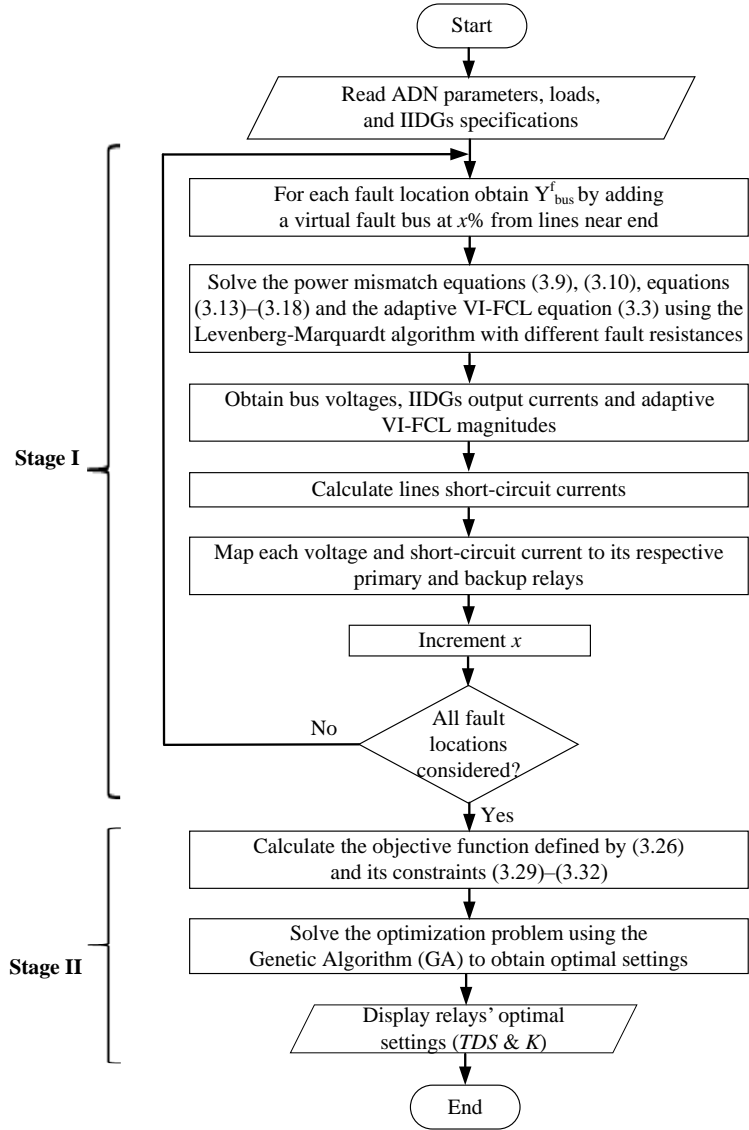


Figure 3.7: Flow chart of the proposed OPC program.

3.2.3 Solving Method

GA is one of the meta-heuristic optimization techniques usually applied to highly nonlinear problems [71]. Each candidate solution is encoded as an array of parameter values. For a problem with Z dimensions, each solution is encoded as a Z -dimensional array. Two settings need to be determined for each DOCR, namely TDS and K . For a distribution system with R relays, the total number of unknowns is $2R$. The GA

chromosome is defined by

$$chromosome = [p_1, p_2, \dots, p_{2R}] \quad (3.33)$$

where p_i denotes a value of a relay parameter.

The OPC program is formulated as an NLP problem, which is time exhaustive to be solved through deterministic methods. GA is an efficient optimization technique to solve intractable problems such as OPC [76], [77]. Hence, it is used to solve Stage II of the OPC problem, as suggested in [31]. The GA exhibits superior performance compared to other meta-heuristic techniques in terms of execution time and accuracy [78]. The GA available in the MATLAB optimization toolbox is used to obtain the optimal relays settings TDS_r and K that guarantee DOCRs' coordination. The nonlinear constraints formulated using short-circuit currents are obtained for different outage contingencies in Stage I and considered simultaneously in the solution.

3.3 Performance Evaluation

The test microgrid is described in this section, and the proposed SCC algorithm is validated by comparing its results with the steady-state values obtained from time-domain simulations. Further, the results of the formulated OPC program are presented.

3.3.1 Test Microgrid

An islanded microgrid representing a section of the Canadian urban benchmark distribution system is used for testing [32], as depicted in Figure 3.8. All lines are 1 km in length with an impedance $Z = 0.1529 + j0.1406 \Omega/\text{km}$. The loads shown are the rated loads and consume 1 MVA at 0.9 power factor each. Four droop-based IIDGs are connected to buses 4, 5, 6, and 9. The IIDGs are identical and rated at 3 MVA. They are connected through 3.5-MVA, 480 V/12.47 kV, dYG transformers with $Z_t = 0.0012 + j0.05 \text{ pu}$. The microgrid is equipped with 16 DOCRs (R_1 — R_{16}) for overcurrent protection. Two case studies were conducted: Case I, all IIDGs are

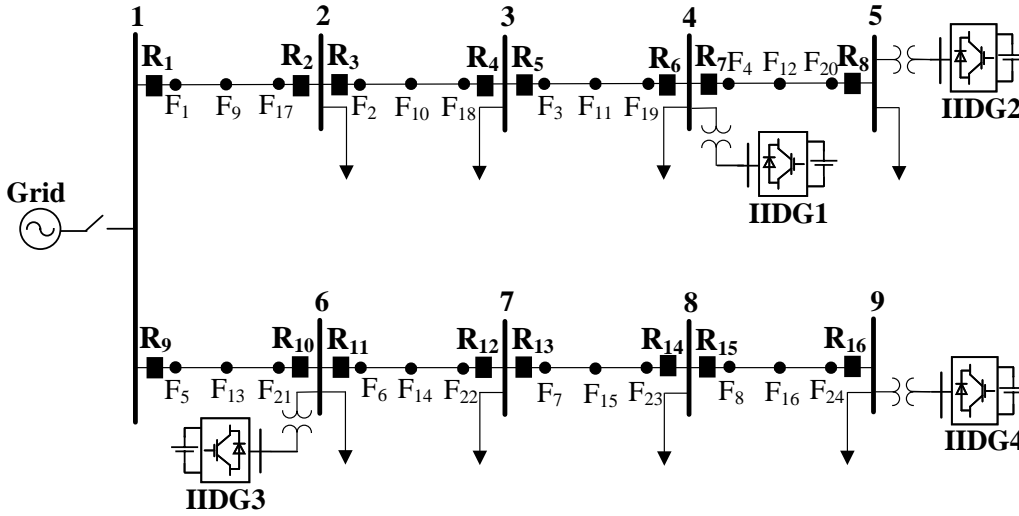


Figure 3.8: Single line diagram of the test microgrid.

droop-based, and in Case II, IIDG4 represents a 2-MW PV source, and the rest are droop-based.

The DOCRs should operate for near-end, far-end faults as well as midline faults within its zone. Three-phase faults (F_1-F_{24}) located at near-end, mid, and far-end locations on the lines are considered, as displayed in Figure 3.8. Due to the bidirectional short-circuit current flow, each fault requires two primary relays, one at each end of the line. For instance, if a fault occurs in the middle of line 3-4, namely F_{11} , R_5 , and R_6 are the primary relays with R_3 operating as a backup for R_5 . While R_8 serves as a backup for R_6 . Short-circuit branch currents are calculated using the proposed SCC algorithm. A map-matrix is defined according to the relays that respond to the defined faults (F_1-F_{24}). This matrix is used to map each branch current and voltage to its relevant relay, and hence the constraints for relays can be checked for satisfaction.

3.3.2 SCC Algorithm Validation and Results

The test microgrid is simulated by PSCAD/EMTDC to validate the SCC algorithm. The proposed SCC algorithm was developed in MATLAB and used to solve for bus

Table 3.1: Validation Results with the Constant VI-FCLs

PSCAD			SCC Algorithm		
Relays currents magnitudes (pu)					
i_o = the IIDG fault current (pu)					
#	Primary	Backup	#	Primary	Backup
F₁₂	R ₇	R ₅	F₁₂	R ₇	R ₅
	3.3916	2.2181		3.4379	2.2082
	R ₈	-		R ₈	-
	1.2153	-		1.2426	-
F₁₅	R ₁₃	R ₁₁	F₁₅	R ₁₃	R ₁₁
	3.3737	3.2340		3.4394	3.1778
	R ₁₄	R ₁₆		R ₁₄	R ₁₆
	1.2131	1.2153		1.2569	1.2604
F₁₂	i_{o1}	i_{o2}	F₁₂	i_{o1}	i_{o2}
	1.2115	1.2211		1.2297	1.2325
	i_{o3}	i_{o4}		i_{o3}	i_{o4}
	1.1622	1.1456		1.1911	1.1787
F₁₅	i_{o1}	i_{o2}	F₁₅	i_{o1}	i_{o2}
	1.1443	1.1390		1.1741	1.1698
	i_{o3}	i_{o4}		i_{o3}	i_{o4}
	1.1995	1.217		1.2104	1.2283

voltages during faults performed one at a time at mid of lines 4-5 and 7-8 when using $R_{flt} = 0.1 \Omega$. The bus voltages obtained are used to calculate the relay currents during faults and compared with the steady-state results obtained from the detailed time-domain PSCAD simulations.

Table 3.1 displays the results with constant VI-FCLs obtained from the detailed time-domain simulations and the proposed SCC algorithm. The maximum error in relays' currents and IIDGs fault currents are 3.71% and 2.89%, respectively. Table 3.2 displays the results with adaptive VI-FCLs obtained from the detailed time-domain

Table 3.2: Validation Results with the Adaptive VI-FCLs

PSCAD			SCC Algorithm		
#	Primary	Backup	#	Primary	Backup
F₁₂	R ₇	R ₅	F₁₂	R ₇	R ₅
	3.4672	2.4053		3.5897	2.3099
	R ₈	-		R ₈	-
	1.2808	-		1.3235	-
F₁₅	R ₁₃	R ₁₁	F₁₅	R ₁₃	R ₁₁
	3.5443	3.5493		3.5852	3.4246
	R ₁₄	R ₁₆		R ₁₄	R ₁₆
	1.2743	1.2765		1.3221	1.3140
F₁₂	i_{o1}	i_{o2}	F₁₂	i_{o1}	i_{o2}
	1.2749	1.2793		1.2824	1.2857
	i_{o3}	i_{o4}		i_{o3}	i_{o4}
	1.2587	1.2571		1.241	1.2274
	$Z_{vi-fcl1}$	$Z_{vi-fcl2}$		$Z_{vi-fcl1}$	$Z_{vi-fcl2}$
	0.779	0.779		0.763	0.761
	$Z_{vi-fcl3}$	$Z_{vi-fcl4}$		$Z_{vi-fcl3}$	$Z_{vi-fcl4}$
	0.749	0.736		0.768	0.764
F₁₅	i_{o1}	i_{o2}	F₁₅	i_{o1}	i_{o2}
	1.2548	1.2541		1.2223	1.2177
	i_{o3}	i_{o4}		i_{o3}	i_{o4}
	1.2664	1.276		1.2616	1.2808
	$Z_{vi-fcl1}$	$Z_{vi-fcl2}$		$Z_{vi-fcl1}$	$Z_{vi-fcl2}$
	0.737	0.733		0.763	0.761
	$Z_{vi-fcl3}$	$Z_{vi-fcl4}$		$Z_{vi-fcl3}$	$Z_{vi-fcl4}$
	0.773	0.778		0.768	0.764

simulations and the proposed algorithm. The maximum error in relays' currents, IIDGs fault currents, and $|Z_{vi-fcl}|$ are 4.13%, 2.99%, and 3.82%, respectively. The results obtained from the proposed SCC algorithm are within a 5% tolerance.

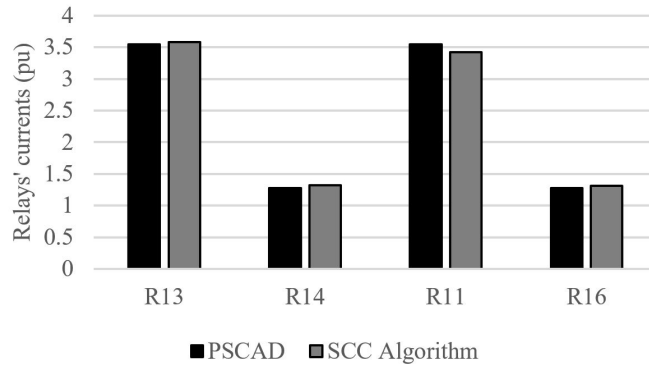

 Figure 3.9: Comparison of relays' currents during F₁₅.

Table 3.3: VI-FCLs Magnitudes in Per Unit (Case I)

R_{ft} (Ω)	Fault Location	Z_{vi-fcl} = the VI-FCL magnitude (pu)			
		IIDG1 $Z_{vi-fcl1}$	IIDG2 $Z_{vi-fcl2}$	IIDG3 $Z_{vi-fcl3}$	IIDG4 $Z_{vi-fcl4}$
0.1	Near-end	0.765	0.763	0.768	0.765
	Midline	0.763	0.761	0.768	0.764
	Far-end	0.762	0.761	0.763	0.765
1	Near-end	0.721	0.718	0.728	0.723
	Midline	0.720	0.718	0.726	0.723
	Far-end	0.720	0.718	0.724	0.722
5	Near-end	0.532	0.53	0.538	0.535
	Midline	0.532	0.53	0.537	0.535
	Far-end	0.531	0.53	0.536	0.535

To reflect the advantage of using adaptive VI-FCLs, the OPC problem was first solved using constant VI-FCLs. These constant VI-FCLs limit the IIDGs fault currents to 150% of their rated currents for bolted faults at the IIDG terminals, and hence, applicable to any faulty conditions. To further elaborate on the results reported in Table 3.2 using the proposed SCC algorithm, the primary and backup relays' currents are displayed in Figure 3.9.

Table 3.3 displays Z_{vi-fcl} for Case study I for selected values of fault resistances

Table 3.4: Relays Optimal Settings for the Test Microgrid (Case I)

#	<i>TDS</i>	I_p	K	#	<i>TDS</i>	I_p	K
	(s)	(pu)			(s)	(pu)	
R₁	1.1588	0.4334	2.5106	R₉	0.6367	0.4334	1.3408
R₂	1.9991	0.4334	2.236	R₁₀	0.9774	0.4334	2.0446
R₃	0.2300	0.4334	1.2745	R₁₁	0.3394	0.4334	0.9727
R₄	0.6105	0.4334	0.8253	R₁₂	1.2617	0.4334	1.9509
R₅	0.1840	0.8667	3.0000	R₁₃	0.5201	0.4334	2.0714
R₆	0.8504	0.8667	1.5117	R₁₄	1.8578	0.4334	2.1512
R₇	0.0915	0.4334	3.0000	R₁₅	0.1121	0.4334	3.0000
R₈	2.3568	0.4334	2.3872	R₁₆	1.3810	0.4334	1.6935

R_{flt} . The table shows a decreasing Z_{vifcl} value with the increase in R_{flt} , which reflects the adaptivity to faults. For example, IIDG1 has a VI-FCL impedance magnitude of 0.765 pu for a 0.1 Ω near-end fault versus 0.532 pu for a 5 Ω near-end fault.

Tables 3.4 and 3.5 furnish the results for Case study I. Table 3.4 shows the optimal values of TDS and K for the test microgrid obtained by solving the OPC problem, as well as the values of the pickup current I_p . The relays' pickup currents are fixed at a value with a safe margin above the rated load current. TDS and K are used as decision variables to satisfy the coordination constraints. Table 3.5 illustrates the relays' operation times for near-end and far-end bolted faults on test microgrid lines. The operation times are calculated using the obtained optimal values of TDS , K , and I_p for each relay. It is observed that all primary and backup relay sets are correctly coordinated by having CTIs at least equal to 0.2 s.

Tables 3.6 and 3.7 display the results for Case study II. The OPC problem is first solved when the microgrid supplies the rated load and the PV source injects its rated power. Secondly, the OPC problem is solved when the microgrid is 15% loaded and the PV source injects 15% of its rated power. Table 3.6 shows the optimal values of TDS and K obtained by solving the OPC problem as well as the values of the pickup current I_p considering the worst pre-fault operating conditions. Table 3.7

Table 3.5: Operation Times in Seconds for Bolted Faults (Case I)

#	Primary	Backup	#	Primary	Backup
F₁	R ₁	R ₁₀	F₁₇	R ₁	R ₁₀
	0.5890	0.7981		0.6094	1.6401
	R ₂	R ₄		R ₂	R ₄
	0.8552	1.0686		0.8296	1.5356
F₂	R ₃	R ₁	F₁₈	R ₃	R ₁
	0.3992	0.6083		0.4217	1.3187
	R ₄	R ₆		R ₄	R ₆
	1.0457	1.3515		1.0014	1.951
F₄	R ₇	R ₅	F₂₀	R ₇	R ₅
	0.022	0.2326		0.02	0.4656
	R ₈	-		R ₈	-
	1.4065	-		1.3724	-
F₅	R ₉	R ₂	F₂₁	R ₉	R ₂
	0.646	0.8549		0.6813	1.2169
	R ₁₀	R ₁₂		R ₁₀	R ₁₂
	0.7978	1.0635		0.7522	1.9134
F₆	R ₁₁	R ₉	F₂₂	R ₁₁	R ₉
	0.4491	0.6729		0.42	0.9294
	R ₁₂	R ₁₄		R ₁₂	R ₁₄
	0.9557	1.165		0.9219	3.2936
F₇	R ₁₃	R ₁₁	F₂₃	R ₁₃	R ₁₁
	0.2268	0.4511		0.227	0.6523
	R ₁₄	R ₁₆		R ₁₄	R ₁₆
	1.1016	1.3338		0.9984	3.7958

illustrates the relays operation times for selected near-end and far-end faults. It is observed that all primary and backup relay sets are correctly coordinated. It is worth mentioning that the relays' operation times can be further enhanced by increasing the IIDG current limit to 2.0 pu, as suggested in [24].

Table 3.6: Relays Optimal Settings for the Test Microgrid (Case II)

#	<i>TDS</i>	<i>I_p</i>	<i>K</i>	#	<i>TDS</i>	<i>I_p</i>	<i>K</i>
	(s)	(pu)			(s)	(pu)	
R₁	1.7024	0.4334	2.1037	R₉	0.6740	0.4334	1.1395
R₂	0.9088	0.4334	1.1846	R₁₀	1.5108	0.4334	1.6717
R₃	1.7571	0.4334	2.5081	R₁₁	0.3547	0.4334	0.7720
R₄	1.2586	0.4334	1.3815	R₁₂	0.6945	0.4334	0.6627
R₅	0.3030	0.8667	1.5888	R₁₃	0.2343	0.4334	1.0273
R₆	1.3514	0.8667	1.7160	R₁₄	1.0312	0.4334	0.9503
R₇	0.0125	0.4334	0.3573	R₁₅	0.1141	0.4334	2.7692
R₈	3.0043	0.4334	2.4074	R₁₆	3.6521	0.4334	3.3150

Table 3.7: Operation Times in Seconds for Selected Bolted Faults (Case II)

Rated Load			Light Load (15%)		
#	Primary	Backup	#	Primary	Backup
F₁	R ₁	R ₁₀	F₁	R ₁	R ₁₀
	0.6171	0.8344		0.6128	0.8288
F₁	R ₂	R ₄	F₁	R ₂	R ₄
	0.8812	1.0936		0.8761	1.0879
F₄	R ₇	R ₅	F₄	R ₇	R ₅
	0.0201	0.2486		0.0201	0.2283
	R ₈	-		R ₈	-
	1.4409		1.4384		
F₆	R ₁₁	R ₉	F₆	R ₁₁	R ₉
	0.4754	0.6998		0.4732	0.6925
	R ₁₂	R ₁₄		R ₁₂	R ₁₄
	1.0108	1.2208	1.011	1.221	
F₈	R ₁₅	R ₁₃	F₈	R ₁₅	R ₁₃
	0.0201	0.2328		0.0201	0.2303
	R ₁₆	-		R ₁₆	-
	1.4296		1.4299		

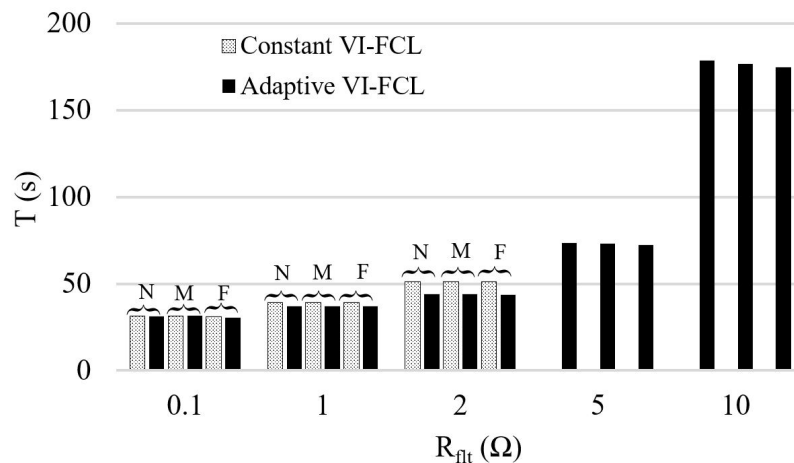


Figure 3.10: Comparison of total relays' operation times for the test microgrid (Case study I) N, M, and F are the near-end, midline, and far-end faults, respectively.

Figure 3.10 displays a bar chart that compares relays' total operation times for the constant VI-FCLs versus the adaptive VI-FCLs for Case study I of the test microgrid. The figure displays the summation of individual relays' operation times in the microgrid (i.e., 16 relays) at different fault locations. The figure shows that the adaptive VI-FCL resulted in comparable relays' total operation times for $R_{flt} \leq 0.1 \Omega$ and less total operation times for $R_{flt} = 1 \Omega$ to 2Ω . It is worth noting that with the adaptive VI-FCLs, relays coordination can be achieved for fault resistances up to 10Ω . In contrast, for constant VI-FCLs, relay coordination cannot be achieved beyond 2Ω , i.e., an indication of infeasible OPC.

3.3.3 Unbalanced faults

During unbalanced faults, the positive-, negative-, and zero-sequence networks should be formed for SCC. These sequence networks are then connected based on the fault type. In the case of single-line-to-ground (SLG) faults, the sequence networks are connected in series with threefold the fault resistance ($3R_{flt}$). Since the VI-FCL is implemented in the positive-sequence frame, only positive-sequence currents have been employed for OPC. To obtain the positive-sequence currents measured by the

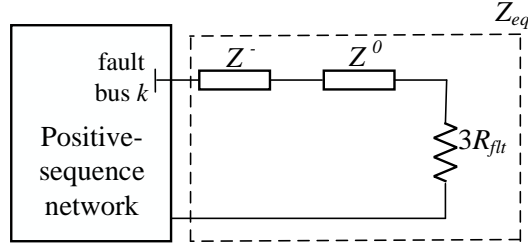


Figure 3.11: Modified sequence networks for SLG faults.

relays, both negative- and zero-sequence networks are replaced by their equivalent impedances, i.e., Z^- and Z^0 , respectively. The justification behind using Z^- and Z^0 is that droop-based IIDGs with VI-FCLs do not generate negative- or zero-sequence voltages. As shown in Figure 3.11, the sequence networks are connected in series for SLG faults, and Z_{eq} is equal to the summation of Z^- , Z^0 , and $3R_{ft}$. As can be noted from the figure, the positive-sequence network during balanced faults becomes identical to that during unbalanced faults if Z_{eq} is replaced by R_{ft} . Thus, the proposed SCC algorithm can also be applied to obtain the relays' positive-sequence currents during unbalanced faults as follows. The bus admittance matrix Y_{bus}^f of the positive-sequence network is built, where $1/Z_{eq}$ is added to the diagonal element that represents the fault location. Then, the power mismatch Equations (3.9), (3.10), (3.13), and (3.14) along with (3.3), (3.15)–(3.18) are solved to obtain positive-sequence components of the bus voltages. The obtained positive-sequence bus voltages during unbalanced fault are then used to calculate the positive-sequence currents seen by each relay. It is worth noting that the microgrid is assumed to be properly grounded to avoid the scenario where the voltages of non-faulted phases increase during unbalanced faults.

A case study that considers SLG faults for OPC has been conducted to support the applicability of the proposed algorithm during unbalanced faults. The ITC was selected for the OPC with the unbalanced faults because the ITC operates based on currents only, i.e., fewer sensors are required. It is also the most used characteristic in the industry [72]. Table 3.8 displays the relays' operation times for SLG and three-phase faults considering various fault resistances. It is observed that all primary and

Table 3.8: Operation Times for Selected Far-end Faults in Seconds

$R_{ft} = 0.1 \Omega$					
SLG			Three-phase		
#	Primary	Backup	#	Primary	Backup
F₉	R ₁	R ₁₀	F₉	R ₁	R ₁₀
	0.7698	1.0099		0.6717	0.8812
	R ₂	R ₄		R ₂	R ₄
	0.9625	1.1946		0.833	1.0464
F₁₂	R ₇	R ₅	F₁₂	R ₇	R ₅
	0.0363	0.3304		0.0323	0.242
	R ₈	-		R ₈	-
	1.74	-		1.3851	-
F₁₄	R ₁₁	R ₉	F₁₄	R ₁₁	R ₉
	0.4777	0.7419		0.4302	0.6392
	R ₁₂	R ₁₄		R ₁₂	R ₁₄
	1.496	1.8357		1.0869	1.4137
	2.2936		1.7565		
$R_{ft} = 3 \Omega$					
F₉	R ₁	R ₁₀	F₉	R ₁	R ₁₀
	0.7924	1.0396		0.7289	0.9562
	R ₂	R ₄		R ₂	R ₄
	0.986	1.1995		0.907	1.1163
F₁₂	R ₇	R ₅	F₁₂	R ₇	R ₅
	0.0377	0.8136		0.0349	0.6589
	R ₈	-		R ₈	-
	1.7074	-		1.5585	-
F₁₄	R ₁₁	R ₉	F₁₄	R ₁₁	R ₉
	0.486	1.1512		0.4571	1.0623
	R ₁₂	R ₁₄		R ₁₂	R ₁₄
	1.7453	1.9554		1.4371	1.6658

Table 3.9: Relays Optimal Settings Considering SLG Faults

#	<i>TDS</i> (s)	<i>I_p</i> (pu)	#	<i>TDS</i> (s)	<i>I_p</i> (pu)
R₁	0.1692	0.4335	R₉	0.1585	0.4334
R₂	0.2107	0.4334	R₁₀	0.222	0.4334
R₃	0.1149	0.4458	R₁₁	0.1343	0.4334
R₄	0.265	0.4334	R₁₂	0.1744	0.4334
R₅	0.0344	0.8667	R₁₃	0.0725	0.4334
R₆	0.1916	0.8667	R₁₄	0.2233	0.4335
R₇	0.0100	0.4334	R₁₅	0.0100	0.4334
R₈	0.2245	0.4334	R₁₆	0.2995	0.4334

backup relay sets remain coordinated with a CTIs of at least 0.2 s. Table 3.9 reports the optimal relays' settings obtained by solving the OPC problem, where three-phase and SLG faults are considered simultaneously.

3.4 Enhanced Adaptive VI-FCL Design

IIDGs can withstand fault currents up to two times their rated current [24]. To limit IIDG fault current below 2.0 pu for bolted fault at the IIDG terminals and other fault locations, Z_{fcl}^{max} magnitude can be approximated by

$$|Z_{fcl_k}^{max}| = \frac{E_{o_k}}{I_{DG}^{max}} \quad (3.34)$$

The characteristics displayed in Figure 3.12 are proposed and utilized to investigate their influence on protective relays' total operation time. Based on Figure 3.12, the proposed characteristics can be expressed as follows:

$$|Z_{fcl_k}| = \begin{cases} k_1|v_{o_k}| + |Z_{fcl_k}^{max}|, & 0 \leq |v_{o_k}| \leq d \\ Z_{f_k}, & d < |v_{o_k}| \leq 1 \end{cases} \quad (3.35)$$

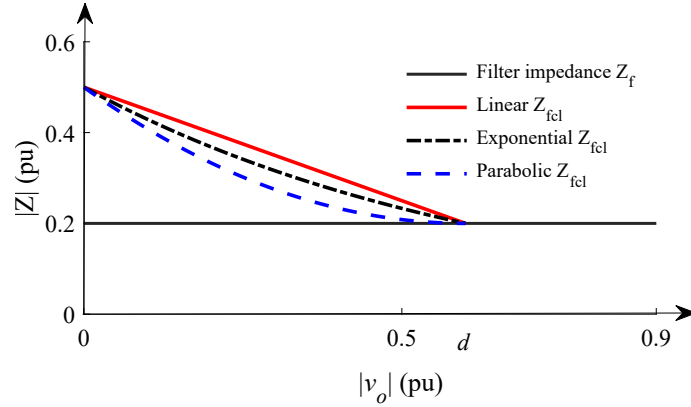


Figure 3.12: Impedance characteristics of the adaptive VI-FCL.

$$|Z_{fcl_k}| = \begin{cases} |Z_{fcl_k}^{max}| k_2^{-|v_{o_k}|}, & 0 \leq |v_{o_k}| \leq d \\ Z_{f_k}, & d < |v_{o_k}| \leq 1 \end{cases} \quad (3.36)$$

$$|Z_{fcl_k}| = \begin{cases} k_3 (|v_{o_k}| - d)^2 + Z_{f_k}, & 0 \leq |v_{o_k}| \leq d \\ Z_{f_k}, & d < |v_{o_k}| \leq 1 \end{cases} \quad (3.37)$$

The droop characteristics represent linear, exponential, and parabolic functions. Z_v adapts to fault severity such that it is at its maximum value for bolted fault and zero at point d for the highest resistive fault. In other words, it diminishes for the highest resistive fault. Thus, the constant d can be approximated by

$$d = E_o - Z_f I_{DG}^{max} \quad (3.38)$$

The constants k_1 , k_2 , and k_3 are the linear, exponential, and parabolic droop characteristic parameters, respectively. The constant k_1 represents the linear characteristic slope and is calculated using the endpoints. k_2 and k_3 are calculated by substituting the points (d, Z_{f_k}) and $(0, Z_{fcl_k}^{max})$ in the exponential and parabolic characteristics, respectively.

The fault is modeled by connecting the fault resistance at the fault location. Then, the set of the nonlinear equations (3.9), (3.10), and (3.13)–(3.18) along with one of (3.35)–(3.37) of the adaptive VI-FCL are solved simultaneously as a minimization

problem using the Levenberg-Marquardt algorithm [71]. The solution furnishes the bus voltages during faults, from which the relays' fault currents are calculated.

3.4.1 Proposed adaptive VI-FCL Characteristics Results

This subsection furnishes the OPC results obtained utilizing the three proposed adaptive VI-FCL characteristics, i.e., linear, exponential, and parabolic. In addition, a breakdown of the relays' operation times for near-end and far-end faults on microgrid's lines is reported. The islanded test microgrid depicted in Figure 3.8 is used to illustrate the impact of adopting different VI-FCL characteristics on relays' operation times. The lines for Case study III are 0.5 km in length.

Case III: *Impact of VI-FCL Characteristic on Protection Coordination*

1) *Optimal DOCRs Settings*: A matrix is used to map each branch current and bus voltage to its relevant relay so that relays' constraints can be checked for satisfaction. The constraints are formulated for a number of fault resistances. Each of the adaptive VI-FCL characteristics is employed while solving for the optimal settings. Table 3.10 lists the optimal settings of TDS , K , and I_p for all DOCRs. The solution with each of the proposed adaptive VI-FCL characteristics results in a different optimal set of settings.

2) *Relays' Operation Times*: Table 3.11 shows the total relays' operation times for each VI-FCL characteristic investigated. The total operation times increase with the distance from the near-end. The total operation time obtained utilizing the parabolic characteristic is the best. A maximum of 5% reduction in the total relays' operation time is achieved, employing the parabolic characteristic for moderate resistive faults. The reduction achieved with the parabolic characteristic is insignificant; therefore, the linear characteristic is implemented in the OPC program.

The relays' operation times are calculated using the optimal settings TDS and K obtained utilizing the linear characteristic. Table 3.12 reports the operation times of the assigned primary and backup DOCRs for near-end and far-end bolted faults on selected lines of the test microgrid. The results indicate that the CTIs for all primary and backup DOCRs sets are at least 0.2 s. Similar results can be obtained

Table 3.10: Relays Optimal Settings with Different VI-FCL Characteristics

#	I_p (A)	Linear		Exponential		Parabolic	
		TDS (s)	K	TDS (s)	K	TDS (s)	K
1	0.3	0.1908	0.0047	0.1968	0.0254	0.2135	0.0859
2	0.3	0.2519	0.0000	0.2548	0.0000	0.2632	0.0000
3	0.3	0.1317	0.0275	0.1331	0.0297	0.1399	0.0560
4	0.3	0.3208	0.0206	0.3266	0.0270	0.3391	0.0330
5	0.6	0.0433	0.0000	0.0440	0.0000	0.0458	0.0000
6	0.6	0.2481	0.0024	0.2645	0.0465	0.2861	0.0821
7	0.3	0.0100	0.3682	0.0134	0.6895	0.0203	1.1540
8	0.3	0.2893	0.0000	0.3029	0.0233	0.3309	0.0721
9	0.3	0.1901	0.0000	0.1981	0.0321	0.1988	0.0000
10	0.3	0.2518	0.0000	0.2549	0.0000	0.2800	0.0745
11	0.3	0.1660	0.0992	0.1884	0.2204	0.1742	0.0967
12	0.3	0.2074	0.0000	0.2125	0.0000	0.2184	0.0000
13	0.3	0.0903	0.1493	0.1000	0.2435	0.0876	0.0580
14	0.3	0.2856	0.1428	0.2906	0.1363	0.2962	0.1278
15	0.3	0.0100	0.3650	0.0110	0.4744	0.0130	0.6500
16	0.3	0.3766	0.2711	0.3798	0.2531	0.3835	0.2321

for different fault resistances.

Table 3.13 displays the OPC results for $R_{flt} = 5\Omega$, with the DOCRs remaining in coordination with CTIs equal to or greater than 0.2 s. The results obtained demonstrate that a universal set of relay settings can be achieved and maintain OPC for a range of bolted fault to the highest possible resistive fault.

Table 3.11: Relays Total Operation Times at Different Fault Resistances with Different VI-FCL Characteristics

$R_{fit}(\Omega)$	#	Values (s)			
		Linear	Exponential	Parabolic	$\Delta T(\%)$ Linear vs Parabolic
0.1	F₁-F₈	23.9699	23.8288	24.0156	-
	F₉-F₁₆	23.8531	23.9063	23.6857	-
	F₁₇-F₂₄	23.7423	23.4705	23.6143	0.54
1	F₁-F₈	24.8788	24.4505	24.1612	2.88
	F₉-F₁₆	24.8586	24.4272	24.1316	2.92
	F₁₇-F₂₄	24.8397	24.4055	24.1045	2.96
3	F₁-F₈	26.1143	25.4173	24.7944	5.05
	F₉-F₁₆	26.0943	25.3983	24.7763	5.05
	F₁₇-F₂₄	26.0744	25.3792	24.7578	5.05
5	F₁-F₈	27.6319	27.9258	28.5982	-
	F₉-F₁₆	27.6100	27.9038	28.5746	-
	F₁₇-F₂₄	27.5879	27.8812	28.5503	-

Table 3.12: Operation Times in Seconds for Near-end and Far-end Bolted Faults

Employing adaptive VI-FCL Linear characteristic					
#	Primary	Backup	#	Primary	Backup
F₁	R ₁	R ₁₀	F₁₇	R ₁	R ₁₀
	0.6442	0.8542		0.6456	0.8561
	R ₂	R ₄		R ₂	R ₄
	0.8562	1.0681		0.8505	1.0605
F₃	R ₅	R ₃	F₁₉	R ₅	R ₃
	0.2282	0.4397		0.2330	0.4430
	R ₆	R ₈		R ₆	R ₈
	1.2690	1.4843		1.2493	1.4593
F₅	R ₉	R ₂	F₂₁	R ₉	R ₂
	0.6457	0.8558		0.6491	0.8603
	R ₁₀	R ₁₂		R ₁₀	R ₁₂
	0.8543	1.0804		0.8512	1.0612
F₈	R ₁₅	R ₁₃	F₂₄	R ₁₅	R ₁₃
	0.0208	0.2308		0.0213	0.2324
	R ₁₆	-		R ₁₆	-
	1.4440	-		1.3826	-

Table 3.13: Operation Times in Seconds for Near-end and Far-end Faults Considering 5Ω Fault Resistance

Employing adaptive VI-FCL Linear characteristic					
#	Primary	Backup	#	Primary	Backup
F₂	R ₃	R ₁	F₁₈	R ₃	R ₁
	0.5050	0.7150		0.5064	0.7166
	R ₄	R ₆		R ₄	R ₆
	1.1523	1.3645		1.1484	1.3584
F₄	R ₇	R ₅	F₂₀	R ₇	R ₅
	0.0262	0.2979		0.0263	0.3007
	R ₈	-		R ₈	-
	1.5785	-		1.5751	-
F₆	R ₁₁	R ₉	F₂₂	R ₁₁	R ₉
	0.4762	0.7158		0.4783	0.7197
	R ₁₂	R ₁₄		R ₁₂	R ₁₄
	1.4026	1.6133		1.3998	1.6098
F₈	R ₁₅	R ₁₃	F₂₄	R ₁₅	R ₁₃
	0.0264	0.2596		0.0265	0.2606
	R ₁₆	-		R ₁₆	-
	1.8136	-		1.8069	-

3.5 Conclusion

Droop-based IIDGs in islanded microgrids switch to current sources under faulty conditions, which could ruin protection coordination and microgrid stability. VI-FCLs are implemented within the IIDG control scheme to keep the IIDG voltage source model intact. The VI-FCLs are adaptively adjusted to protect inverters and optimally tune the DOCRs settings. An SCC algorithm that accommodates the VI-FCLs is developed to formulate an OPC program that involves two stages. Stage I is dedicated to the SCC algorithm and VI-FCLs sizing. In Stage II, one set of settings

that maintain relays coordination for a range of low to medium fault resistances is obtained. The studies also investigate the impact of various adaptive VI-FCL characteristics on the total operation time of protection relays. The results assure that the VI-FCLs act as a means for fault current discrimination, which facilitates OPC. Further, the adaptive VI-FCLs reduced the relays' total operation times in the presence of droop-based and current-controlled IIDGs and achieved coordination. The VI-FCLs represent a non-costly current limiting method, enable the IIDGs voltage source model to remain intact, and are beneficial to microgrid transient stability.

Chapter 4

Protection Coordination of IBIM Considering N-1 Contingency

Conventional distribution networks have a unidirectional power flow from a utility substation to loads. Traditional distribution systems have recently undergone tremendous changes that include integrating DGs derived from increasing interest in green energy and smart grids. These changes led to the emergence of microgrids [1]. To ensure a reliable operation of distribution networks, they should be adequately defended against faults using protection schemes that quickly isolate the minimum portion of faulty elements. This isolation reduces load interruption and equipment damage, and improves the power quality. Protective relays need to respond in a coordinated manner to ensure the microgrid reliable operation. OPC is usually solved for the original network topology with all lines, loads, and generation intact. However, power grids may experience contingencies due to transient events, e.g., generation or line outages. Low fault currents of IIDGs necessitate a sensitive and reliable protection scheme.

4.1 Adaptive Piecewise VI-FCL Design

As mentioned earlier, the fault severity can be inferred by measuring the IIDG output voltage, v_{o_k} . A smaller value of v_{o_k} indicates a more severe fault. The worst-case scenario is a bolted fault at the IIDG terminals, resulting in $v_{o_k} = 0$ and the maximum IIDG fault current, I_{DG}^{max} . Therefore, to limit IIDG fault current below 1.5 pu for this fault scenario, an impedance Z_{fcl_k} of a magnitude

$$|Z_{fcl_k}^{max}| = \frac{E_{o_k}}{I_{DG}^{max}} \quad (4.1)$$

is sufficient. where k is the IIDG index.

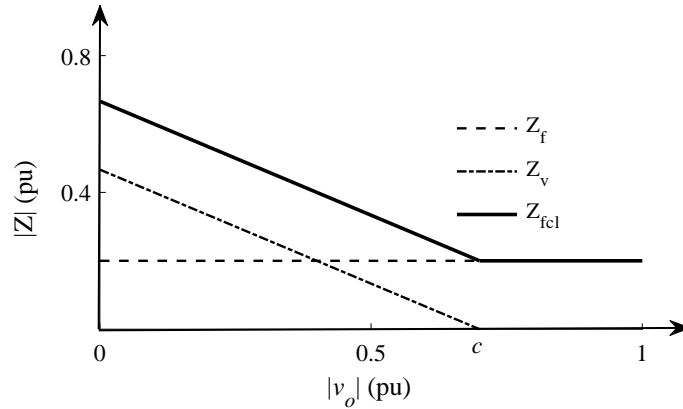


Figure 4.1: Impedance characteristic of the adaptive VI-FCL.

The characteristic displayed in Figure 4.1 is proposed. From Figure 4.1, it can be deduced

$$|Z_{fcl_k}| = \begin{cases} k_1 |v_{o_k}| + k_2, & 0 \leq |v_{o_k}| \leq c \\ Z_{f_k}, & c < |v_{o_k}| \leq 1 \end{cases} \quad (4.2)$$

The characteristic is a straight line from 0 to c and constant from c to 1.0. It is split into two segments to adapt to fault such that it is at its maximum value for bolted faults and zero at point c for the highest resistive faults. The constants k_1 and k_2 are the parameters of the droop characteristic in Figure 4.1. The slope k_1 is calculated using the line endpoints and assuming v_{o_k} dips to c pu. k_2 is equal to $|Z_{fcl_k}^{max}|$. With reference to Figure 4.1, Z_{v_k} diminishes for relatively high resistive faults. Thus, the constant c can be approximated by

$$c = E_{o_k} - Z_{f_k} I_{DG}^{max} \quad (4.3)$$

The proposed SCC method utilizes adaptive VI-FCLs to limit the IIDG fault currents contribution. The engagement of VI-FCLs prevents inverter current saturation, resulting in different short-circuit currents measured by DOCRs during low resistive faults, i.e., enhancing selectivity.

The fault is modeled by connecting the fault resistance as an additional branch

at the fault location. Then, the set of the nonlinear equations (3.9), (3.10), and (3.13)–(3.18) along with (4.2) of the VI-FCL are solved simultaneously as a minimization problem using the Levenberg-Marquardt algorithm [71]. The solution provides the voltages at each bus during the fault, and hence, the lines' and relays' fault currents are calculated.

4.2 Proposed Optimal Protection Coordination

The proposed OPC problem formulation is revisited in this section.

4.2.1 OPC Problem Formulation

The main goal of protection coordination is to minimize all relays' operation times for fast fault isolation while maintaining coordination of the assigned primary and backup relays. Hence, the objective function is defined as the sum of all relays' operation times due to their respective near-end, midline, and far-end fault, T , i.e.,

$$\min T = \sum_{r=1}^R \sum_{l=1}^L (t_{rl}^p + \sum_{b=1}^{BK} t_{rl}^{b_k}) \quad (4.4)$$

where l is the fault location with a total of L fault locations, r is the relay identifier, where R is the total number of relays. The subscript p denotes a primary relay, and b_k refers to a backup relay k for a primary relay p with BK as the total number of backup relays for each primary relay. t_{rl}^p is the operation time of relay r as a primary relay for fault location l and $t_{rl}^{b_k}$ is the operation time of the backup relay b_k of relay r for fault location l .

The operation time for the TCV characteristic is given by

$$t_{rl} = e^{(V_{rl}^f - 1)K_r} TDS_r \frac{A}{\left(\frac{I_{sc_{rl}}/CTR}{I_{pr}}\right)^B - 1} \quad (4.5)$$

where TDS_r , I_{pr} are the time dial setting and the pickup current for relay r , respectively. $I_{sc_{rl}}$ is the fault current in the primary of the current transformer (CT) for

fault location l . CTR is the current transformer ratio. V_{rl}^f is the phase voltage measured by relay r due to a fault at location l and K_r is a constant parameter. A and B are constants that determine the DOCR characteristic. Assuming the standard ITC characteristic, the constants A and B are 0.14 and 0.02, respectively.

For DOCR coordination, the relay settings and coordination constraints are included in the OPC program. The pickup current I_p is selected to have a minimum value of 30% higher than the rated load current of the respective protected line. Enforcing this condition ensures that DOCRs only trip when a fault occurs. The TDS of each relay is bounded by minimum and maximum values. Thus, the constraints imposed on I_p and TDS can be written as

$$I_{pr,min} \leq I_{pr} \leq I_{pr,max} \quad \forall r \quad (4.6)$$

$$TDS_{min} \leq TDS_r \leq TDS_{max} \quad \forall r \quad (4.7)$$

where $I_{pr,min}$ and $I_{pr,max}$ are the lower and upper bounds of I_{pr} , respectively, which are set at 1.3 and 1.5 of the nominal line current at the rated load. TDS_{min} and TDS_{max} denote the lower and upper bounds of TDS_r , respectively, with values of 0.01 and 1. Similarly, the parameter K has bounds defined by

$$K_{min} \leq K_r \leq K_{max} \quad \forall r \quad (4.8)$$

where K_{min} and K_{max} are the lower and upper bounds of K_r . K_{min} and K_{max} are set at 0 and 4.0, respectively.

A coordination time that represents the time delay between the operation of a primary relay and its backup relay, known as CTI, must be preserved for all fault scenarios. The CTI is set at 200 ms to adhere to the IEEE Standard 242-2001. The 200 ms includes circuit breaker opening time and a safety factor for CT saturation and relay setting errors. Thus, the following constraint is defined

$$t_{crl}^{bk} - t_{crl}^p \geq CTI \quad \forall c, [l, r, k] \quad (4.9)$$

where t_{clr}^p and $t_{clr}^{b_k}$ are the operation time of the primary relay r and its backup relay b_k for a fault at location l when the microgrid topology c is triggered. The relay constraints remain the same for the islanded topology with all IIDGs and lines engaged and any IIDG outage. In contrast, every topology formed due to a line outage has different set of constraints corresponding to the faults considered in the resulting topology. The typical operation time of a DOCR is one cycle to three cycles [75]. A constraint on the minimum relay operation time is imposed as

$$t_{clr}^p, t_{clr}^{b_k} \geq t_{min} \quad \forall c, [l, r, k] \quad (4.10)$$

where t_{min} is the minimum relay operation time. t_{min} is set to 20 ms. This study considers phase relays subjected to three-phase faults for phase overcurrent protection [6], [39]–[45].

SBDGs have high fault currents; therefore, they do not introduce issues to overcurrent protection schemes. On the contrary, islanded microgrids dominated by IIDGs face protection challenges due to their limited fault current contributions. Therefore, in an islanded microgrid with both SBDGs and IIDGs, DOCRs measure different levels of fault currents based on the locations and types of DGs. To explain this point, Figure 4.2 displays a four-bus islanded microgrid with two IIDGs and an SBDG connected to bus 1. Three cases can be extracted for the measured currents by the relays: (i) A relay only measures an SBDG fault current (R_1) (ii) A relay only measures an IIDG fault current (R_3 and R_5) (iii) A relay measures a mix of the SBDG and IIDG fault currents (R_2 , R_4 , and R_6).

The VI-FCL effect would be diminished if the fault current is dominated by the SBDG fault current, i.e., Cases 1 and 3. In these cases, networks do not face issues with overcurrent protection due to the high fault current level. On the other hand, the VI-FCL is beneficial in Case 2.

4.2.2 OPC Program for IIDGs with VI-FCLs

The conventional OPC formulation involves calculating short-circuit currents assuming SGs as the primary power source [4]–[6], [39]. On the contrary, the proposed OPC

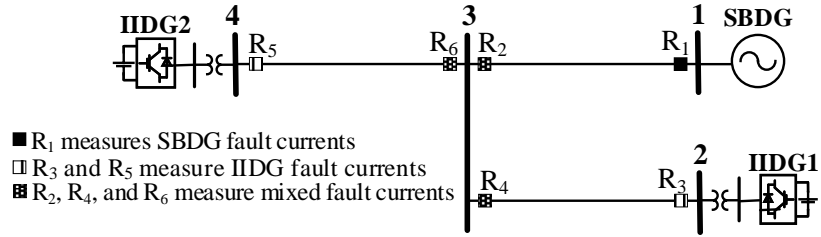


Figure 4.2: A 4-bus microgrid with two IIDGs and one SBDG.

formulation considers limiting the IIDGs fault currents using an adaptive VI-FCL. Thus, it protects the inverter's switches from overcurrent and prevents reference current saturation. In addition, the inclusion of the VI-FCL keeps the voltage source model of IIDGs intact during faults and enhances the microgrid transient stability. Further, the proposed adaptive VI-FCL has the advantage of furnishing more tangible fault current levels depending on fault severity, enhancing protection selectivity.

The IIDG is modeled as a voltage source behind an impedance for short-circuit analysis, owing to the employment of the proposed VI-FCL. This impedance includes the proposed VI-FCL impedance and the IIDG filter impedance. The algorithm starts by constructing a modified bus admittance matrix Y_{bus}^f , which comprises the fault location as a virtual bus. It is formulated for each topology resulting from an N-1 contingency and each fault location in the test microgrid. The optimization program unfolds two stages, as demonstrated by the flow chart in Figure 4.3. In Stage I, the VI-FCL voltage equations and the power mismatch equations are solved simultaneously to obtain bus voltages during faults conducted on virtual fault buses. The virtual fault buses are selected to represent near-end, midline, and far-end locations. The proposed OPC formulation can be applied for microgrids hosting droop-based IIDGs with VI-FCLs and current-controlled IIDGs without VI-FCLs. The current-controlled IIDGs are interpreted in the power mismatch equations as negative loads with powers equal to the pre-fault settings if the IIDG terminal voltage is higher than $1/I_{DG}^{max}$ pu [24]. Otherwise, the current-controlled IIDGs are modeled as constant current sources with $i_{ok} = I_{DG}^{max}$ pu. MATLAB's Levenberg-Marquardt built-in algorithm is used to solve

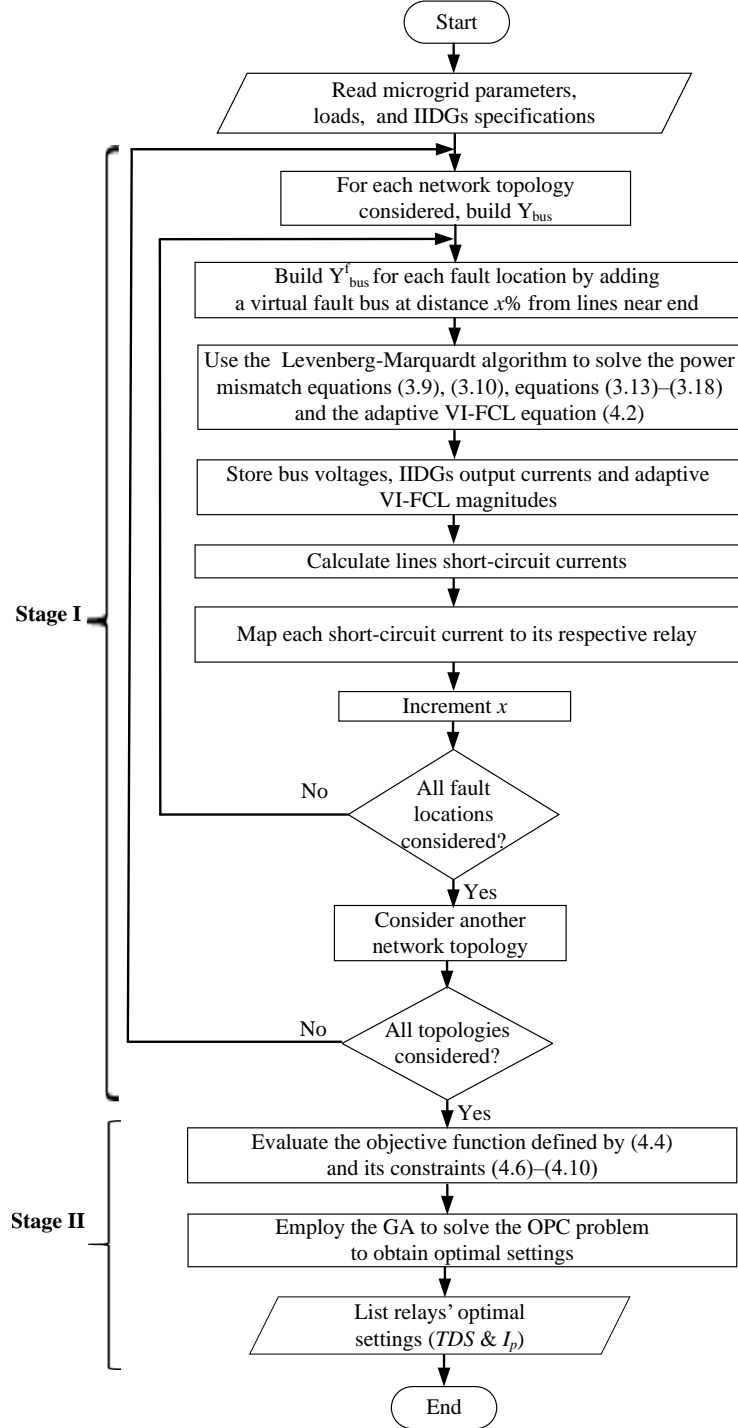


Figure 4.3: Flow chart of the proposed OPC program.

for bus voltages employing the SCC algorithm in subsection 3.2.2. The algorithm restarts for each fault location. A row vector with all bus voltages for different fault

locations considering bolted faults is obtained. The bus voltages obtained during the fault are used to calculate the lines' short-circuit currents. A map-matrix is then used to map each short-circuit current to its respective primary and backup relays.

4.3 Microgrid Adequacy and Models Under Contingencies

This section discusses microgrid adequacy, which is needed to comply with the N-1 criterion. Further, it explains the different OPC models considered in this study.

4.3.1 Microgrid Adequacy

Adequacy is an assessment of the available generation and its sufficiency to supply loads and network losses. The microgrid should be capable of supplying its planned demand and losses under all operating conditions, including contingencies such as lines and IIDG outages. In such events, contingency planning decisions are implemented to shed loads when there is a power inadequacy, e.g., an IIDG planned or transient outage or switching off a part of the microgrid under a scheduled or a transient line contingency. The contingency planning decisions are mainly enforced to ensure islanded microgrid's successful operation. These constraints include maintaining the voltage profile between the permissible limits (i.e., 0.95–1.05 pu) and providing sufficient generation to supply the microgrid loads and losses.

To elaborate on microgrid adequacy, the microgrid displayed in Figure 4.4(a) is considered. It has two IIDGs rated at 1.0 MVA connected to buses 1 and 5. The loads displayed are represented by their rated powers, i.e., 0.4 MVA at 0.9 power factor. For instance, the contingency resulting from IIDG2 being out of service is shown in Figure 4.4(b), which requires the shedding of the loads at buses 4 and 5 since IIDG1 cannot adequately supply the total microgrid load and network losses. On the other hand, as illustrated by Figure 4.4(c), the microgrid topology splits into two separate sub-microgrids, A and B, with the removal of Line 4-5 due to a transient contingency

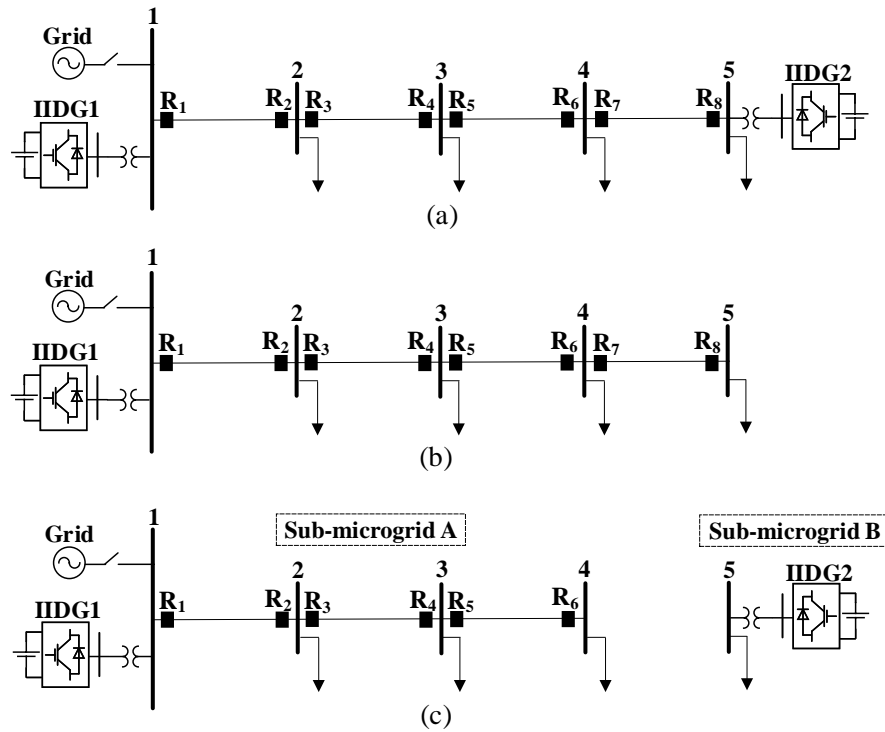


Figure 4.4: Network topologies of a sample microgrid: (a) Islanded topology. (b) IIDG2 outage topology. (c) Line 4-5 outage topology.

or scheduled maintenance. IIDG1 cannot supply the total demand of sub-microgrid A. Therefore, the load at bus 4 should be shed to ensure the successful operation of sub-microgrid A. Sub-microgrid B comprises only IIDG2, which supplies only the load at bus 5. In other words, Line 4-5 outage makes IIDG1 remain connected to the distribution feeder and IIDG2 be isolated. The OPC formulation in Model 3 simultaneously considers all topologies resulting from all single IIDG and line outages as well as the main topology. Therefore, a single set of relays' settings is obtained utilizing Model 3, which works for all possible topologies.

4.3.2 Models Considering Contingencies

The islanded microgrid used for testing is displayed in Figure 3.8. Each DOCR has a continuous TDS and a range for I_p . The CTR for each DOCR is 1000/5. The ratio is chosen such that the minimum pickup current is higher than the rated current of the

Table 4.1: OPC Models Description

Model	Topologies considered
1	Islanded mode topology
2	Islanded mode topology + all topologies due to single IIDG contingencies
3	Islanded mode topology + all topologies due to single IIDG contingencies + all topologies due to single line contingencies

respective line. A short-circuit analysis is performed for faults (F_1 – F_{24}) that involve the fault resistance at near-end, midline, and far-end as shown in Figure 3.8, for the islanded microgrid with no outages and all other possible outages. Each line requires two primary DOCRs because of the bidirectional flow of the short-circuit currents. Each primary relay is backed-up by one DOCR.

It is worth mentioning that the OPC for microgrid topologies resulting from different outage contingencies has been investigated in the literature only for SBDGs. This study considers all single outages (line and IIDG contingency) in multi-IIDG islanded microgrids. The bus-admittance matrix is modified to reflect the contingency by eliminating the parameters corresponding to the outage. Then, the modified matrices are used to calculate the short-circuit currents in the resulting topologies. The models used are listed in Table 4.1. Model 1 considers only the islanded topology, whereas Model 2 accounts for the islanded topology and all topologies resulting from single IIDG contingencies.

The proposed model (Model 3) is the most inclusive, where the islanded topology and all possible single outages are considered. The objective function defined by (4.4) is used for all models for fair performance evaluation.

Although the dissertation focuses on the islanded operation of microgrids, the proposed OPC method can be applied to the grid-connected mode. To accommodate the grid-connected mode, bus 1 is modeled as a slack bus (i.e., $V_1 = 1.0\angle 0^\circ$ pu) and is integrated into the proposed SCC as an equality constraint. The relays' settings should

be changed when switching between the islanded and grid-connected modes due to the change in the fault current levels. Therefore, relays can be equipped with dual trip characteristics, namely islanded and grid-connected trip characteristics. Switching between the relays' characteristics can be achieved using an islanding detection technique or a communication link.

4.4 Results and Analysis

This section presents the OPC results obtained using the three models in Table 4.1. Then, a thorough investigation of the results obtained from each model is conducted. Further, the relays' operation times are obtained for faults on all lines of the test microgrid. The test microgrid in Figure 3.8 is used to conduct two case studies.

Case I: Microgrid Powered only by Droop-based IIDGs

1) *Optimal DOCRs Settings at Different Topologies:* The network contingencies are interpreted through a set of constraints corresponding to the contingency considered. These constraints are then employed by the different OPC models while solving for the optimal settings, employing the ITC. Table 4.2 displays the optimal TDS and I_p settings for all DOCRs of the test microgrid using the ITC. The solution of each model leads to different optimal settings. Thus, the OPC based on the original topology cannot meet the N-1 criterion because each model has a different set of settings.

Table 4.3 displays the sum of relays' operation times for near-end, midline, and far-end faults for each model. The total operation times follow the same pattern, in which the times decrease with distance from the near-end. The total operation time obtained for Model 3 is higher than its corresponding total operation times achieved for Models 1 and 2. This higher total operation time reflects that more cases have been considered in Model 3 to account for all possible microgrid topologies. The total operation time achieved for Model 2 is slightly higher than that obtained for Model 1. This slight difference can be interpreted as no significant variation in short-circuit current levels with the single IIDG outage.

The miscoordination between primary and backup relay sets occurs when the

Table 4.2: Relays Optimal Settings for the Test Microgrid (Case I)

Relay	Model 1		Model 2		Model 3	
	TDS	I_p	TDS	I_p	TDS	I_p
	(s)	(A)	(s)	(A)	(s)	(A)
R₁	0.1080	0.5291	0.1642	0.3010	0.1639	0.3000
R₂	0.0698	0.9503	0.2345	0.3090	0.2395	0.3001
R₃	0.1074	0.3199	0.1123	0.3010	0.1121	0.3000
R₄	0.1560	0.6152	0.2928	0.3010	0.5367	0.3001
R₅	0.0466	0.4393	0.0610	0.3010	0.0605	0.3028
R₆	0.4812	0.3000	0.3488	0.3010	0.4307	0.4805
R₇	0.0100	0.3000	0.0101	0.3010	0.0100	0.3000
R₈	0.2867	0.3335	0.3819	0.3101	0.4541	0.4765
R₉	0.0486	0.9979	0.1864	0.3013	0.1748	0.3316
R₁₀	0.1421	0.5296	0.2159	0.3010	0.2158	0.3002
R₁₁	0.1308	0.3177	0.1353	0.3010	0.1346	0.3004
R₁₂	0.1582	0.3000	0.2465	0.3011	0.2464	0.3002
R₁₃	0.0493	0.5692	0.0723	0.3010	0.0723	0.3001
R₁₄	0.1899	0.3000	0.2972	0.3011	0.1637	0.4666
R₁₅	0.0100	0.3000	0.0101	0.3011	0.0100	0.3000
R₁₆	0.1634	0.3939	0.1382	0.5611	0.4921	0.4281

Table 4.3: Sum of Operation Times for Bolted Faults in the Test Microgrid (Case I)

#	Values (s)		
	Model 1	Model 2	Model 3
F₁–F₈	27.0816	31.9437	46.8655
F₉–F₁₆	26.9505	31.6881	46.4431
F₁₇–F₂₄	26.7987	31.3949	45.9166

backup relay operates before the primary relay for a given fault or the backup relay operates after the primary relay but with a time delay less than the defined CTI. If a backup relay does not operate for a fault in its assigned zone, it also leads to

miscoordination. For instance, a bolted fault at F_9 on the test microgrid with Line 3-4 outage results in a fault current of 2.3579 pu passing through the primary relay R_1 and 2.3720 pu through its backup relay R_{10} . Using Model 1's optimal settings, R_1 and R_{10} operate in 0.6616 s and 0.8581 s, respectively. Thus, R_{10} operates after R_1 but with a time delay of 196.5 ms, which is less than the CTI. Using Model 2 optimal settings relays R_1 and R_{10} operate in 0.6671 s and 0.8649 s, respectively. The backup relay operates after the primary relay with a time gap of 197.8 ms, less than the CTI. However, using Model 3 (i.e., the proposed OPC model), optimal settings relays R_1 and R_{10} operate in 0.6646 s and 0.8723 s, respectively, coordinated with $CTI = 207.8$ ms.

An example of a backup relay that does not operate is R_5 , which backs up R_7 for any faults on lines 3-4 or 4-5 with Line 2-3 out of service. This issue happens because R_5 is connected to an open end, i.e., R_5 barely sees a fault current. Thus, it is not considered in the coordination constraints of Model 3. Also, unfeasible constraints under some lines' outages are excluded. For example, considering Line 1-2 outage, the test microgrid splits into two sub-microgrids. The upper feeder has a unidirectional power flow; therefore, only the upstream relays (R_5 and R_7) are considered for coordination constraints. The optimal relays' settings obtained by solving the OPC problem are used to test the relay sets coordination for all topologies in Table I. This analysis highlights the number of coordination violations resulting from considering each model's settings. All violations are listed in Table 4.4. The violations resulting from using Model 1 are much higher than those resulting from using Model 2. Utilizing Model 3 results in proper coordination for all DOCR pairs in each topology. Therefore, it is the best option for the OPC.

2) *Relays' Operation Times:* To calculate the operation times of each DOCR, short-circuit currents passing through each relay obtained in Stage I of the OPC program are needed. Besides, relay's optimal settings TDS and I_p attained in Stage II utilizing the proposed model (Model 3) are employed. The operation times of the assigned DOCRs are shown in Table 4.5 for selected near-end and far-end faults for the original islanded topology. Similar results can be obtained for all other topolo-

Table 4.4: Coordination Violations for Bolted Faults in the Test Microgrid (Case I)

Topology	Number of coordination violations		
	Model 1	Model 2	Model 3
Islanded	0	0	0
IIDG1 outage	16	0	0
IIDG2 outage	13	0	0
IIDG3 outage	6	0	0
IIDG4 outage	1	0	0
Line 1-2 outage	9	0	0
Line 2-3 outage	9	0	0
Line 3-4 outage	10	1	0
Line 4-5 outage	15	0	0
Line 1-6 outage	8	3	0
Line 6-7 outage	2	0	0
Line 7-8 outage	1	0	0
Line 8-9 outage	1	0	0
Total violations	91	4	0

gies. The results reveal that the primary and backup DOCRs sets remain correctly coordinated with a CTI of at least 200 ms under all considered topologies.

Severe voltage drops are unavoidable in islanded microgrids during short-circuit faults with all current limiting methods, including VI-FCLs. Despite the voltage drop during faults, the relays' operation times mainly depend on the fault current magnitude. The successful operation of the proposed OPC is reported at different fault resistances in Table 4.6. The table displays the assigned relays operation times during fault F_4 on the upper feeder for $R_{flt} = 1 \Omega$, $R_{flt} = 5 \Omega$, and $R_{flt} = 10 \Omega$. The relays' operation times are obtained using the optimal settings of Model 3. The primary and backup relay sets remain coordinated with CTIs of at least 200 ms. The results demonstrate that a single set of relay settings can be obtained and guarantees

Table 4.5: Operation Times for Selected Near-end and Far-end Bolted Faults in the Test Microgrid (Case I)

Relays operation times (s)					
#	Primary	Backup	#	Primary	Backup
F₁	R ₁	R ₁₀	F₁₇	R ₁	R ₁₀
	0.6632	0.8735		0.6658	0.8769
	R ₂	R ₄		R ₂	R ₄
	0.9703	2.1702		0.9658	2.1611
F₂	R ₃	R ₁	F₁₈	R ₃	R ₁
	0.4562	0.6660		0.4582	0.6686
	R ₄	R ₆		R ₄	R ₆
	2.1601	2.4631		2.1466	2.4451
F₄	R ₇	R ₅	F₂₀	R ₇	R ₅
	0.0387	0.2492		0.0344	0.2533
	R ₈	-		R ₈	-
	5.4003	-		5.3248	-
F₆	R ₁₁	R ₉	F₂₂	R ₁₁	R ₉
	0.4803	0.7562		0.4548	0.7659
	R ₁₂	R ₁₄		R ₁₂	R ₁₄
	1.6796	1.9613		1.6644	1.9385
F₇	R ₁₃	R ₁₁	F₂₃	R ₁₃	R ₁₁
	0.2442	0.4545		0.2427	0.4516
	R ₁₄	R ₁₆		R ₁₄	R ₁₆
	1.9459	5.0545		1.8455	4.8976

optimal coordination of DOCRs under an N-1 contingency (i.e., considering IIDG and line outages). The operation times increase with the increase of R_{flt} . This increase in operation times is expected due to the lower short-circuit currents measured by DOCRs, and following the ITC, the relays take longer times to operate. It is worth mentioning that using constant VI-FCLs, feasible OPC solutions are only obtained for severe faults (i.e., when the fault resistance does not exceed 2Ω). On the con-

Table 4.6: Operation Times for a Three-phase Fault at F_4 with Selected Fault Resistances (Case I)

R_{ft} (Ω)	Relays operation times (s)			
	Primary		Backup	
1	R ₇	0.0325	R ₅	0.2476
	R ₈	4.9392	-	-
5	R ₇	0.0349	R ₅	0.2867
	R ₈	5.3897	-	-
10	R ₇	0.0396	R ₅	0.3674
	R ₈	6.3405	-	-

trary, utilizing the adaptive VI-FCL attains the OPC feasibility up to 10 Ω . Table 4.6 demonstrates the ability of adaptive VI-FCLs to enhance the sensitivity of the proposed OPC.

Model 3 increases the summation of the relays' operation times because it considers more topologies. However, the relay's individual operation time is relatively low due to the optimal protection coordination. A further reduction in the relays' operation times can be achieved using adaptive protection schemes, but it requires communication. Alternative relay characteristics can be used to further reduce the relays' operation times, such as the TCV characteristic [73]. This alternative provides a non-assisted protection scheme.

The OPC problem is also solved using Model 3, employing the TCV characteristic. As displayed in Table 4.7, the TCV characteristic with the proposed model results in a significant reduction of 44% in the total relays' operation time. Tables 4.8 and 4.9 report the optimal settings and operation times for selected DOCRs of the test microgrid utilizing the TCV characteristic. Several primary relays on the upper feeder and the lower feeder have a significant reduction in their operation times, i.e., R_4 , R_6 , R_8 , and R_{16} .

Case II: Microgrid Powered by Droop-based and Current-controlled IIDGs

In this case study, two current-controlled IIDGs rated at 2-MVA each replace

Table 4.7: ITC vs TCV characteristic (Case I)

	ITC		TCV
OPC	achieved	achieved	
#	Sum of operation times (s)	Reduction percentage	
F1–F8	46.6466	26.2453	44.00 %
F9–F16	46.2260	26.3490	43.27 %
F17–F24	45.7019	25.4867	44.49 %

Table 4.8: Relays Optimal Settings for the Test Microgrid (Case I)

Using TCV characteristic							
#	<i>TDS</i>	<i>I_p</i>	<i>K</i>	#	<i>TDS</i>	<i>I_p</i>	<i>K</i>
	(s)	(pu)			(s)	(pu)	
R₁	0.2743	0.3	0.1521	R₉	0.9986	0.3	1.9615
R₂	1.0000	0.3	1.6781	R₁₀	0.8740	0.3	1.1496
R₃	0.7587	0.3	1.4306	R₁₁	0.2933	0.3	1.0169
R₄	1.0000	0.3	1.4518	R₁₂	0.4842	0.3	0.9011
R₅	0.0976	0.6	1.1132	R₁₃	0.5182	0.3	2.2985
R₆	0.3737	0.6	0.7958	R₁₄	0.9893	0.3	1.4898
R₇	0.0109	0.3	0.7102	R₁₅	0.1634	0.3	3.5545
R₈	1.0000	0.3	1.6341	R₁₆	1.0000	0.3	1.3985

IIDG3 and IIDG4 in the test microgrid. Firstly, the OPC problem is solved when the microgrid is fully loaded and the current-controlled IIDGs inject their rated powers before faults. Secondly, the OPC problem is solved when the microgrid is lightly loaded (i.e., 20% of the rated load) and the current-controlled IIDGs inject 20% of their rated powers. The OPC settings separately obtained for the two scenarios are different. The pre-fault generation condition for current-controlled IIDGs does affect the OPC because these IIDGs do not share the fault current as in the case of

Table 4.9: Operation Times for Selected Near-end and Far-end Bolted Faults in the Test Microgrid (Case I)

Relays operation times (s)					
Using TCV characteristic					
#	Primary	Backup	#	Primary	Backup
F₂	R ₃	R ₁	F₁₈	R ₃	R ₁
	0.7658	0.9700		0.7776	0.9773
	R ₄	R ₆		R ₄	R ₆
	0.9793	1.1795		0.9586	1.1557
F₃	R ₅	R ₃	F₁₉	R ₅	R ₃
	0.2346	0.7774		0.2400	0.7904
	R ₆	R ₈		R ₆	R ₈
	1.1491	1.3723		1.0940	1.2946
F₄	R ₇	R ₅	F₂₀	R ₇	R ₅
	0.0212	0.2404		0.0216	0.2652
	R ₈	-		R ₈	-
	1.2802	-		1.2268	-
F₇	R ₁₃	R ₁₁	F₂₃	R ₁₃	R ₁₁
	0.2008	0.4007		0.2160	0.4180
	R ₁₄	R ₁₆		R ₁₄	R ₁₆
	1.4934	1.6896		1.2382	1.5429
F₈	R ₁₅	R ₁₃	F₂₄	R ₁₅	R ₁₃
	0.0203	0.2202		0.0292	0.2592
	R ₁₆	-		R ₁₆	-
	1.5161	-		1.3586	-

droop-based IIDGs. Therefore, the OPC should simultaneously consider the worst-case pre-fault operating scenarios in the presence of current-controlled IIDGs. Table 4.10 shows the optimal TDS and I_p settings for all DOCRs considering the worst pre-fault operating scenarios. The displayed results are obtained utilizing Model 3 and the ITC. Table 4.11 lists the operation times of the assigned DOCRs for selected

Table 4.10: Relays Optimal Settings for the Test Microgrid (Case II)

Relay	TDS (s)	I_p (A)
R₁	0.1345	0.3002
R₂	0.1781	0.3000
R₃	0.0356	0.6951
R₄	0.2220	0.3004
R₅	0.0234	0.6098
R₆	0.2663	0.3000
R₇	0.0100	0.3000
R₈	0.3476	0.3063
R₉	0.1355	0.3000
R₁₀	0.1771	0.3001
R₁₁	0.1356	0.3003
R₁₂	0.1061	0.7565
R₁₃	0.0727	0.3000
R₁₄	0.3005	0.3001
R₁₅	0.0100	0.3000
R₁₆	0.3494	0.3001

near-end and far-end faults for the original islanded topology. These results confirm the effectiveness of the proposed OPC when the microgrid is powered by a mix of

Table 4.11: Operation Times for Selected Near-end Bolted Faults for the Test Microgrid (Case II)

		Rated Load		Light Load (20%)	
Relays operation times (s)					
#	Primary	Backup	#	Primary	Backup
F₃	R ₅	R ₃	F₁₉	R ₅	R ₃
	0.2396	0.4465		0.2469	0.4511
	R ₆	R ₈		R ₆	R ₈
	1.2979	1.5072		1.2837	1.5072
F₄	R ₇	R ₅	F₂₀	R ₇	R ₅
	0.0353	0.2466		0.0335	0.2389
	R ₈	-		R ₈	-
	1.5072	-		1.5072	-
F₅	R ₉	R ₂	F₂₁	R ₉	R ₂
	0.6734	0.8847		0.6832	0.8976
	R ₁₀	R ₁₂		R ₁₀	R ₁₂
	0.8641	1.0773		0.8542	1.0773
F₆	R ₁₁	R ₉	F₂₂	R ₁₁	R ₉
	0.4759	0.6828		0.4520	0.6717
	R ₁₂	R ₁₄		R ₁₂	R ₁₄
	1.0773	1.2865		1.0773	1.2865
F₇	R ₁₃	R ₁₁	F₂₃	R ₁₃	R ₁₁
	0.2435	0.4519		0.2413	0.4494
	R ₁₄	R ₁₆		R ₁₄	R ₁₆
	1.2865	1.4957		1.2865	1.4957
F₈	R ₁₅	R ₁₃	F₂₄	R ₁₅	R ₁₃
	0.0334	0.2412		0.0333	0.2413
	R ₁₆	-		R ₁₆	-
	1.4957	-		1.4957	-

droop-based and current-controlled IIDGs.

4.5 Conclusion

In designing a reliable OPC scheme, it is essential to consider all possible microgrid topologies that may result from operation conditions and transients. This chapter considers the islanded topology of a microgrid and all microgrid topologies that result from single IIDG and line contingencies. An SCC method that utilizes VI-FCLs to limit IIDGs fault currents is proposed. The VI-FCLs contribute to microgrid transient stability, keep the IIDG voltage model intact, and represent a cost-effective current limiting. The VI-FCLs are selected to be adaptive to enhance the relay sensitivity to faults with relatively high fault resistances. The OPC program comprises two stages. In Stage I, the fault currents measured by DOCRs are calculated. Stage II aims at obtaining the optimal settings of the DOCRs. The typical OPC formulation that considers no contingencies results in 91 violations. However, including single IIDG outages reduces OPC violations by 95%. Further, no violations are obtained when all single IIDG and line outages are considered. As opposed to the ITC characteristic, the TCV reduces the total relays' operation time by 44%. The results confirm that DOCRs in an islanded microgrid can have a single set of optimal settings to maintain relays' coordination under all microgrid topologies resulting from different N-1 contingencies.

Chapter 5

Harmonic-based Dual-setting

Protection for IBIM

IIDGs limit their output fundamental currents to 150% of the inverter's rated current [30]. These low fault currents have an adverse impact on the available protection devices such as overcurrent relays and render their coordination troublesome or infeasible [1], [69]. Moreover, the IIDG controllers adversely impact the existing commercial directional elements [69]. Thus, a reliable relaying scheme is required.

5.1 Proposed Harmonic-based Protection

This chapter proposes a protection scheme that triggers a harmonic voltage generation at the inverter's terminals upon fault detection. Consequently, harmonic current flows from IIDGs to the fault location. The deliberately generated harmonic currents are decoupled from the fundamental currents. Further, the decoupled harmonic currents can be discriminated from load harmonic currents. Then, HDOCRs are utilized to measure the harmonic voltages and currents to achieve OPC for islanded microgrids.

5.1.1 IIDG controller and harmonic generation characteristic

The modulation index of the IIDG is augmented with a harmonic modulation index, m^h , before being fed to the pulse width modulation (PWM) block, as illustrated by Figure 5.1(a). m^h determines the magnitude of the adaptive generated harmonic voltage at the inverter's terminals and h pertains to the order of the individual injected harmonic.

As shown in Figure 5.1(a), neither the magnitude nor the angle of the generated harmonic voltage is regulated by the IIDG droop controller [Figure 5.1(b)] or PQ

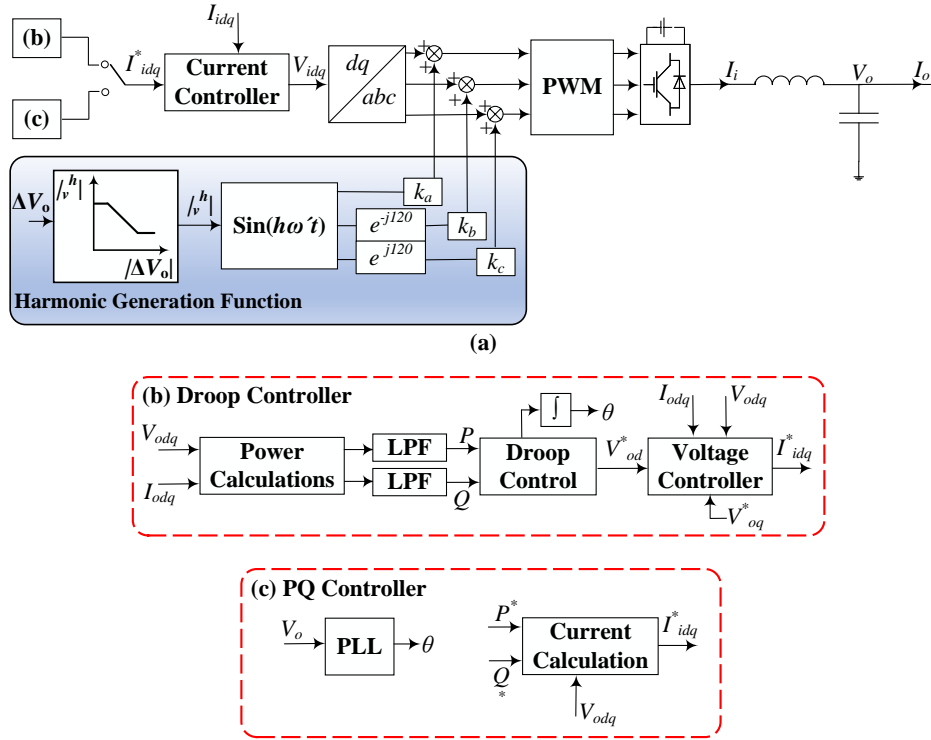


Figure 5.1: The IIDG control block diagram with the proposed adaptive harmonic generation.

controller [Figure 5.1(c)]. By setting the angular frequency, ω' , and magnitude of m^h , two decoupled layers (i.e., fundamental and harmonic) are formed during faults. Therefore, the HDOCRs operate based on the measured harmonic currents that are not impacted by the IIDGs' limited fundamental current. On the other hand, the IIDG controller limits the inverter's current in the fundamental layer, resulting in a constant current source model for the IIDG.

Upon fault detection, binary variables $k_{a,b,c}$ are set at 1.0, activating the respective harmonic generation system as shown in Figure 5.1. These variables switch to zero once the fault is cleared to deactivate the harmonic generation system. Therefore, the harmonic injection exists only during faults. HDOCRs are then coordinated based on the measured harmonic voltages and currents. It is worth mentioning that injected harmonics have a minor effect on power quality since the fault condition typically lasts for a short time. Other system applications, such as microgrid islanding detec-

tion, have employed limited harmonics injection for a short period of time [79], [80]. Further, the load harmonics have a phase angle of $h\delta$, i.e., zero-sequence third-order harmonics. In contrast, the proposed harmonic injection system injects synthetic harmonics, which are positive-sequence and has a phase angle of δ . Thus, the proposed HDOCRs can differentiate between load harmonics and generated harmonics.

Fault currents change based on fault severity, i.e., the fault resistance and location. Establishing a deliberate harmonic current flow during faults can be attained by a constant or adaptive harmonic voltage generation. However, the constant harmonic voltage may fail to produce sensible fault currents for a broader range of fault resistances, especially at the farthest point from the IIDG's terminals. This study proposes a scheme that guarantees reliable protection coordination for higher fault resistances in islanded microgrids. Employing an adaptive harmonic voltage generation produces higher harmonic fault currents for high resistive faults.

The harmonic voltage is adapted to faults such that its maximum and minimum magnitudes are generated during the highest resistive faults at the feeder end and for bolted faults at the IIDG terminals, respectively. The sample microgrid displayed in Figure 5.2 is considered to elaborate on the harmonic voltage generation. Figure 5.3 depicts the equivalent circuit of the sample microgrid in the harmonic layer. In Figure 5.3, v_1^h and v_2^h denote the generated harmonic voltages at the IIDGs' inverter terminals. Z_f , Z_{tr} , and Z_{line} are the filter, transformer, and line impedances, respectively. The superscript h indicates harmonic quantities. In that figure, the fault F may result in an unappreciable harmonic fault current measured by relay R_2 , considering a high resistive fault. In this case, I_{F2}^h is expected to be low because IIDG2 is far away from the fault location.

Fault severity can be inferred by sensing the voltage sag, ΔV_o , in the fundamental layer at the IIDG's terminals, i.e.,

$$\Delta V_o = V_{min} - V_o^f \quad (5.1)$$

where V_{min} is the lowest normal IIDG output voltage and V_o^f denotes the IIDG

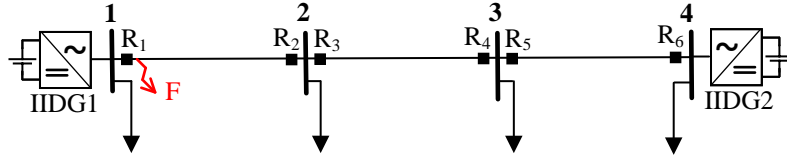


Figure 5.2: A sample microgrid.

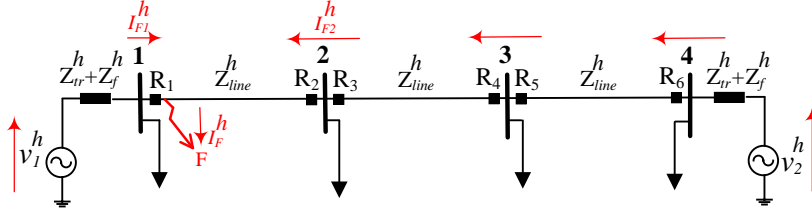


Figure 5.3: Microgrid equivalent model in the harmonic layer.

output voltage during faults, which is lower than V_{min} . V_{min} is set at 0.88 pu as recommended by the IEEE Standard 1547 [15]. V_o is obtained using PSCAD/EMTDC simulations. The extreme fault scenarios are bolted and high resistive faults at the farthest point from the IIDG's terminals, resulting in the maximum and minimum ΔV_o , respectively. Promoting higher harmonic voltage generation at the IIDG's terminals that adapt to fault severity leads to higher harmonic currents at high resistive faults. Three harmonic voltage characteristics are proposed (i.e., linear, piecewise linear, and quadratic), tested, and compared as displayed in Figure 5.4 and defined respectively by (5.2)–(5.4).

$$|v^h| = k_1 |\Delta V_o| + \lceil v^h \rceil \quad (5.2)$$

$$|v^h| = \begin{cases} \frac{y_1 - \lceil v^h \rceil}{\Delta_1} |\Delta V_o| + \lceil v^h \rceil, & 0 \leq |\Delta V_o| \leq 0.2 \\ \frac{y_2 - y_1}{\Delta_2} (|\Delta V_o| - 0.2) + y_1, & 0.2 < |\Delta V_o| \leq 0.5 \\ \frac{y_3 - y_2}{\Delta_3} (|\Delta V_o| - 0.5) + y_2, & 0.5 < |\Delta V_o| \leq 0.7 \\ \frac{\lceil v^h \rceil - y_3}{\Delta_4} (|\Delta V_o| - 0.7) + y_3, & 0.7 < |\Delta V_o| \leq 0.88 \end{cases} \quad (5.3)$$

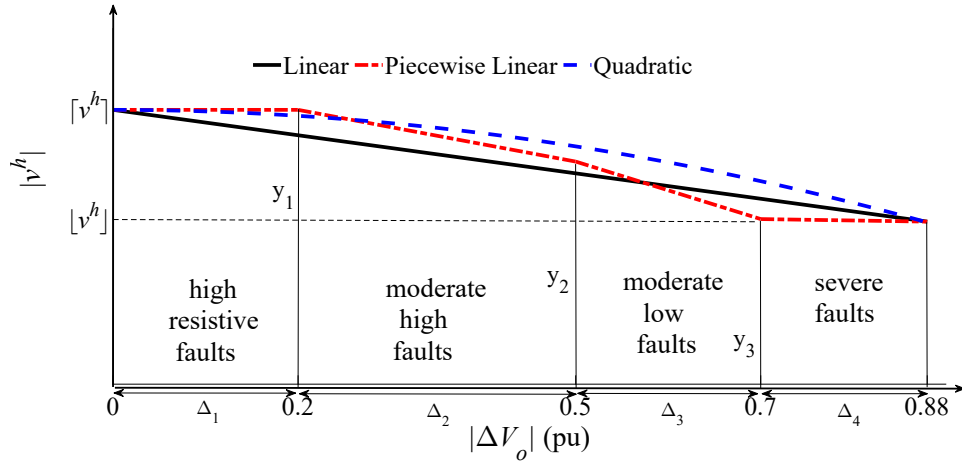


Figure 5.4: Proposed adaptive harmonic voltage characteristics.

$$|v^h| = k_2|\Delta V_o|^2 + k_3|\Delta V_o| + k_4 \quad (5.4)$$

where $|v^h|$ is the generated harmonic voltage magnitude at the inverter's terminals. The slope, k_1 , of the linear characteristic is calculated using the endpoints representing the minimum, $[v^h]$, and maximum, $[v^h]$, magnitudes of v^h , respectively. Unlike the linear characteristic, the piecewise linear characteristic assumes different line segments based on fault harshness, i.e., high, moderate, or severe. The slope for each line segment is calculated using its endpoints having the ordinates y_1 , y_2 , and y_3 , as indicated in Figure 5.4. The constants k_2 , k_3 , and k_4 are the quadratic characteristic coefficients. The boundaries of each characteristic are set such that v^h is at its maximum value for the highest resistive fault and at its minimum value for bolted fault at the IIDG's terminals.

The main objective of the adaptive harmonic voltage generation is to maximize the generated voltage based on fault severity while maintaining the IIDG output current below or equal to its maximum allowable value, I_{DG}^{max} , i.e., 1.5 pu, according to [30]. Thus, an objective function is defined to maximize the sum of all generated harmonic voltages, V^h , i.e.,

$$\max V^h = \sum_{k=1}^{nDG} \sum_{l=1}^L \sum_{r_f=1}^{R_{tot}} v_{klr_f}^h \quad (5.5)$$

where k is the IIDG index, nDG is the total number of IIDGs, and $v_{klr_f}^h$ is the individual IIDG's generated harmonic voltage due to a fault at location l involving fault resistance r_f . L and R_{tot} are the total numbers of fault locations and resistances, respectively. All characteristics are bounded by lower and upper bounds defined by

$$\lfloor v^h \rfloor \leq y_1, y_2, y_3 \leq \lceil v^h \rceil \quad (5.6)$$

$$\lfloor v^h \rfloor \leq |v^h| \leq \lceil v^h \rceil \quad (5.7)$$

Equality constraints are set at the endpoints of the adaptive quadratic characteristic by replacing ΔV_o with zero and ΔV_o^{max} as follows:

$$k_4 = \lceil v^h \rceil \quad (5.8)$$

$$k_2 |\Delta V_o^{max}|^2 + k_3 |\Delta V_o^{max}| + \lceil v^h \rceil - \lfloor v^h \rfloor = 0 \quad (5.9)$$

The quadratic characteristic can be expressed as a parabola in its vertex form, with only one coefficient that can be determined using the endpoint $(\Delta V_o^{max}, \lfloor v^h \rfloor)$. The determined coefficients are used to set the lower and upper bounds for k_2 and k_3 , i.e.,

$$lb \leq k_2, k_3 \leq ub \quad (5.10)$$

where lb and ub are the lower and upper bounds of k_2 and k_3 .

Due to the intractability and nonlinearity of the piecewise linear and quadratic characteristics, a meta-heuristic optimization technique is utilized to optimize their parameters. The GA has a superior performance compared to other meta-heuristic algorithms in terms of accuracy and execution time [78]. Therefore, the GA in MATLAB is used to optimize the piecewise linear and quadratic characteristics parameters, such that it results in the minimum total relays' operation time.

Harmonic voltage generation at the inverter's terminals can be achieved by directly changing the harmonic modulation signals. The minimum generated voltage is adapted when a bolted fault is applied at the IIDG's terminals, such that the amplitude of the peak output current does not exceed I_{DG}^{max} to protect the inverter's switches from excessive current. Further, the fundamental current is limited by the current limiter in the current control loop. Thus, the constraints imposed on the lowest injected harmonic current, I_{low}^h , can be established by

$$[v^h] = I_{low}^h |Z_{tr}^h + Z_f^h| \quad (5.11)$$

$$I_{sat}^{fund} + I_{low}^h \leq I_{DG}^{max} \quad (5.12)$$

where I_{sat}^{fund} is the saturated fundamental fault current, set at 1.2 pu. The maximum generated voltage is adjusted when the maximum fault resistance, R_{flt}^{max} , is applied at the farthest point from the IIDG's terminals such that it results in the highest harmonic fault current, I_{high}^h . The IIDGs operate near their nominal current at high resistive faults, allowing 50% room for the harmonic current. Therefore, $[v^h]$ can be approximated by

$$[v^h] = I_{high}^h |Z_{tr}^h + Z_f^h + Z_{feed} + R_{flt}^{max}| \quad (5.13)$$

where Z_{feed} is the impedance between the IIDG's terminals and the farthest point on the feeder.

5.1.2 Trip characteristics of HDOCRs

Typically, overcurrent protection schemes adopt the ITC characteristic, according to the IEC standard 60255-151 [72]. Applying the standard ITC for the HDOCR results in a harmonic ITC (HITC) characteristic defined by

$$t_{rl} = TDS_r \frac{A}{\left(\frac{I_{scrl}^h}{I_{pr}^h}\right)^B - 1} \quad (5.14)$$

where TDS_r and I_{pr}^h are the time dial setting and the harmonic pickup current for relay r , respectively. $I_{sc_{rl}}^h$ denotes the harmonic fault current measured by relay r for a fault location l . t_{rl} is the operation time of relay r for a fault location l . A and B are constants that determine the HDOCR characteristic. Assuming the standard ITC characteristic, the constants A and B are 0.14 and 0.02, respectively. To enhance the operation time of HDOCR, the TCV characteristic is implemented in the harmonics layer. The operation time for the harmonic TCV (HTCV) characteristic can be obtained as

$$t_{rl} = e^{(v_{f_{rl}}^h)^{-1}K} TDS_r \frac{A}{\left(\frac{I_{sc_{rl}}^h}{I_{pr}^h}\right)^B - 1} \quad (5.15)$$

where $v_{f_{rl}}^h$ is the harmonic fault phase voltage measured by relay r for a fault location l and K is a constant parameter.

5.1.3 The harmonic directional element

The HDOCRs measure harmonic fault voltages and currents; therefore, they can identify the fault's current direction [68]. The directional element can be implemented using

$$T_r^h = v_{fr}^h I_{sc_r}^h \overbrace{\cos(\delta_{vr}^h - (\delta_{Ir}^h + \delta_Z^h))}^{\delta_r^h} \quad (5.16)$$

where T_r^h is the developed torque by relay r . δ_{vr}^h and δ_{Ir}^h pertain to the phase angles of the relay's measured harmonic voltage and current, respectively, and δ_Z^h denotes the angle of the harmonic impedance of the protected line. The relay's harmonic torque angle is represented by δ_r^h . The harmonic directional element logic is given by

$$Zone = \begin{cases} forward, & -90^\circ \leq \delta_r^h \leq 90^\circ \\ reverse, & otherwise \end{cases} \quad (5.17)$$

The harmonic directional element is utilized along with the harmonic voltages and currents measured by HDOCRs to implement the proposed protection scheme.

5.2 Harmonic Short Circuit Calculations

As a prerequisite step, SCCs should be performed for OPC. This study adopts the modified nodal method (MNM) initially proposed in [81] and applied by [68] as an SCC method. The MNM is selected due to its superior computational capabilities that offer flexible modeling of all system components and handling different system topologies. Further, the MNM has an outstanding performance compared to the backward-forward sweep and current injection methods used to solve the power flow problem in distribution networks [82].

The developed SCC method is denoted in this study by the harmonic short-circuit current calculation (HSCC) method. The bus admittance matrix is a function of the harmonic order and models the microgrid buses, including virtual fault buses. The relationship between voltages and currents in the HSCC is given by

$$\begin{bmatrix} Y_N^h & B_1 \\ B_2 & B_3 \end{bmatrix} \begin{bmatrix} V_N^h \\ I_u^h \end{bmatrix} = \begin{bmatrix} I_N^h \\ V_u^h \end{bmatrix} \quad (5.18)$$

where Y_N^h is the harmonic bus admittance matrix neglecting the harmonic voltage sources' contributions. N denotes the total number of system buses, including the virtual fault locations and the IIDGs' internal buses. u is the total number of components that are not included in Y_N^h . V_N^h and I_u^h comprise the unknown bus harmonic voltages and the unknown harmonic currents, respectively. V_u^h and I_N^h define the magnitudes of the known independent harmonic voltages and the known injected harmonic currents, respectively. The matrices B_1 and B_2 are determined by the voltage sources and their connection to system buses. B_1 is a binary matrix with an element equal to zero if the respective element of I_u^h is not related to the corresponding nodal equation and 1.0 otherwise. B_2 is also a binary matrix with elements equal to 1.0 only if the corresponding elements of V_N^h and V_u^h are equal. B_3 is a square matrix defined by source type (i.e., dependent or independent).

Since IIDGs generate only harmonic voltages, (5.18) can be rewritten as

$$\begin{bmatrix} Y_N^h & B_1 \\ B_2 & 0_u \end{bmatrix} \begin{bmatrix} V_N^h \\ I_u^h \end{bmatrix} = \begin{bmatrix} 0_N \\ V_u^h \end{bmatrix} \quad (5.19)$$

u defines the number of independent harmonic voltage sources regulated by IIDGs. 0_N and 0_u are columns with N zeros and $u \times u$ matrix with all its elements equal to zero, respectively. The off-diagonal elements of Y_N^h are calculated as

$$y_{ij}^h = \frac{-1}{z_{ij}^h} \quad (5.20)$$

z_{ij}^h denotes line ij impedance (i.e., between buses i and j) and is calculated by

$$z_{ij}^h = R_{ij} + jhL_{ij}\omega \quad (5.21)$$

where R_{ij} and L_{ij} are the resistance and inductance of line ij , respectively. The diagonal elements of Y_N^h are given by

$$y_{ii}^h = \sum_{j=1}^N \frac{1}{z_{ij}^h} + \sum_{g=1}^G \frac{1}{z_{ig}^h} \quad (5.22)$$

z_{ig}^h models the total impedance from bus i to ground, including the fault impedance connected to the virtual fault bus v_{bus} , which is calculated as follows:

$$Z_{v_{bus}} = \begin{cases} R_{flt}, & \text{fault at } v_{bus} \\ \infty, & \text{no fault at } v_{bus} \end{cases} \quad (5.23)$$

The inline fault is modeled by an impedance $Z_{v_{bus}}$ connected to v_{bus} , where R_{flt} is the fault resistance. Solving (5.19) for the unknown nodal harmonic fault voltages and currents results in

$$\begin{bmatrix} V_N^h \\ I_u^h \end{bmatrix} = \begin{bmatrix} Y_N^h & B_1 \\ B_2 & 0_u \end{bmatrix}^{-1} \begin{bmatrix} 0_N \\ V_u^h \end{bmatrix} \quad (5.24)$$

Then, the harmonic fault current is obtained using the nodal harmonic voltages during the fault:

$$i_{fij}^h = \frac{v_{fi}^h - v_{fj}^h}{z_{ij}^h} \quad (5.25)$$

where v_{fi}^h and v_{fj}^h are the harmonic voltages of buses i and j during a fault, respectively.

5.3 Proposed Protection Coordination

This section explains the proposed OPC problem formulation and describes the OPC program.

5.3.1 OPC problem formulation

In contrast to the conventional directional relays, which operate only in a forward direction, the dual setting directional relays can operate in both forward and reverse directions utilizing two different settings. This study proposes an HDOCR equipped with a dual setting TCV characteristic for islanded microgrid overcurrent protection to enhance the relays' total operation time. The operation times of the dual setting HDOCR are defined as

$$t_{rl, fwd} = e^{(v_{fri}^h - 1)K_{r, fwd}} TDS_{r, fwd} \frac{A}{\left(\frac{I_{scrl}^h}{I_{pr}^h}\right)^B - 1} \quad (5.26)$$

$$t_{lr, rev} = e^{(v_{fri}^h - 1)K_{r, rev}} TDS_{r, rev} \frac{A}{\left(\frac{I_{scrl}^h}{I_{pr}^h}\right)^B - 1} \quad (5.27)$$

where $t_{lr,fwd}$, $TDS_{r,fwd}$, and $K_{r,fwd}$ pertain to the relay operation time for a fault location l , time dial setting, and constant parameter for the forward operation, respectively. Likewise, $t_{lr,rev}$, $TDS_{r,rev}$, and $K_{r,rev}$ are the relay operation time for a fault location l , time dial setting, and constant parameter for the reverse operation, respectively.

The main aim of protection coordination is to minimize the HDOCRs total operation time while satisfying the coordination constraints. Thus, the objective function is defined as follows:

$$\begin{aligned} \min T = \sum_{r=1}^R \sum_{l=1}^L (t_{rl,fwd}^p + \sum_{k=1}^K (t_{rl,fwd}^{b_k} + t_{rl,rev}^{b_k})) \\ + t_{rl,rev}^p + \sum_{k=1}^K t_{rl,rev}^{b_k} \end{aligned} \quad (5.28)$$

where l is the fault location with a total number of L locations, and r is the relay identifier with R as the total number of relays. p and b_k denote the primary and the k^{th} backup relay, respectively. $t_{rl,fwd}^p$, $t_{rl,fwd}^{b_k}$, $t_{rl,rev}^p$, and $t_{rl,rev}^{b_k}$ are computed for each relay r , employing the harmonic fault voltage and current calculated using the HSCC.

The OPC program considers a set of constraints to be satisfied to ensure a feasible solution for the forward and reverse operation of every HDOCR. For the HDOCRs coordination purposes, the relay settings and coordination constraints should be included in the OPC program. The constraints imposed on the relay settings are

$$TDS_{min} \leq TDS_{r,fwd}, TDS_{r,rev} \leq TDS_{max} \quad \forall r \quad (5.29)$$

$$K_{min} \leq K_{fwd}, K_{rev} \leq K_{max} \quad \forall r \quad (5.30)$$

where TDS_{min} and TDS_{max} denote the lower and upper bounds of $TDS_{r,fwd}$ and $TDS_{r,rev}$, respectively, with values set at 0.01 and 1.0. K_{min} and K_{max} are the minimum and maximum values for K_{fwd} and K_{rev} , respectively. K_{min} and K_{max} are equal to 0 and 4.0, respectively.

A minimum CTI should be maintained between the operation of primary and backup relays. CTI is set at 0.2 s as recommended by the IEEE Standard 242-2001. Hence, the CTI constraints are formulated as follows:

$$t_{rl,fwd}^{b_k} - t_{rl,fwd}^p \geq CTI \quad \forall r \quad (5.31)$$

$$t_{rl,fwd}^{b_k} - t_{rl,rev}^p \geq CTI \quad \forall r$$

The IEEE Standard 519 mandates a maximum harmonic current distortion of 0.04 pu for harmonic orders 3–11 during normal operation. Further, the accuracy of CT measurements is guaranteed if the measured currents are equal to or above 0.05 pu [83]. Hence, to distinguish the generated harmonics, the pickup current of the HDOCR is selected to have a value of 0.1 pu. A constraint on the minimum relay operation time is enforced through the following constraint:

$$t_{rl,fwd}^p, t_{rl,fwd}^{b_k} \geq t_{min} \quad \forall r \quad (5.32)$$

$$t_{rl,rev}^p, t_{rl,rev}^{b_k} \geq t_{min} \quad \forall r$$

where t_{min} is the minimum relay operation time set to 20 ms.

5.3.2 OPC program

The algorithm starts by building the bus admittance matrix Y_N^h , which includes the fault location as a virtual bus and is formulated for each fault location. The OPC program unfolds two stages, as illustrated by the flow chart depicted in Figure 5.5. The first stage aims at maximizing the generated harmonic voltage to promote higher harmonic currents at high fault resistances. In Stage I, the harmonic voltage generation characteristics are tested. The GA in MATLAB is used to obtain optimized values for the coefficients starting with an initial guess for characteristic coefficients. Then, the HSCC is employed to obtain bus voltages during faults for several fault resistances utilizing the optimized harmonic generation characteristic. Next, the bus

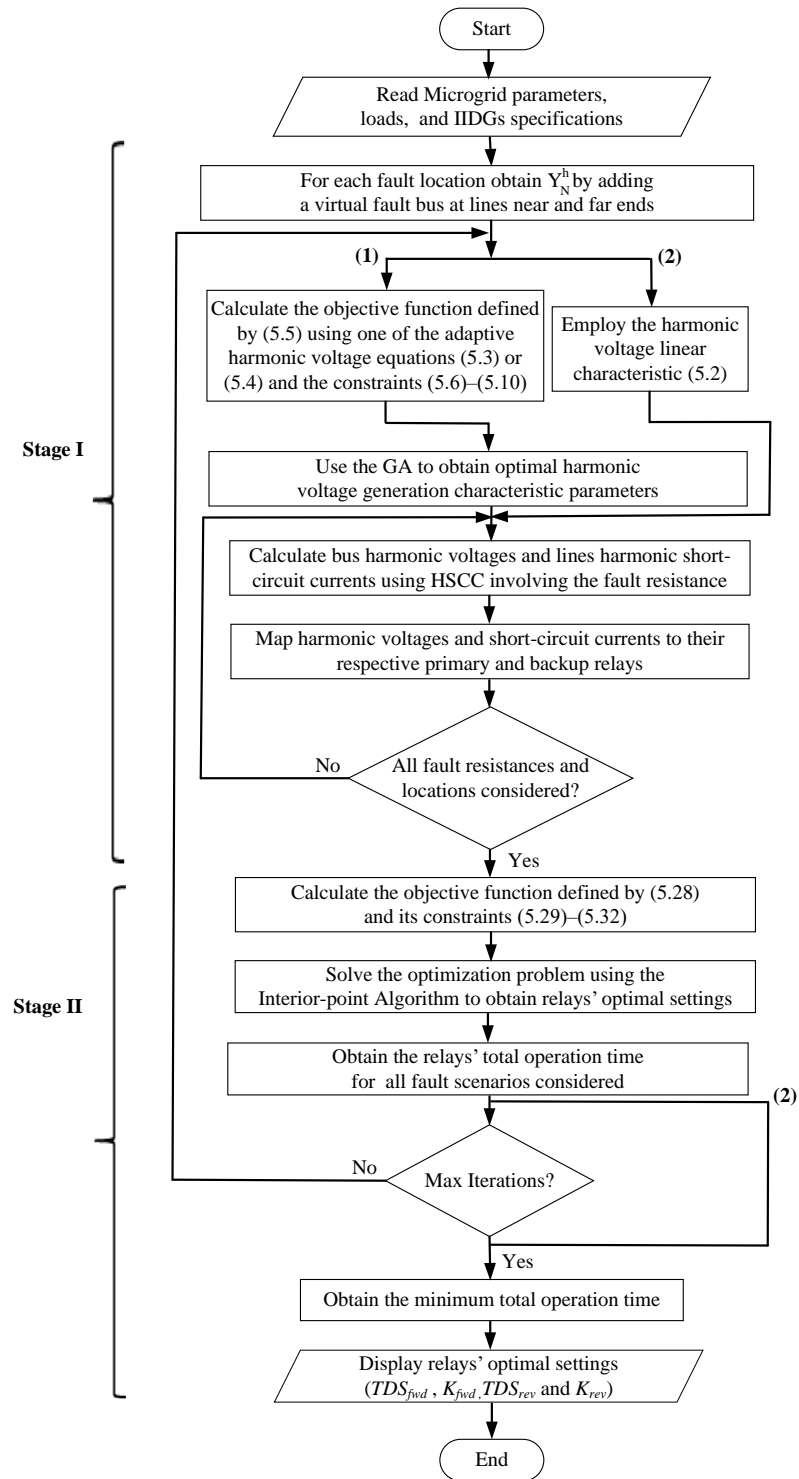


Figure 5.5: Flow chart of the proposed OPC program.

voltages obtained are used to calculate the lines' short-circuit currents. Finally, the harmonic short-circuit currents and voltages are mapped to their respective relays.

The second stage determines the optimal relays' dual setting. The harmonic short-circuit currents and voltages are used in Stage II, employing the interior-point algorithm to obtain the optimal relays' settings TDS_{fwd} , TDS_{rev} , K_{fwd} , and K_{rev} that guarantee OPC. The nonlinear constraints formulated using the harmonic short-circuit currents and voltages resulting from involving several fault resistances are considered simultaneously in the solution. The solution obtained results in a single relays' setting that guarantees optimal coordination under all fault scenarios.

5.4 Performance Evaluation

5.4.1 Test system

The performance of the proposed protection scheme is assessed on the same microgrid in Figure 3.8. IIDG1 and IIDG3 are replaced with IIDGs having a 2-MVA rating, as displayed in Figure 5.6. Faults (F_1 – F_{16}) at the near and far ends are marked as indicated. Each line hosts two primary relays due to the bidirectional power flow. As a result, 16 HDOCRs are used for overcurrent protection.

5.4.2 The harmonic layer measurements

The islanded microgrid in Figure 5.6 is simulated using PSCAD/EMTDC, and a bolted fault at F_{10} is considered to demonstrate the operation of the proposed protection scheme. The fault is detected by monitoring the change in the IIDG output voltage. IIDGs reduce their output voltages upon fault inception to limit their output currents. As a consequence, a severe network-wide voltage sag dominates in the microgrid. A harmonic voltage is superimposed on the faulted phase once a voltage sag below 0.88 pu is detected at the IIDG's terminals. Figure 5.7(a) displays the IIDG1 output current during F_{10} . This current enfolds a 3rd harmonic component excited by the superimposed 3rd harmonic voltage and a fundamental component. A

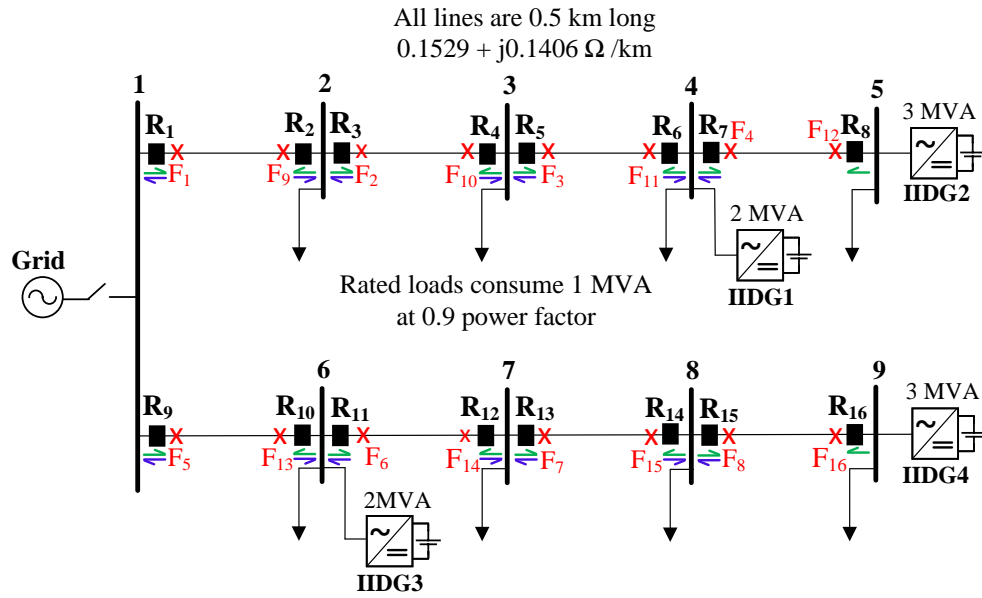


Figure 5.6: Single line diagram of the test microgrid.

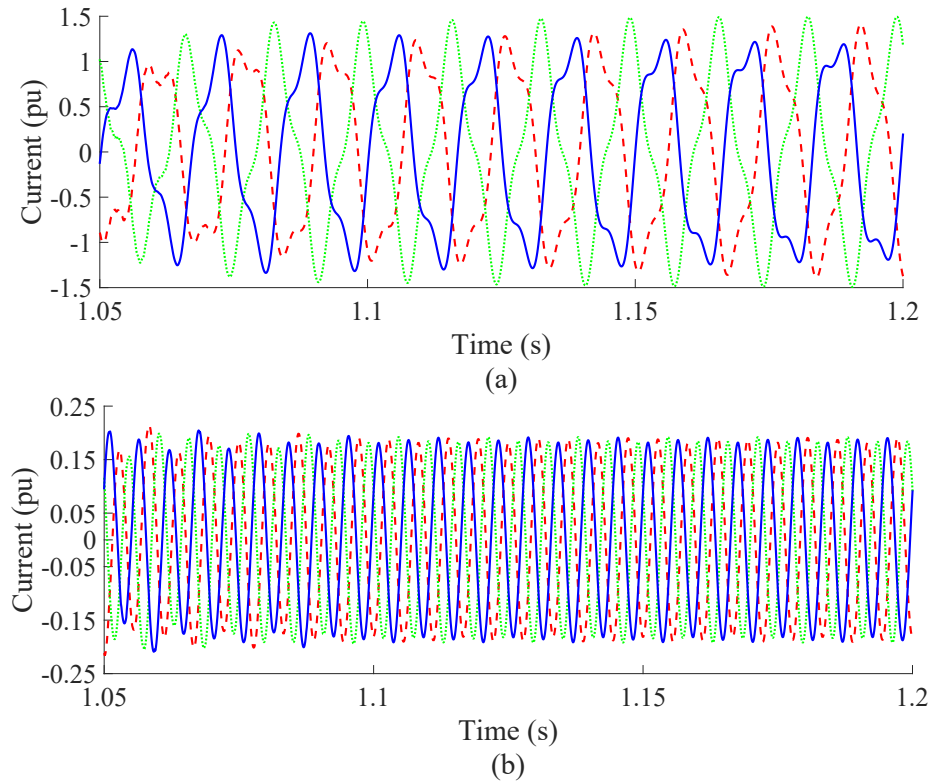
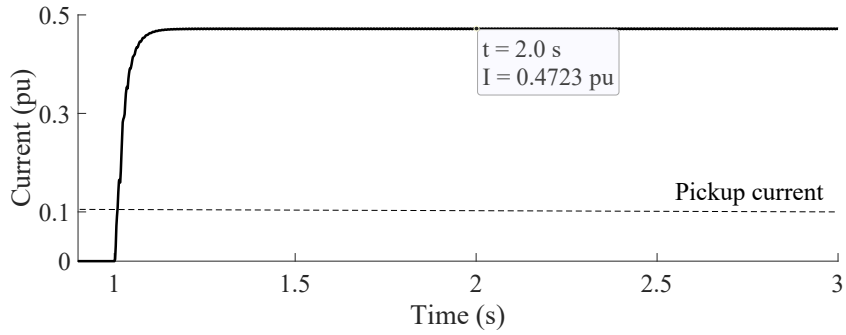
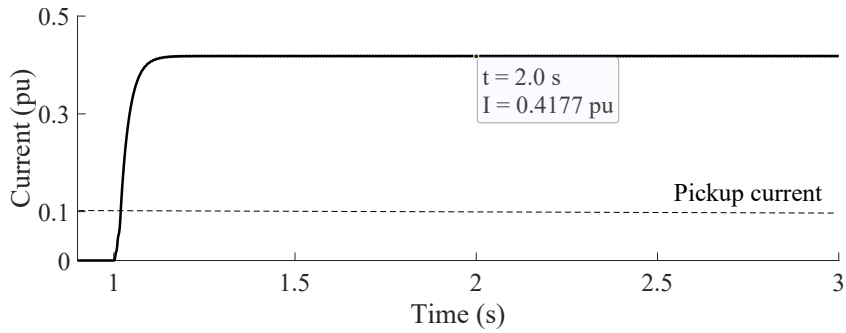


Figure 5.7: IIDG1 currents during F_{10} : (a) output current. (b) harmonic current.

Figure 5.8: The harmonic current measured by R_4 during F_{10} .Figure 5.9: The harmonic current measured by R_1 during F_1 .

fast Fourier transform (FFT) is used to extract the positive-sequence 3^{rd} harmonic current, depicted in Figure 5.7(b). The IIDGs' harmonic fault currents flow towards the fault at F_{10} . As a result, the harmonic current measured by R_4 is the sum of IIDG1's and IIDG2's injected harmonic currents, as demonstrated in Figure 5.8. Another fault scenario at F_1 is considered to illustrate the sensitivity of the proposed protection scheme to the highest resistive fault ($R_{flt}^{max} = 15 \Omega$). Figure 5.9 shows the 3^{rd} harmonic current measured by the primary relay R_1 . The harmonic torque angles of R_2 and R_3 are displayed in Figure 5.10. The relays R_2 and R_3 identify a forward and a reverse fault, respectively, as noted by the angles in Figure 5.10. Since the harmonic pickup current is exceeded for F_1 , relays R_4 , R_6 , and R_8 are triggered due to the identification of a forward fault. Therefore, R_1 and R_2 must be designed to have the fastest operation times for a fault at their primary protection zone.

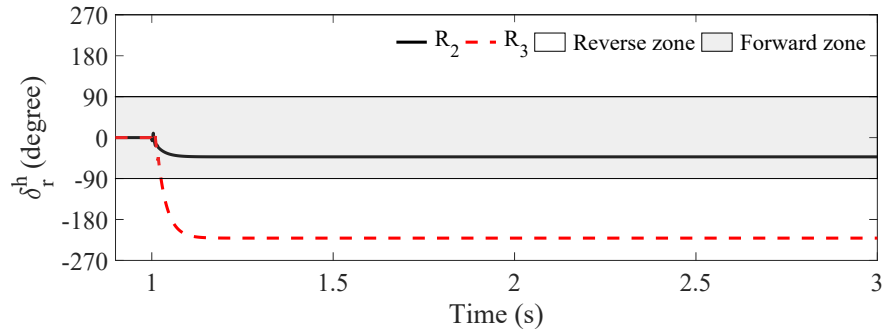


Figure 5.10: The harmonic torque angles measured by R_2 and R_3 during F_1 .

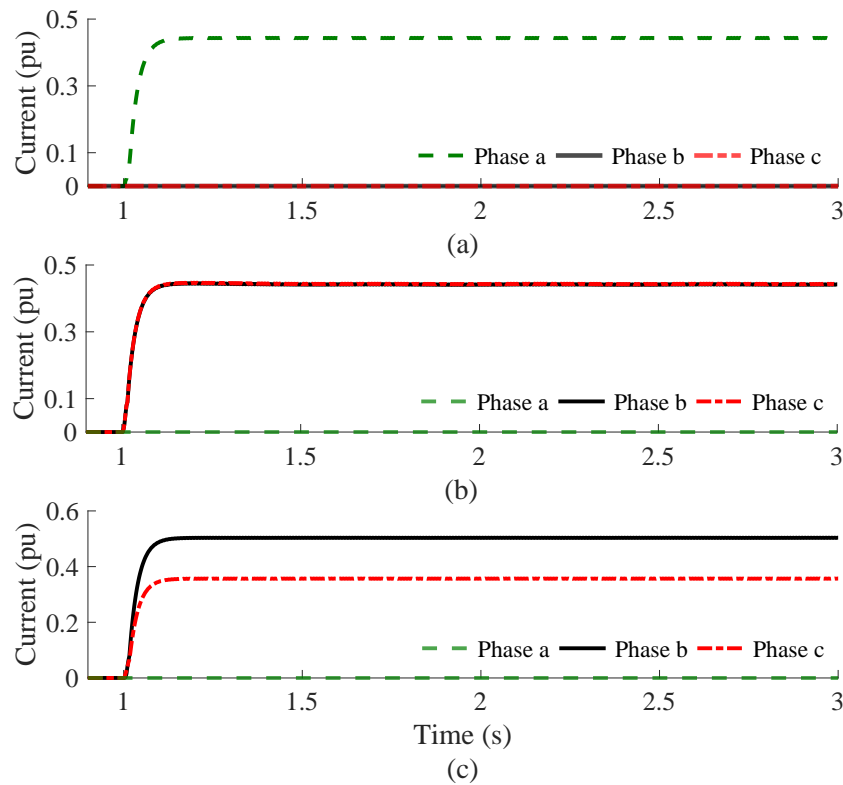


Figure 5.11: The magnitude of the harmonic currents measured by relay R_1 due to (a) SLG (b) LL (c) DLG during F_1 .

Single-line-to-ground (SLG), line-to-line (LL), and double-line-to-ground (DLG) are applied at F_1 with R_{flt}^{max} to illustrate the capability of the proposed harmonic voltage generation in producing tangible harmonic currents during unbalanced faults. Figure 5.11 displays the harmonic fault currents measured by R_1 during SLG, LL,

and DLG faults at F_1 with R_{flt}^{max} . During unbalanced faults, the 3rd harmonic voltage is activated only at the faulted phase(s). As noted in Figure 3.11, the harmonic fault currents of the faulted phase(s) are well above the pickup current (0.1 pu). Hence, the proposed protection scheme can work with different fault types. It is worth noting that harmonic-based protection schemes should be immune to faults in unbalanced IBIMs, but it needs to be tested and could be considered a future work.

5.4.3 OPC using constant and adaptive harmonic voltage generation

Table 5.1 compares the relays' total operation times for constant and adaptive harmonic voltage generation considering relays equipped with only the forward trip characteristic. First, the OPC is solved using constant harmonic voltage generation [67], optimized for bolted to the highest resistance faults. Although the OPC is feasible in all fault scenarios, the relays' total operation times have high values, as noted in the second column of Table 5.1. Then, the OPC is solved employing a linear adaptive harmonic voltage generation optimized for bolted to R_{flt}^{max} resistance faults. The results in Table 5.1 reveal that the adaptive harmonic protection scheme has two advantages, a significant reduction of 30.58% and 62.69% in relays' total operation time at bolted and high fault resistances and a feasible OPC up to the highest fault resistance (i.e., R_{flt}^{max}).

Table 5.2 displays the optimal settings of TDS and K obtained for all HDOCRs of the test microgrid by solving the OPC problem utilizing constant and adaptive harmonic voltages. The solution leads to different optimal settings. Table 5.3 reports the relays' total operation times adopting different adaptive v^h characteristics and the dual setting. Testing various adaptive v^h characteristics aims at obtaining the minimum relays' total operation times. The results demonstrate that optimized characteristic coefficients lead to further reducing the total relays' operation time compared to the linear characteristic. The minimum relays' total operation time for high resistive faults is obtained using the piecewise linear characteristic. The optimal

Table 5.1: Relays Total Operation Times in Seconds for Near-end Faults Considering Forward Characteristic

$R_{ft}(\Omega)$	Values (s)		
	v^h Charcteristic		
	Constant [67]	Adaptive	$\Delta T(\%)$ Constant vs Adaptive
0.1	35.172	24.416	30.58
1	36.507	24.646	32.49
3	40.041	24.978	37.62
5	44.252	25.690	41.95
10	58.222	28.396	51.23
15	85.472	31.893	62.69

Table 5.2: Relays Optimal Settings Considering Forward Characteristic

Relay	v^h characteristic			
	Constant		Adaptive	
	TDS (s)	K	TDS (s)	K
R₁	1.0000	1.7363	0.2100	0.3204
R₂	0.3627	0.6812	0.2822	0.3377
R₃	1.0000	2.2778	0.1082	0.0492
R₄	0.7194	1.1456	0.4679	0.6228
R₅	0.4092	0.0000	0.0538	0.0000
R₆	1.0000	1.2638	0.7063	0.8508
R₇	0.0100	0.5478	0.0100	0.5146
R₈	0.2488	0.0974	0.5902	0.8671
R₉	0.1385	0.0000	0.1519	0.0000
R₁₀	1.0000	1.3767	0.3643	0.5896
R₁₁	0.1153	0.0000	0.1330	0.0605
R₁₂	0.1987	0.0000	0.1710	0.0000
R₁₃	0.0602	0.0000	0.0654	0.0000
R₁₄	1.0000	0.7512	0.6703	1.1861
R₁₅	0.0100	0.5599	0.0100	0.5216
R₁₆	1.0000	0.2848	1.0000	1.3121

Table 5.3: Relays Total Operation Times in Seconds for Near-end Faults with TCV Dual Setting and Various Characteristic

$R_{flt}(\Omega)$	Values (s)			
	Linear	Piecewise Linear	Quadratic	$\Delta T(\%)$ Linear vs Piecewise Linear
0.1	34.809	34.726	35.833	0.24
1	35.138	35.139	35.530	0.00
3	35.623	35.625	35.048	0.00
5	36.652	36.373	35.882	0.76
10	40.560	37.980	40.660	6.36
15	45.591	45.470	47.838	0.27

Table 5.4: Relays Optimal Dual Setting with Piecewise Characteristic

Relay	TDS_{fwd} (s)	K_{fwd}	TDS_{rev} (s)	K_{rev}
R₁	0.2048	0.3587	0.2690	0.3352
R₂	0.2692	0.3365	0.2046	0.3571
R₃	0.1047	0.0801	0.4447	0.6170
R₄	0.4446	0.6174	0.1047	0.0797
R₅	0.0504	0.000	0.6716	0.8459
R₆	0.6709	0.8455	0.0504	0.0000
R₇	0.0100	0.5705	0.7991	1.2527
R₈	0.7991	1.2536	-	-
R₉	0.1451	0.0000	0.3560	0.6285
R₁₀	0.3565	0.6308	0.1451	0.0000
R₁₁	0.1314	0.1026	0.1638	0.0000
R₁₂	0.1638	0.0000	0.1248	0.0457
R₁₃	0.0619	0.0000	0.6262	1.1612
R₁₄	0.6267	1.1629	0.0619	0.0000
R₁₅	0.0100	0.5763	1.0000	1.3774
R₁₆	1.0000	1.3784	-	-

dual setting obtained achieved OPC for bolted faults and up to $15\ \Omega$ fault resistance.

Table 5.4 lists the relays' optimal settings for forward and reverse fault directions obtained from solving the OPC problem employing the piecewise linear characteristic.

The relay's optimal settings, along with the calculated harmonic voltages and short-circuit currents, are used to obtain the relay's operation time. Table 5.5 reports a breakdown of the relays' operation times in response to bolted faults. The primary and backup relay sets are adequately coordinated with CTIs of at least 0.2 s. Furthermore, the backup relays on the lines adjacent to the faulty line have the same operation times, enabling the clearance of the fault instantly from both sides. The relays' operation times are obtained using the optimal dual setting displayed in Table 5.4.

Table 5.6 displays the relays' operation times in response to R_{flt}^{max} . The results are obtained using the same optimal dual setting of Table 5.4. Using the same settings confirms the capability of the proposed dual setting protection scheme to achieve OPC up to the maximum fault resistance and its sensitivity to high resistive faults. The primary and backup relays remain coordinated without violating the minimum value of the CTI.

Table 5.5: Operation Times in Seconds for Bolted Faults Utilizing the Proposed Scheme with TCV Dual Setting

#	Primary	Backup1	Backup2	#	Primary	Backup1	Backup2
F₁	R ₁	R ₉	R ₁₀	F₉	R ₁	R ₉	R ₁₀
	0.6121	0.8121	0.8121		0.6158	0.8169	0.8172
	R ₂	R ₃	R ₄		R ₂	R ₃	R ₄
	0.8135	1.0147	1.0154		0.8098	1.0101	1.0105
F₂	R ₃	R ₂	R ₁	F₁₀	R ₃	R ₂	R ₁
	0.4159	0.6159	0.6159		0.4185	0.6197	0.6199
	R ₄	R ₅	R ₆		R ₄	R ₅	R ₆
	1.0103	1.2141	1.2153		1.0054	1.2083	1.2089
F₄	R ₇	R ₆	R ₅	F₁₂	R ₇	R ₆	R ₅
	0.0200	0.2200	0.2200		0.0202	0.2220	0.2220
	R ₈	-	-		R ₈	-	-
	1.4025	-	-		1.3962	-	-
F₅	R ₉	R ₁	R ₂	F₁₃	R ₉	R ₁	R ₂
	0.6137	0.8137	0.8137		0.6165	0.8175	0.8177
	R ₁₀	R ₁₁	R ₁₂		R ₁₀	R ₁₁	R ₁₂
	0.8120	1.0248	1.0248		0.8068	1.0171	1.0171
F₆	R ₁₁	R ₁₀	R ₉	F₁₄	R ₁₁	R ₁₀	R ₉
	0.4162	0.6166	0.6166		0.4186	0.6204	0.6204
	R ₁₂	R ₁₃	R ₁₄		R ₁₂	R ₁₃	R ₁₄
	1.0169	1.2181	1.2186		1.0124	1.2124	1.2124
F₇	R ₁₃	R ₁₂	R ₁₁	F₁₅	R ₁₃	R ₁₂	R ₁₁
	0.2187	0.4208	0.4187		0.2200	0.4232	0.4211
	R ₁₄	R ₁₅	R ₁₆		R ₁₄	R ₁₅	R ₁₆
	1.2122	1.5583	1.5519		1.2066	1.5517	1.5517

Table 5.6: Operation Times in Seconds for 15 Ω Resistance Faults Utilizing the Proposed Scheme with TCV Dual Setting

#	Primary	Backup1	Backup2	#	Primary	Backup1	Backup2
F₁	R ₁	R ₉	R ₁₀	F₉	R ₁	R ₉	R ₁₀
	0.8593	1.0603	1.0603		0.8677	1.0677	1.0677
	R ₂	R ₃	R ₄		R ₂	R ₃	R ₄
	1.0202	1.2202	1.2202		1.0123	1.2130	1.2130
F₂	R ₃	R ₂	R ₁	F₁₀	R ₃	R ₂	R ₁
	0.6663	0.8679	0.8679		0.6754	0.8754	0.8754
	R ₄	R ₅	R ₆		R ₄	R ₅	R ₆
	1.2128	1.4128	1.4128		1.2049	1.4055	1.4054
F₄	R ₇	R ₆	R ₅	F₁₂	R ₇	R ₆	R ₅
	0.0313	0.4838	0.4838		0.0315	0.4940	0.4940
	R ₈	-	-		R ₈	-	-
	1.6716				1.6584		
F₅	R ₉	R ₁	R ₂	F₁₃	R ₉	R ₁	R ₂
	0.8194	1.0204	1.0204		0.8274	1.0274	1.0274
	R ₁₀	R ₁₁	R ₁₂		R ₁₀	R ₁₁	R ₁₂
	1.0602	1.5418	1.5418		1.0519	1.5148	1.5148
F₇	R ₁₃	R ₁₂	R ₁₁	F₁₅	R ₁₃	R ₁₂	R ₁₁
	0.2754	0.4935	0.4970		0.2772	0.4960	0.4994
	R ₁₄	R ₁₅	R ₁₆		R ₁₄	R ₁₅	R ₁₆
	1.6965	1.8965	1.8965		1.6779	1.8829	1.8829

5.5 Conclusion

The limited fault current contributions from IIDGs introduce formidable protection challenges in islanded microgrids. Consequently, overcurrent protection may fail to distinguish between normal load and short-circuit currents. A harmonic-based protection scheme that does not rely on communication is developed for islanded microgrids to ensure reliable overcurrent protection. Once a fault is detected, a harmonic

current flow is established by utilizing the IIDG controller to generate adaptive harmonic voltages based on fault severity. The adaptive harmonic voltage is optimized to maximize the harmonic current flow during faults, thus, reducing the relays' total operation time. A two-stage OPC program is developed that employs an HSCC method. Stage I determines the optimized coefficients of the harmonic generation characteristics and the relays' harmonic voltages and currents. In Stage II, a universal set of dual settings that maintain HDOCRs coordination is obtained utilizing the HTCVC characteristic and a harmonic directional element. The proposed protection scheme provides non-expensive and reliable overcurrent protection for islanded microgrids powered by IIDGs. Further, the adaptive harmonic voltage reduces the total relays' operation time and achieves coordination for bolted to the highest resistance faults.

Chapter 6

Harmonic-based Protection of IBIM Considering N-1 Contingency

Solving the OPC problem for the main network topology results in coordination violations when the network experiences a contingency. Therefore, all possible single outages of IIDGs and lines should be considered in the OPC formulation to ensure a reliable protection scheme.

6.1 Proposed Harmonic-based Protection

The linear adaptive harmonic voltage generation system devised in Chapter 5 is employed to design a new overcurrent protection scheme. In addition, the OPC formulation accommodates all single IIDGs and lines outages to guarantee protection coordination under N-1 contingencies.

The new protection scheme activates the harmonic voltage generation at the inverter's terminals upon fault detection. As a result, harmonic current flows from IIDGs to the fault location. The HDOCRs are utilized to measure the harmonic voltages and currents to achieve OPC for islanded microgrids.

6.1.1 OPC problem formulation

HDOCRs are equipped with a single TCV characteristic for islanded microgrid overcurrent protection. The operation time of the HDOCR is given by

$$t_{rl} = e^{(v_{f_{rl}}^h - 1)K_r} TDS_r \frac{A}{\left(\frac{I_{sc_{rl}}^h}{I_{pr}^h}\right)^B - 1} \quad (6.1)$$

where t_{rl} , TDS_r , and K_r denote the relay operation time for a fault location l , time dial setting, and constant parameter for the forward operation, respectively. The constants A and B determine the relay characteristic. Assuming the standard ITC characteristic, the constants A and B are 0.14 and 0.02, respectively.

The objective function is defined as follows:

$$\min T = \sum_{r=1}^R t_r \quad (6.2)$$

where t_r is the operation time of relay r in response to its respective near-end fault. t_r is calculated for all the HDOCRs, utilizing the harmonic fault voltages and currents computed using the HSCC (Subsection 5.2).

The OPC program considers a set of constraints representing all possible IIDG and line outages to be satisfied to ensure a feasible solution for the OPC. The constraints imposed on the relay settings are

$$I_{pr,min} \leq I_{pr} \leq I_{pr,max} \quad \forall r \quad (6.3)$$

$$TDS_{min} \leq TDS_r \leq TDS_{max} \quad \forall r \quad (6.4)$$

$$K_{min} \leq K_r \leq K_{max} \quad \forall r \quad (6.5)$$

where $I_{pr,min}$ and $I_{pr,max}$ pertain to the minimum and maximum pickup current, respectively. TDS_{min} and TDS_{max} denote the lower and upper bounds of TDS_r , respectively, with values set at 0.01 and 1.0. K_{min} and K_{max} are the minimum and maximum values for K_r , respectively. K_{min} and K_{max} are equal to 0 and 4.0, respectively. A CTI is set at 200 ms as recommended by the IEEE Standard 242-2001. Thus, the CTI constraint is defined as:

$$t_{cr}^{b_k} - t_{cr}^p \geq CTI \quad \forall r \quad (6.6)$$

where t_{cr}^p and $t_{cr}^{b_k}$ are the operation time of the primary relay r and its backup relay b_k when the microgrid topology c is formed. The relay constraints remain the same for the islanded topology with all IIDGs and lines engaged and any IIDG outage. In contrast, every topology formed due to a line outage has different set of constraints corresponding to the faults considered in the resulting topology.

A constraint on the minimum relay operation time is imposed through the following constraint:

$$t_{cr}^p, t_{cr}^{b_k} \geq t_{min} \quad \forall r \quad (6.7)$$

where t_{min} is the minimum relay operation time set to 20 ms.

According to [83], the accuracy of CT measurements is guaranteed for current measurements at least 0.05 pu. Further, adhering to the IEEE Standard 519 that mandates a maximum harmonic current distortion of 0.04 pu for harmonic orders 3–11 during normal operation. Thus, the HDOCR $I_{pr,min}$ and $I_{pr,max}$ are set at 0.06 pu and 0.1 pu, respectively.

6.1.2 OPC program

The algorithm starts by building the bus admittance matrix Y_N^h , including the virtual fault bus, formulated for each fault location. The OPC program encompasses two stages, as illustrated by the flow chart displayed in Figure 6.1. In Stage I, the adaptive linear harmonic voltage generation characteristic is employed. Firstly, bus voltages during faults are obtained for several fault resistances using the HSCC. Secondly, the bus voltages obtained are used to calculate the lines' short-circuit currents. Finally, the harmonic short-circuit currents and voltages are mapped to their respective relays.

The harmonic short-circuit currents and voltages are used in Stage II, utilizing the interior-point algorithm to obtain the optimal relays' settings TDS and K that guarantee OPC. The nonlinear constraints formulated using the harmonic short-circuit currents and voltages resulting from involving several fault resistances under different contingencies are considered simultaneously in the solution. The obtained solution results in universal relays' settings that ensure optimal coordination under all con-

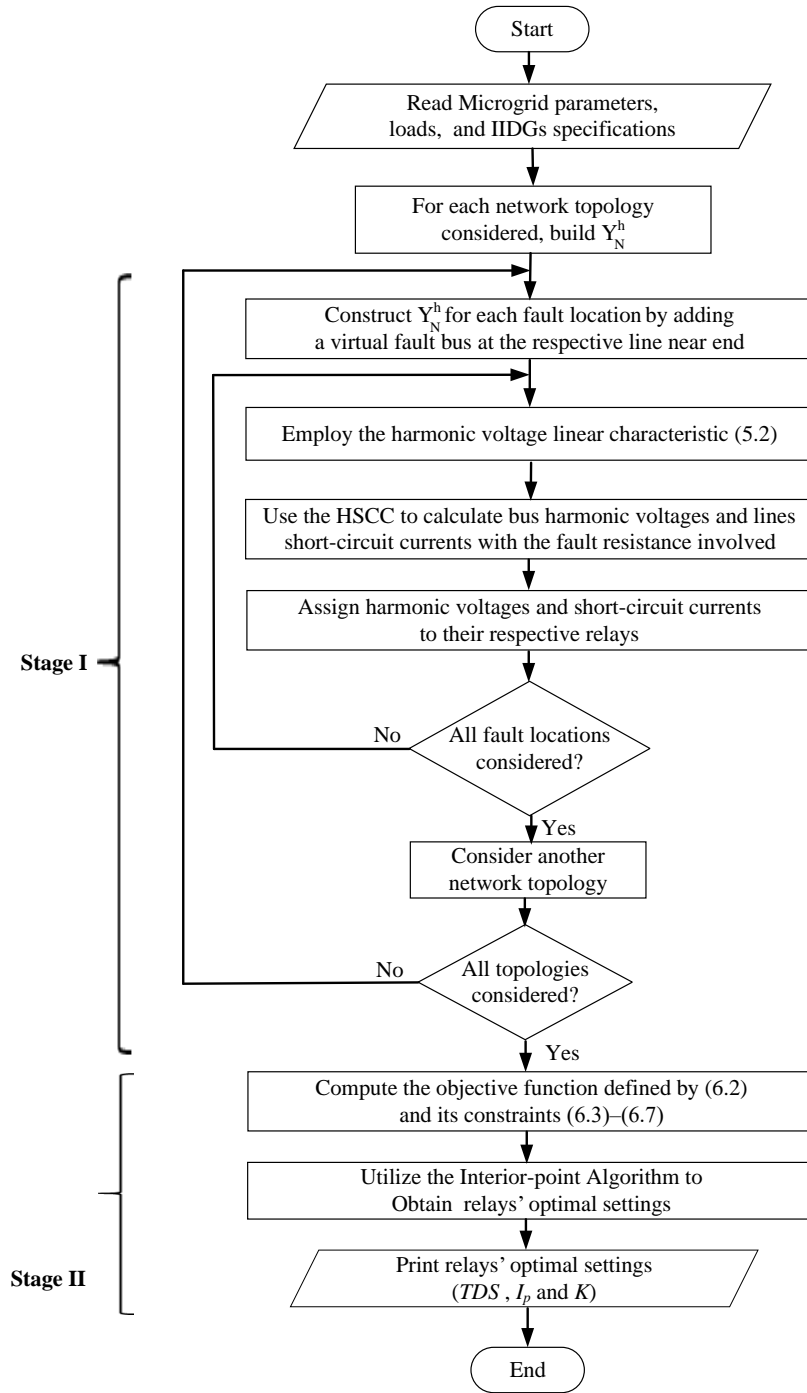


Figure 6.1: Flow chart of the proposed OPC program.

sidered network topologies.

Table 6.1: Relays Optimal Settings for the Test Microgrid (Case I)

Relay	Model 1		Model 2		Model 3	
	TDS	K	TDS	K	TDS	K
	(s)		(s)		(s)	
\mathbf{R}_1	0.2091	0.3175	0.2403	0.1486	0.2439	0.1508
\mathbf{R}_2	0.2825	0.3411	0.3604	0.1936	0.3687	0.2160
\mathbf{R}_3	0.1075	0.0451	0.1512	0.0912	0.1514	0.0713
\mathbf{R}_4	0.4666	0.6205	0.5152	0.3292	0.5363	0.3740
\mathbf{R}_5	0.0535	0.0000	0.0731	0.0112	0.0751	0.0022
\mathbf{R}_6	0.7053	0.8487	0.6713	0.3971	0.7204	0.4803
\mathbf{R}_7	0.0100	0.5643	0.0108	0.3938	0.0100	0.0046
\mathbf{R}_8	0.6093	0.9007	0.5382	0.0031	0.5402	0.0133
\mathbf{R}_9	0.1517	0.0000	0.2287	0.0070	0.2312	0.0128
\mathbf{R}_{10}	0.3623	0.5846	0.3593	0.2527	0.3667	0.2641
\mathbf{R}_{11}	0.1330	0.0628	0.1687	0.0590	0.1619	0.0058
\mathbf{R}_{12}	0.1716	0.0000	0.3484	0.0019	0.3514	0.0018
\mathbf{R}_{13}	0.0651	0.0000	0.0852	0.0298	0.0848	0.0046
\mathbf{R}_{14}	0.6763	1.1928	0.7491	0.5928	0.7627	0.6057
\mathbf{R}_{15}	0.0100	0.5718	0.0202	1.0366	0.0100	0.1172
\mathbf{R}_{16}	1.0000	1.3070	0.7531	0.3095	0.7584	0.3095

6.2 Performance Evaluation

This section provides the OPC results obtained using the three models described in Table 4.1. Two case studies are conducted on the test microgrid in Figure 5.6.

Case I: Non-identical IIDGs and Fixed Pickup Current

In this case study, two IIDGs rated at 2-MVA (IIDG1 and IIDG3) and two rated at 3 MVA (IIDG2 and IIDG4). The resulting contingencies are interpreted by a set of constraints that correspond to each contingency considered. Then, these constraints are utilized by the different OPC models while solving for the optimal relays' settings.

Table 6.1 lists the optimal settings of TDS and K for all HDOCRs of the test

Table 6.2: Coordination Violations for Considered Fault Resistances in the Test Microgrid

Topology	Number of coordination violations		
	Model 1	Model 2	Model 3
Islanded	0	0	0
IIDG1 outage	8	0	0
IIDG2 outage	6	0	0
IIDG3 outage	16	0	0
IIDG4 outage	6	0	0
Line 1-2 outage	0	0	0
Line 2-3 outage	0	0	0
Line 3-4 outage	0	0	0
Line 4-5 outage	6	2	0
Line 1-6 outage	0	0	0
Line 6-7 outage	0	0	0
Line 7-8 outage	0	0	0
Line 8-9 outage	3	2	0
Total violations	45	4	0

microgrid using the three models. The optimal settings obtained for each model are different. Hence, considering the main topology cannot satisfy the N-1 criterion. Table 6.2 displays the coordination violations. Model 3 results in proper coordination of all HDOCRs pairs for all topologies considered.

The relays' optimal settings obtained utilizing Model 3 (the proposed model), along with the harmonic voltages and short-circuit currents, are used to calculate the HDOCRs' operation times. The obtained operation times for selected near-end and far-end bolted faults for the main topology are displayed in Table 6.3. The results reveal that the assigned primary and backup HDOCRs pairs are coordinated under all considered topologies without coordination violations.

Table 6.3: Operation Times for Selected Near-end and Far-end Bolted Faults with Fixed I_p (Case I)

Relays operation times (s)					
#	Primary	Backup	#	Primary	Backup
F₁	R ₁	R ₁₀	F₉	R ₁	R ₁₀
	0.8860	1.1890		0.8903	1.1946
	R ₂	R ₄		R ₂	R ₄
	1.2595	1.5644		1.2538	1.5574
F₂	R ₃	R ₁	F₁₀	R ₃	R ₁
	0.5984	0.8904		0.6016	0.8950
	R ₄	R ₆		R ₄	R ₆
	1.5572	1.8812		1.5499	1.8724
F₃	R ₅	R ₃	F₁₁	R ₅	R ₃
	0.3203	0.6017		0.3220	0.6048
	R ₆	R ₈		R ₆	R ₈
	1.8722	3.2804		1.8636	3.2628
F₄	R ₇	R ₅	F₁₂	R ₇	R ₅
	0.0351	0.3221		0.0353	0.3245
	R ₈	-		R ₈	-
	3.2623	-		3.2508	-
F₅	R ₉	R ₂	F₁₃	R ₉	R ₂
	0.9681	1.2599		0.9727	1.2659
	R ₁₀	R ₁₂		R ₁₀	R ₁₂
	1.1888	2.1895		1.1827	2.1729

Case II: Identical IIDGs and Variable Pickup Current

The test microgrid in Figure 3.8 is used to conduct this case study for a fair comparison with the VI-FCL overcurrent protection scheme. Table 6.4 displays the HDOCRs' optimal settings with variable I_p . The relays' optimal settings in Table 6.4 are used to obtain the relays' operation times. Table 6.5 reports the operation times of the HDOCRs of the test microgrid for bolted faults. The primary and backup relay pairs

Table 6.4: Relays Optimal Settings for the Test Microgrid (Case II)

Relay	TDS (s)	I _p (pu)	K
R₁	0.1716	0.0991	0.0000
R₂	0.3649	0.0694	0.2096
R₃	0.1300	0.0796	0.0000
R₄	0.4946	0.0779	0.3637
R₅	0.0781	0.0600	0.0000
R₆	0.6624	0.0857	0.5323
R₇	0.0100	0.0600	0.2310
R₈	1.0000	0.0600	0.4630
R₉	0.2669	0.0600	0.0857
R₁₀	0.2722	0.1000	0.0000
R₁₁	0.1748	0.0600	0.0038
R₁₂	0.5753	0.0600	0.0000
R₁₃	0.0906	0.0600	0.0000
R₁₄	1.0000	0.0851	0.6358
R₁₅	0.0100	0.0600	0.2395
R₁₆	1.0000	0.1000	0.4399

are coordinated with CTIs of at least 0.2 s.

Employing variable pickup current results in further reduction of individual relays' operation times, as noted in Table 6.6. Table 6.7 displays the operation times of the HDOCRs of the test microgrid for the highest resistive fault (i.e., $R_{flt}^{max} = 15 \Omega$). The primary and backup relay pairs remain coordinated with CTIs equal to or greater than 0.2 s.

Table 6.8 compares the harmonic generation and the VI-FCL overcurrent protection schemes from a speed and sensitivity perspective. The VI-FCL results in a feasible OPC considering N-1 contingency up to 10 ohms in the main topology. In contrast, with the harmonic-based protection scheme, an OPC can be achieved under N-1 contingency up to R_{flt}^{max} . Further, the harmonic-based protection scheme signifi-

Table 6.5: Operation Times for Selected Near-end and Far-end Bolted Faults with Variable I_p (Case II)

Relays operation times (s)					
#	Primary	Backup	#	Primary	Backup
F₁	R ₁	R ₁₀	F₉	R ₁	R ₁₀
	0.6501	1.0358		0.6535	1.0408
	R ₂	R ₄		R ₂	R ₄
	0.9385	1.1539		0.9344	1.1484
F₂	R ₃	R ₁	F₁₀	R ₃	R ₁
	0.4408	0.6536		0.4430	0.6571
	R ₄	R ₆		R ₄	R ₆
	1.1483	1.3659		1.1428	1.3587
F₃	R ₅	R ₃	F₁₁	R ₅	R ₃
	0.2329	0.4431		0.2340	0.4453
	R ₆	R ₈		R ₆	R ₈
	1.3585	2.6600		1.3516	2.6445
F₄	R ₇	R ₅	F₁₂	R ₇	R ₅
	0.0200	0.2340		0.0201	0.2356
	R ₈	-		R ₈	-
	2.6442	-		2.6368	-
F₅	R ₉	R ₂	F₁₃	R ₉	R ₂
	0.7271	0.9388		0.7302	0.9430
	R ₁₀	R ₁₂		R ₁₀	R ₁₂
	1.0356	2.4510		1.0302	2.4348

cantly reduces the total relays operation times by 20.62% and 51.63% at bolted and moderate high resistance faults, respectively.

Table 6.9 reports a sensitivity analysis for the harmonic and VI-FCL schemes. The VI-FCL scheme maintains the protection coordination for resistive faults up to 10 ohms compared to 15 Ω for the harmonic scheme for the main topology. Under N-1 contingency, the VI-FCL scheme can maintain protection coordination for severe

Table 6.6: Reduction in Individual Relays' Operation Times for Selected Near-end Bolted Faults (Case II)

Relays operation times (s)							
Fixed I_p			Variable I_p		Δt (s)		Δt (s)
#	Primary	Backup	#	Primary	Backup	Primary	Backup
F₁	R ₁	R ₁₀	F₁	R ₁	R ₁₀	0.2359	0.1532
	0.8860	1.1890		0.6501	1.0358		
	R ₂	R ₄		R ₂	R ₄		
	1.2595	1.5644		0.9385	1.1539		
F₂	R ₃	R ₁	F₂	R ₃	R ₁	0.1576	0.2368
	0.5984	0.8904		0.4408	0.6536		
	R ₄	R ₆		R ₄	R ₆		
	1.5572	1.8812		1.1483	1.3659		
F₃	R ₅	R ₃	F₃	R ₅	R ₃	0.0874	0.1586
	0.3203	0.6017		0.2329	0.4431		
	R ₆	R ₈		R ₆	R ₈		
	1.8722	3.2804		1.3585	2.6600		
F₄	R ₇	R ₅	F₄	R ₇	R ₅	0.0151	0.0881
	0.0351	0.3221		0.0200	0.2340		
	R ₈	-		R ₈	-		
	3.2623	-		2.6442	-		
F₅	R ₉	R ₂	F₅	R ₉	R ₂	0.2410	0.3211
	0.9681	1.2599		0.7271	0.9388		
	R ₁₀	R ₁₂		R ₁₀	R ₁₂		
	1.1888	2.1895		1.0356	2.4510		

Table 6.7: Operation Times for Selected Near-end and Far-end 15 Ω resistance Faults with Variable I_p (Case II)

Relays operation times (s)					
#	Primary	Backup	#	Primary	Backup
F₃	R ₅	R ₃	F₁₁	R ₅	R ₃
	0.4002	0.6743		0.4034	0.6779
	R ₆	R ₈		R ₆	R ₈
	1.5629	2.9796		1.5594	2.9685
F₄	R ₇	R ₅	F₁₂	R ₇	R ₅
	0.0266	0.4035		0.0267	0.4074
	R ₈	-		R ₈	-
	2.9681	-		2.9620	-
F₇	R ₁₃	R ₁₁	F₁₅	R ₁₃	R ₁₁
	0.2715	0.4966		0.2726	0.4982
	R ₁₄	R ₁₆		R ₁₄	R ₁₆
	4.1948	4.4063		4.1576	4.3848
F₈	R ₁₅	R ₁₃	F₁₆	R ₁₅	R ₁₃
	0.0266	0.2726		0.0267	0.2736
	R ₁₆	-		R ₁₆	-
	4.3840	-		4.3612	-

Table 6.8: Relays Total Operation Times Considering Near-end Faults

R_{ft}	Adaptive		$\Delta T(\%)$
	VI-FCL	Harmonic Voltage	
0.1	48.2272	38.2836	20.62
1	48.2393	38.5716	20.04
3	55.6110	39.0422	29.79
5	63.8686	40.1193	37.18
10	91.2693	44.1455	51.63
15	-	49.2848	-

Table 6.9: Protection Schemes Sensitivity

Outage	R_{ft} (Ω)	Harmonic	VI-FCL
No outage	0-3	✓	✓
	3-10	✓	✓
	10-15	✓	×
All single IIDG outages	0-3	✓	✓
	3-10	✓	×
	10-15	×	×
All single line outages	0-1	✓	✓
	1-10	✓	×
	10-15	×	×

faults (up to 3 Ω), while the harmonic scheme can preserve the coordination up to moderate high resistance faults (up to 10 Ω).

6.3 Conclusion

The fault currents measured by overcurrent protective relays in IBIM are comparable to the nominal load current even at low resistive faults. Therefore, a communication-less harmonic-based protection scheme is developed for islanded microgrids to provide reliable overcurrent protection. In addition, the IIDG controller is modified to include a linear adaptive harmonic voltage generation function that generates a harmonic voltage based on fault severity. A two-stage program is developed which utilizes an HSCC method. The first stage calculates the relays' harmonic voltages and currents. In Stage II, a single relays' settings that preserve HDOCRs coordination employing the HTCVC characteristic and a harmonic directional element are obtained. The proposed protection scheme achieves coordination for bolted to the highest resistance faults for the main topology. Further, it is capable of maintaining coordination up to 10 Ω for all single IIDG and line outages.

Chapter 7

Conclusions

7.1 Summary

The effect of IIDGs limited fault current contributions on overcurrent protective relays has been tackled. The studies were based on time-domain simulations using PSCAD/EMTDC software and algorithms developed in the MATLAB environment. The objective of the studies was threefold: unveiling any transient stability issues associated with IIDG current saturation under low resistive fault conditions, devising a modified IIDG controller to confront these problems without the need for communication, extra hardware, and protecting the inverter's switches from overcurrent. The studies broadly utilized two layers, namely fundamental and harmonic. The dissertation has focused on two topics in the overcurrent protection of IBIM:

1. *Fundamental-based overcurrent protection*: A control algorithm is developed utilizing an adaptive VI-FCL that adapts to fault severity to enhance the overcurrent protection scheme. The adaptive VI-FCL serves two objectives: protecting the inverter's switches from overcurrent while ensuring a feasible OPC for IBIM under various fault scenarios. The OPC problem is formulated as a constrained nonlinear programming problem and solved to obtain the optimal DOCRs settings. The results confirm that DOCRs in an islanded microgrid can have a single set of optimal settings to maintain relays' coordination under all microgrid topologies resulting from different N-1 contingencies.
2. *Harmonic-based overcurrent protection*: An adaptive harmonic generation system is proposed by modifying the IIDG controller to generate a third harmonic voltage based on fault severity. The generated harmonic voltage results in a harmonic layer formed during short-circuit faults and is decoupled from the fun-

damental fault current, i.e., limited by IIDGs. The harmonic-based protection scheme utilizes the generated harmonic voltages and currents at the relay location to ensure the OPC of IBIM. In addition, the proposed protection scheme employs dual-setting HDOCRs capable of operating in forward and reverse directions. The results demonstrate the ability of the proposed scheme to protect islanded microgrids without communication and its capability to reduce relays' operation times. The proposed adaptive harmonic generation system is utilized in another protection scheme employing HDOCRs equipped with forward trip characteristic. The results reflect that the proposed scheme can protect IBIM under different N-1 contingencies using universal relays' settings. The OPC is achieved up to the maximum resistive fault in the main topology.

7.2 Contributions

The contributions of this dissertation can be summarized as follows:

Development of a new OPC framework with an SCC algorithm for islanded microgrids, in which:

- A VI-FCL is developed to limit the inverter's fault current, avoid the reference current saturation, and enhance microgrid transient stability. Further, the VI-FCL keeps the voltage source model intact, which reduces the complexity of the SCC;
- A two-stage OPC algorithm is proposed for islanded microgrids. The algorithm adaptively adjusts the VI-FCLs and calculates relays' currents in Stage I, which are used in Stage II for protection coordination based on the standard ITC and the TCV characteristics. The adaptive VIFCLs allow for solving the OPC problem at a broader range of fault resistances and enhance the DOCR sensitivity;
- The OPC problem is solved considering N-1 contingency, including all possible single line and IIDG outages during the islanding mode. Including contingencies

guarantees the reliable operation of islanded microgrids.

Development of an OPC algorithm based on an adaptive harmonic voltage generated by IIDGs, which makes microgrid protection independent of the limited fundamental current during faults, in which:

- An adaptive harmonic voltage generation characteristic produces tangible fault current measurements for a broader range of fault resistances. The use of the adaptive harmonic voltage enhances protection sensitivity;
- A new OPC formulation is developed for islanded microgrids involving a two-stage algorithm. The algorithm tests various harmonic voltage generation characteristics in the first stage to maximize the harmonic voltage resulting in more tangible harmonic currents;
- In the second stage, the harmonic voltages and currents are used to achieve protection coordination utilizing HDOCRs equipped with dual TCV characteristics. The dual setting reduces relays' total operation time and handles reverse fault currents without communication;
- A new overcurrent protection scheme is proposed utilizing an adaptive harmonic linear characteristic using relays with a forward trip characteristic. The two-stage OPC algorithm is used and the protection coordination problem is solved considering all possible N-1 contingencies. Including contingencies ensures a secure and dependable operation of islanded microgrids.

It is worth mentioning that although the optimal settings obtained considering balanced faults, the relay might take longer to respond to unbalanced faults because of the change in the fault current levels. However, using relays equipped with fault-type classifiers can be programmed to switch between multiple characteristics based on fault type. Low-bandwidth communication can be used as means to select the appropriate trip characteristic. Hence, achieving enhanced relay operation times can be considered in future work.

7.3 Future Work

Building on the results obtained in this dissertation, further research on the protection of IBIM may include the following topics:

1. OPC for IBIM utilizing the harmonic-based overcurrent protection considering unbalanced faults,
2. Enhancement of the harmonic-based overcurrent protection scheme speed under contingencies, and
3. Planning of overcurrent protection coordination for IBIM.

Bibliography

- [1] A. Hooshyar, R. Iravani, “Microgrid protection,” *Proc. IEEE*, vol. 105, no. 7, pp. 1332–1353, Jul. 2017.
- [2] *IEEE press, Microgrid architecture and control*, Wiley, 2014, pp. 83–84.
<https://ieeexplore.ieee.org/book/6685216>.
- [3] T. E. Sati and M. A. Azzouz, “Optimal protection coordination for inverter dominated islanded microgrids considering N-1 contingency,” *IEEE Trans. Power Deliv.*, vol. 37, no.3, pp. 2256–2267, Jun. 2022.
- [4] E. Dehghanpour, H. Kazemi Karegar, R. Kheirollahi, and T. Soleymani, “Optimal coordination of directional overcurrent relays in microgrids by using cuckoo-linear optimization algorithm and fault current limiter,” *IEEE Trans. Smart Grid*, vol. 9, no. 2, pp. 1365–1375, 2018.
- [5] H. M. Sharaf, H. H. Zeineldin, and E. El-Saadany, “Protection coordination for microgrids with grid-connected and islanded capabilities using communication assisted dual setting directional overcurrent relays,” *IEEE Trans. Smart Grid*, vol. 9, no. 1, pp. 143–151, Jan. 2018.
- [6] L. Huchel and H. H. Zeineldin, “Planning the coordination of directional overcurrent relays for distribution systems considering DG,” *IEEE Trans. Smart Grid*, vol. 7, no. 3, pp. 1642–1649, May 2016.
- [7] A. Gururani, S. R. Mohanty, and J. C. Mohanta, “Microgrid protection using

- Hilbert–Huang transform based-differential scheme,” *IET Gener. Transm. Distrib.*, vol. 10, no. 15, pp. 3707–3716, 2016.
- [8] E. Casagrande, W. L. Woon, H. H. Zeineldin, and D. Svetinovic, “A differential sequence component protection scheme for microgrids with inverter-based distributed generators,” *IEEE Trans. Smart Grid*, vol. 5, no. 1, pp. 29–37, Jan. 2014.
- [9] F. Katiraei and M. R. Iravani, “Power Management strategies for a microgrid with multiple distributed generation units,” *IEEE Trans. Power Syst.*, vol. 21, no. 4, pp. 1821–1831, Nov. 2006.
- [10] A. Tuladhar, H. Jin, T. Unger and K. Mauch, “Parallel operation of single phase inverter modules with no control interconnections,” *Proceedings of APEC Applied Power Electron. Conf.*, pp. 97–100, 1997.
- [11] N. Pogaku, M. Prodanovic and T. C. Green, “Modeling, analysis and testing of autonomous operation of an inverter-based microgrid,” *IEEE Trans. Power Electron.*, vol. 22, no. 2, pp. 613–625, Mar. 2007.
- [12] A. Yazdani and R. Iravani, *Voltage-sourced converters in power systems*, Wiley, 2010.
- [13] J. A. P. Lopes, C. L. Moreira, and A. G. Madureira, “Defining control strategies for microgrids islanded operation,” *IEEE Trans. Power Syst.*, vol. 21, no. 2, pp. 916–924, May 2006.
- [14] K. T. Tan, X. Y. Peng, P. L. So, Y. C. Chu, and M. Z. Q. Chen, “Centralized control for parallel operation of distributed generation inverters in microgrids,” *IEEE Trans. Smart Grid*, vol. 3, no. 4, pp. 1977–1987, Dec. 2012.
- [15] *IEEE guide for design, operation, and integration of distributed resource island systems with electric power systems*, IEEE Standard 1547.4, Jul. 2011.

- [16] J. M. Guerrero, J. C. Vasquez, J. Matas, L. G. de Vicuna, and M. Castilla, “Hierarchical control of droop-controlled AC and DC microgrids—a general approach toward standardization,” *IEEE Trans. Ind. Electron.*, vol. 58, no. 1, pp. 158–172, Jan. 2011.
- [17] H. Bevrani and S. Shokoochi, “An intelligent droop control for simultaneous voltage and frequency regulation in islanded microgrids,” *IEEE Trans. Smart Grid*, vol. 4, no. 3, pp. 1505–1513, Sep. 2013.
- [18] Y. Mohamed and E. F. El-Saadany, “Adaptive decentralized droop controller to preserve power sharing stability of paralleled inverters in distributed generation microgrids,” *IEEE Trans. Power Electron.*, vol. 23, no. 6, pp. 2806–2816, Nov. 2008.
- [19] A. Yazdani and R. Iravani, “An accurate model for the DC-side voltage control of the neutral point diode clamped converter,” *IEEE Trans. Power Deliv.*, vol. 21, no. 1, pp. 185–193, Jan. 2006.
- [20] M. A. U. Khan, Q. Hong, A. Egea-Àlvarez, A. Dyško, and C. Booth, “A communication-free active unit protection scheme for inverter dominated islanded microgrids,” *Electr. Power Syst. Res.*, vol. 142, Art. no. 108125, May 2022.
- [21] K. Saleh, M. A. Allam, and A. Mehrizi-Sani, “Protection of inverter-based islanded microgrids via synthetic harmonic current pattern injection,” *IEEE Trans. Power Deliv.*, vol. 36, no. 4, pp. 2434–2445, Aug 2021.
- [22] L. V. Strezoski and M. D. Prica, “Short-circuit analysis in large-scale distribution systems with high penetration of distributed generators,” *IEEE/CAA J. Autom. Sing.*, vol. 4, no. 2, pp. 243–251, Apr. 2017.
- [23] L. V. Strezoski, B. Dumnici, B. Popadic, M. Prica and K. A. Loparo, “Novel fault models for electronically coupled distributed energy resources and their

- laboratory validation,” *IEEE Trans. Power Syst.*, vol. 35, no. 2, pp. 1209–1217, Mar. 2020.
- [24] H. Hooshyar and M. E. Baran “Fault analysis on distribution feeders with high penetration of PV systems,” *IEEE Trans. Power Syst.*, 2013, vol. 28, no. 3, pp. 2890–2896, 2013.
- [25] M. Ghanaatian and S. Lotfifard, “Sparsity-based short-circuit analysis of power distribution systems with inverter interfaced distributed generators,” *IEEE Trans. Power Syst.*, vol. 34, no. 6, pp. 4857–4868, Nov. 2019.
- [26] Z. Shuai, C. Shen, X. Yin, X. Liu and Z. J. Shen, “Fault analysis of inverter-interfaced distributed generators with different control schemes,” *IEEE Trans. Power Deliv.*, vol. 33, no. 3, pp. 1223–1235, Jun. 2018.
- [27] K. Jia, Q. Liu, B. Yang, L. Zheng, Y. Fang and T. Bi, “Transient fault current analysis of IRESs considering controller saturation,” *IEEE Trans. on Smart Grid*, vol. 13, no. 1, pp. 496–504, 2022.
- [28] Q. Zhang, D. Liu, Z. Liu and Z. Chen, “Fault modeling and analysis of grid-connected inverters with decoupled sequence control,” *IEEE Trans. on Ind. Electron.*, p.1-1, 2021.
- [29] X. Shi, H. Zhang, C. Wei, Z. Li and S. Chen, “Fault modeling of IIDG considering inverter’s detailed characteristics,” *IEEE Access*, vol. 8, pp. 183401–183410, 2020.
- [30] J. Keller and B. Kroposki, “Understanding fault characteristics of inverter based distributed energy resources,” Natl. Renew. Energy Lab., pp. 1–41, 2010, [Online]. Available: <http://www.nrel.gov/docs/fy10osti/46698.pdf>.
- [31] A. D. Paquette, D. M. Divan, “Virtual impedance current limiting for inverters in microgrids with synchronous generators,” *IEEE Trans. Ind. Appl.*, vol. 51, no. 2, pp. 1630–1638, Mar. 2015.

- [32] W. K. A. Najy, H. H. Zeineldin, W. L. Woon, “Optimal protection coordination for microgrids with grid-connected and islanded capability,” *IEEE Trans. Ind. Electron.*, vol. 60, no. 4, pp. 1668–1677, 2013.
- [33] T. Qoria, F. Gruson, F. Colas, X. Kestelyn and X. Guillaud, “Current limiting algorithms and transient stability analysis of grid-forming VSCs,” *Electr. Power Syst. Res.*, vol. 189, pp. 106726, Dec. 2020.
- [34] S. Beheshtaein, M. Savaghebi, R. M. Cuzner, S. Golestan and J. M. Guerrero, “Modified secondary-control-based fault current limiter for inverters,” *IEEE Trans. Ind. Electron.*, vol. 66, no. 6, pp. 4798–4804, Jun. 2019.
- [35] V. A. Papaspiliotopoulos, G. N. Korres, V. A. Kleftakis and N. D. Hatziargyriou, “Hardware-in-the-loop design and optimal setting of adaptive protection schemes for distribution systems with distributed generation,” *IEEE Trans. Power Deliv.*, vol. 32, no. 1, pp. 393–400, Feb. 2017.
- [36] A. Karthikeyan, D. G. Abhilash Krishna and C. Nagamani, “Virtual impedance based DFCL for DVR during downstream faults,” *Proceedings of 2018 IEEE International Conference on Power Electronics, Drives and Energy Systems, PEDES*, 2018.
- [37] X. Wang, Y. W. Li, F. Blaabjerg and P. C. Loh, “Virtual-impedance-based control for voltage-source and current-source converters,” *IEEE Trans. Power Electron.*, vol. 30, no. 12, pp. 7019–7037, Dec. 2015.
- [38] X. Lu, J. Wang, J. M. Guerrero, and D. Zhao, “Virtual impedance- based fault current limiters for inverter dominated AC microgrids,” *IEEE Trans. Smart Grid*, vol. 9, no. 3, pp. 1599–1612, May 2018.
- [39] K. A. Saleh, M. S. El Moursi, and H. H. Zeineldin, “A new protection scheme considering fault ride through requirements for transmission level interconnected wind parks,” *IEEE Trans. Ind. Informatics*, vol. 11, no. 6, pp. 1324–1333, Dec. 2015.

- [40] A. Korashy, S. Kamel, T. Alquthami, and F. Jurado, "Optimal Coordination of Standard and Non-Standard Direction Overcurrent Relays Using an Improved Moth-Flame Optimization," *IEEE Access*, vol. 8, pp. 87378–87392, 2020.
- [41] D. Solati Alkaran, M. R. Vatani, M. J. Sanjari, G. B. Gharehpetian, and M. S. Naderi, "Optimal overcurrent relay coordination in interconnected networks by using fuzzy-based GA method," *IEEE Trans. Smart Grid*, vol. 9, no. 4, pp. 3091–3101, Jul. 2018.
- [42] P. P. Bedekar and S. R. Bhide, "Optimum coordination of directional overcurrent relays using the hybrid GA-NLP approach," *IEEE Trans. Power Deliv.*, vol. 26, no. 1, pp. 109–119, Jan. 2011.
- [43] V. N. Rajput, F. Adelnia, and K. S. Pandya, "Optimal coordination of directional overcurrent relays using improved mathematical formulation," *IET Gener., Transm. and Distrib.*, vol. 12, no. 9, pp. 2086–2094, May 2018.
- [44] D. Saha, A. Datta and P. Das, "Optimal coordination of directional overcurrent relays in power systems using Symbiotic Organism Search Optimization technique," *IET Gener., Transm. and Distrib.*, vol. 10, no. 11, pp. 2681–2688, 2016.
- [45] H. Usama, M. Moghavvemi, H. Mokhlis, N.N. Mansor, H. Farooq, and A. Pourdaryaei, "Optimal protection coordination scheme for radial distribution network considering on/off-grid," *IEEE Access*, vol. 9, pp. 34921–34937, Jan. 2021.
- [46] U. F. E. R. Commission et al., "Mandatory reliability standards for the bulk power systems," Federal Egenegy Regulatory Commission, Washington, DC, USA Docket no. RM06-16-000, Order no. 693, Mar. 2007.
- [47] M. Ojaghi and V. Mohammadi, "Use of clustering to reduce the number of different setting groups for adaptive coordination of overcurrent relays," *IEEE Trans. Power Deliv.*, vol. 33, no. 3, pp. 1204–1212, Jun. 2018.

- [48] M. N. Alam, "Adaptive protection coordination scheme using numerical directional overcurrent relays," *IEEE Trans. Ind. Informatics*, vol. 15, no. 1, pp. 64–73, Jan. 2019.
- [49] A. S. Noghabi, H. R. Mashhadi, and J. Sadeh, "Optimal coordination of directional overcurrent relays considering different network topologies using interval linear programming," *IEEE Trans. Power Deliv.*, vol. 25, no. 3, pp. 1348–1354, Jul. 2010.
- [50] A. Sharma and B. K. Panigrahi, "Phase fault protection scheme for reliable operation of microgrids," *IEEE Trans. on Indust. Appl.*, vol. 54, no. 3, pp. 2646–2655, 2018.
- [51] J. Qi, J. Xie, X. Ling, Y. Li, and T. Lan, "Optimal-probabilistic coordination of directional overcurrent relays considering network topological uncertainties," *IEEE Power and Energy Society General Meeting*, vol. 2019, August 2019.
- [52] K. A. Saleh, H. H. Zeineldin, and E. F. El-Saadany, "Optimal protection coordination for microgrids considering N - 1 contingency," *IEEE Trans. Ind. Informatics*, vol. 13, no. 5, pp. 2270–2278, Oct. 2017.
- [53] I. Sadeghkhani, M. E. Hamedani Golshan, A. Mehrizi-Sani, J. M. Guerrero, and A. Ketabi, "Transient monitoring function-based fault detection for inverter-interfaced microgrids," *IEEE Trans. Smart Grid*, vol. 9, no. 3, pp. 2097–2107, May 2018.
- [54] D. P. Mishra, S. R. Samantaray, and G. Joos, "A combined wavelet and data-mining based intelligent protection scheme for microgrid," *IEEE Trans. Smart Grid*, vol. 7, no. 5, pp. 2295–2304, Sep. 2016.
- [55] S. A. Saleh, R. Ahshan, M. S. Abu-Khaizaran, B. Alsayid, and M. A. Rahman, "Implementing and testing d-q WPT-based digital protection for microgrid systems," *IEEE Trans. Ind. Appl.*, vol. 50, no. 3, pp. 2173–2185, May/June 2014.

- [56] S. F. Zarei, H. Mokhtari, and F. Blaabjerg, "Fault detection and protection strategy for islanded inverter-based microgrids," *IEEE J. Emerg. Sel. Top. Power Electron.*, vol. 9, no. 1, pp. 472–484, Dec. 2019.
- [57] A. A. Balyith, H. M. Sharaf, M. Shaaban, E. F. EL-saadany, and H. H. Zeineldin, "Non-communication based time-current-voltage dual setting directional overcurrent protection for radial distribution systems with DG," *IEEE Access*, vol. 8, no. 5, pp. 190572–190581, Oct. 2020.
- [58] K. O. Oureilidis and C. S. Demoulias, "A fault clearing method in converter-dominated microgrids with conventional protection means," *IEEE Trans. Power Electron.*, vol. 31, no. 6, pp. 4628–4640, Jun. 2016.
- [59] F. Alasali, E. Zarour, W. Holderbaum, and K. N. Nusair, "Highly fast innovative overcurrent protection scheme for microgrid using metaheuristic optimization algorithms and nonstandard tripping characteristics," *IEEE Access*, vol. 10, pp. 42208–42231, Apr. 2022.
- [60] X. Li, A. Dysko, and G. M. Burt, "Traveling wave-based protection scheme for inverter-dominated microgrid using mathematical morphology," *IEEE Trans. Smart Grid*, vol. 5, no. 5, pp. 2211–2218, Sep. 2014.
- [61] H. Muda and P. Jena, "Superimposed adaptive sequence current based microgrid protection: A new technique," *IEEE Trans. Power Del.*, vol. 32, no. 2, pp. 757–767, Apr. 2017,
- [62] K. Dubey, and P. Jena "Impedance angle-based differential protection scheme for microgrid feeders," *IEEE Syst. J.*, vol. 15, no. 3, pp. 3291–3300, Sept. 2021.
- [63] U.Orji et al., "Adaptive zonal protection for ring microgrids," *IEEE Trans. Smart Grid*, vol. 8, no. 4, pp. 1843–1851, Jul. 2017.
- [64] J. Nsengiyaremye, B. C. Pal, and M. M. Begovic, "Microgrid protection using low-cost communication systems," *IEEE Trans. Power Del.*, vol. 35, no. 4, pp. 2011–2020, Aug. 2020

- [65] K. Pandakov , C. M. Adrah , H. K. Høidalen, and Ø. Kure, “Experimental validation of a new impedance-based protection for networks with distributed generation using co-simulation test platform,” *IEEE Trans. Power Del.*, vol. 35, no. 3, pp. 1136–1145, Jun. 2020.
- [66] Z. Chen, X. Pei, M. Yang, L. Peng, and P. Shi, “A novel protection scheme for inverter-interfaced microgrid (IIM) operated in islanded mode,” *IEEE Trans. Power Electron.*, vol. 33, no. 9, pp. 7684–7697, Sep. 2018.
- [67] K. A. Saleh and A. Mehrizi-Sani, “Harmonic directional overcurrent relay for islanded microgrids with inverter-based DGs,” *IEEE Syst. J.*, vol. 15, no. 2, pp. 2720 - 2731, Jun. 2021.
- [68] W. T. El-Sayed, M. A. Azzouz, H. H. Zeineldin, and E. F. El-Saadany, “A harmonic time-current-voltage directional relay for optimal protection coordination of inverter-based islanded microgrids,” *IEEE Trans. Smart Grid*, vol. 12, no. 3, pp. 1904–1917, May. 2021.
- [69] A. Hooshyar and R. Iravani, “A new directional element for microgrid protection,” *IEEE Trans. Smart Grid*, vol. 9, no. 6, pp. 6862–6876, Nov. 2018.
- [70] A. Banaiemoqadam, A. Hooshyar, and M. A. Azzouz, “A comprehensive dual current control scheme for inverter-based resources to enable correct operation of protective relays,” *IEEE Trans. Power Delivery*, vol. 36, no. 5, pp. 2715–2729, 2021
- [71] J. Nocedal, S. J. Wright, *Numerical Optimization*, Second ed. Springer Verlag, Berlin, 2006.
- [72] *Relays. IEC Measuring and Equipment—Part, Protection, 151: Functional Requirements for Over/Under Current Protection*, IEC Standard 60255-151, 2009.
- [73] K. A. Saleh, H. H. Zeineldin, A. Al-Hinai, E. F. El-Saadany, “Optimal coordination of directional overcurrent relays using a new time-current- voltage characteristic,” *IEEE Trans. Power Delivery*, vol. 30, no. 2, pp. 537–544, 2015.

- [74] *IEEE Recommended Practice for Protection and Coordination of Industrial and Commercial Power Systems (IEEE Buff Book)*, IEEE Standard 242–2001, pp. 1–710, Dec. 2001.
- [75] J. L. Blackburn, T. J. Domin, *Protective Relaying: Principles and Applications*, 4th ed., CRC Press, Boca Raton, FL, 2014.
- [76] A. S. A. Awad, T. H. M. EL-Fouly, and M. M. A. Salama, “Optimal ESS allocation for benefit maximization in distribution networks,” *IEEE Trans. Smart Grid*, vol. 8, no. 4, pp. 1668–1678, Jul. 2017.
- [77] H. M. A. Ahmed, A. S. A. Awad, M. H. Ahmed, and M. M. A. Salama, “Mitigating voltage-sag and voltage-deviation problems in distribution networks using battery energy storage systems,” *Electr. Power Syst. Res.*, vol. 184, Art. no. 106294, 2020.
- [78] S. Kannan, S. M. R. Slochanal, and N. P. Padhy, “Application and comparison of metaheuristic techniques to generation expansion planning problem,” *IEEE Trans. Power Syst.*, vol. 20, no. 1, pp. 466–475, Feb. 2005.
- [79] T. B. Soeiro, F. Vancu, and J. W. Kolar, “Hybrid active third-harmonic current injection mains interface concept for DC distribution systems,” *IEEE Trans. Power Electron.*, vol. 28, no. 1, pp. 7–13, Jan. 2013,
- [80] W. Cai, B. Liu, S. Duan, and C. Zou, “An islanding detection method based on dual-frequency harmonic current injection under grid impedance unbalanced condition,” *IEEE Trans. Ind. Informat.*, vol. 9, no. 2, pp. 1178–1187, May 2013.
- [81] C.-W. Ho, A. Ruehli, and P. Brennan, “The modified nodal approach to network analysis,” *IEEE Trans. Circuits Syst.*, vol. CS-22, no. 6, pp. 504–509, Jun. 1975.
- [82] O. S. Nduka, Y. Yu, B. C. Pal, and E. N. C. Okafor, “A robust augmented nodal analysis approach to distribution network solution,” *IEEE Trans. Smart Grid*, vol. 11, no. 3, pp. 2140–2150, May 2020.

- [83] GE Digital Energy ITI. (2020). Instrument Transformer Basic Technical Information and Application. [Online]. Available: <https://www.gegridsolutions.com/products/manuals/ititechinfo.pdf>

Appendix A

A1. Parameters based on IIDG rating

Paramter	Value (pu)
m_p	0.022
n_q	0.229
R_f	0.003
L_f	0.2
C_f	0.04
K_{vp}	1.0
T_{vi}	0.1
K_{ip}	0.1
T_{ii}	2.0
H	0.5

Vita Auctoris

NAME: Talal Sati

PLACE OF BIRTH: Sudan

EDUCATION: University of Windsor, Ph.D. in Electrical Engineering, Windsor, Ontario, Canada, 2022

The University of Western Ontario, MEng in Electrical Engineering, London, Ontario, Canada, 2017.

University of Khartoum, M.Sc. in Electrical Power Engineering, Faculty of Engineering, Khartoum, Sudan, 2009.

University of Khartoum, B.Sc. in Electrical Power Engineering, Faculty of Engineering, Khartoum, Sudan, 1994.

ProQuest Number: 29391492

INFORMATION TO ALL USERS

The quality and completeness of this reproduction is dependent on the quality and completeness of the copy made available to ProQuest.



Distributed by ProQuest LLC (2022).

Copyright of the Dissertation is held by the Author unless otherwise noted.

This work may be used in accordance with the terms of the Creative Commons license or other rights statement, as indicated in the copyright statement or in the metadata associated with this work. Unless otherwise specified in the copyright statement or the metadata, all rights are reserved by the copyright holder.

This work is protected against unauthorized copying under Title 17, United States Code and other applicable copyright laws.

Microform Edition where available © ProQuest LLC. No reproduction or digitization of the Microform Edition is authorized without permission of ProQuest LLC.

ProQuest LLC
789 East Eisenhower Parkway
P.O. Box 1346
Ann Arbor, MI 48106 - 1346 USA